Analysis of an enclosure for a MEMS DC electric field sensor

by

Sadna Isik

A Thesis submitted to the Faculty of Graduate Studies of

The University of Manitoba

in partial fulfillment of the requirements of the degree of

MASTER OF SCIENCE

Department of Electrical and Computer Engineering
University of Manitoba
Winnipeg, MB

Abstract

MEMS DC electric field sensors are successful candidates in the field of monitoring power utility infrastructure. Their delicate size and nature require them to be placed in a protective enclosure when used in an outdoor environment. The enclosure surrounding an electric field sensor affects the measurement conditions and sensor performance. This thesis presents an enclosure for MEMS DC electric field sensors with a height-adjustable floating pin conductor to augment the signal. The enclosure top assembly includes a metal pin extending into the enclosure to augment the signal seen by the sensor. A floating metal plate and an adjustable floating pin on the enclosure body are included to pass the electric field into the enclosure and onto the sensor. The electric field strength variation is computed while changing the distance between the sensor and the body of the sensor enclosure by changing the length of the floating pin. The behaviors of electric field strength on the sensor are studied by varying parameters. A capacitance model is studied and proposed for the enclosure structure.

Simulation and experimental tests are performed for a conducting electrically floating plate, which is placed 14.6 mm above the sensor and a conducting pin, which is located at different heights above the sensor. For the enclosure design considered, when the pin is placed 1 mm above the sensor, the measured electric field is 18.3 times stronger than when the same electric field is measured without the pin. Simulation and experiment results show that a floating pin can help to reduce signal loss due to the gap by extending into the enclosure, which significantly increases the incident electric field upon the sensor located deeper inside the enclosure box. These enclosures can be integrated with other sensor types, such as field mills, to eliminate the potential disadvantages of locating sensors inside protective enclosures.

Acknowledgments

First and foremost, I would like to express my sincere gratitude to my advisor Dr. Cyrus Shafai giving me the opportunity to study and work at the University of Manitoba and NSFL (Nano System Fabrication Laboratory) and for the continuous support for my master's degree. Thank you for your patience, motivation, discussions, and guidance.

A special thank goes to all my colleagues Dr. Elnaz Afsharipour, Dr. Tao Chen, and Brandon Hill, Sampath Liyanage for their support in my research.

I am very much thankful to graduate advisor Samuel Kidd (present) and graduate advisor Amy Dario (previous) for their support.

I would also like to thank Nanofabrication Laboratory manager Dwayne Chrusch, and my friends in Dr. Cyrus Shafai's research group for their support.

I thank all ECE department administrative and technical staff.

Last but not the least, I would like to thank my family members Omer, Muhammed, Nazan, Sunara, Mehran, Imtiyaz, Kaleem and Memet.

Contents

List of Figures

List of Tables

Notations and Abbreviations

The following notations and abbreviations are used in the thesis:

List	Description
DC	Direct current
MEMS	Micro-electro-mechanical systems
FMP	Floating metal plate
AC	Alternating current
Al	Aluminum
FMP	Floating metal plate
Si	Silicon
HVDC	High voltage direct current
SOI	Silicon on Insulator
2D	Two dimensional
3D	Three dimensional
es	Electrostatics
MEFM	Micromechanical electric field mills

Dedication

To children;

Hamza Mirac
Muhammed Zain
Manha Suleiha
Manara Bathul

Chapter 1

Introduction

This thesis presents the modeling, fabrication, and testing of an enclosure for MEMS-based DC electric field sensors. This was achieved through the optimization of the geometric shape of the sensor enclosure and the metal aperture over the sensor using COMSOL Multiphysics software, which utilizes finite element analysis (FEA) [1]. This study was carried out in collaboration with the MEMS sensor and electronic design group, as well as the partner organization Manitoba Hydro International (MHI), and involved close collaboration in conducting research and experimental work to apply it to electric power utilities and smart grid concept applications.

1.1 Background and history

The DC electrical field sensors sector presents a remarkable potential within the electric power industry. An instance of this is the Smart Grid concept [3], which incorporates a sensor network for gathering information that is integrated across the entire electrical distribution grid. This network is used to monitor thousands of power transformers, capacitors, breakers, and thousands of kilometers of power lines. Within the category of electric field monitoring, arrays of electric field sensors could be positioned in the proximity of electrical utility installations and transmission line networks.

Reported DC electric field sensor applications

Exploring and monitoring natural and man-made electric fields is very important for the better understanding of the power and transmission line systems as well as hazard prevention that exists in our vicinity [2]. There is value in measuring large electric fields due to high-voltage direct current (HVDC) power transmission lines that are widely distributed to deliver power from remote renewable power generation centers, such as solar, wind, hydro, etc., to the load center cities located hundreds of kilometers away [3,4]. These lines could be overhead, underground, or underwater, and the efficiency and reliability of these cables are critical to power utilities. Sensors used to measure DC electric fields are one of the effective ways to monitor the high-voltage DC infrastructure. For example, they can be applied to monitor the voltage remotely [5], monitor the electromagnetic effect on the environment [6], improve insulation systems [7], detect faulty insulators [8], or ensure the safety of operators in live line work [9,10]. Moreover, measuring DC fields are useful to observe and take precautions in advance in the field of lighting observation [11], thunderstorm observations [12,38], cosmic observation [13] earthquake prediction [14], and natural electric fields at different sea depths [15]. Measuring small electric field strength can provide information on wound healing in health applications [16,17] and exploring electric fields in the body for medical applications were also reported [19,20]. Electric field measurement is also being applied to musical applications. According to the Joseph A. et al. in p.1 “The Theremin was one of the first electronic musical instruments, yet it provides a degree of expressive real-time control that remains lacking in most modern electronic music interfaces. Underlying the deceptively simple capacitance measurement used by it and its descendants are a few surprisingly interesting current transport mechanisms” [18].

The different functions of sensors in electric field monitoring

There are many applications were measuring electric field could be useful in the high voltage and electric utility industry.

- Monitoring the condition of insulators.
- Alert of surface contamination on insulators.
- Warn of potential dangers of flashover.
- Measure ionic generation and ionic travel caused by wind.
- Detect surface charge accumulation on infrastructure.
- Detect high electric fields caused by dusty conditions.
- Monitor for fast transient changes in atmospheric electromagnetic field (indicative of lightning).
- Detect changes such as charge separation in a cloud (observed by monitoring local strengthening in magnitude and/or reversal of electrostatic field) that can warn of potentially hazardous weather conditions.
- Measure voltage remotely with proper calibration, eliminating the need for bulky and expensive insulators when measuring high voltages.

Some of the challenges associated with measuring DC electric fields

Many challenges exist in measuring DC electric fields in long term and high voltage applications. Some are listed below.

- Charging of the instrument itself, resulting in difficulties with long-term monitoring.
- Charge attraction onto instrument surfaces.

- Settling of ionic atmospheric particles on the instrument.
- Difficulties with long-term use of rotating field mills, such as limited battery life and wear and tear of moving parts.
- High maintenance costs associated with remote field mill installations used for extended periods of time.
- Other economic disadvantages associated with the widespread deployment of DC electric field mills across the electrical grid.

There are different types of instruments currently employed for measuring DC electric fields, including induction probes, rotating field mills, and vibration field probes. Rotating field mills [36] are commonly utilized by many utilities for long-term monitoring of atmospheric and high voltage DC electric fields, as they are capable of functioning in ionic environments. Electric field mills typically employ a motor to rotate a perforated shield, which intermittently exposes the sensing electrodes to the incoming electric field.

However, the extended use of rotating field mills can lead to various issues, including limited battery life and wear and tear of moving parts. Utilities often deploy these devices in remote locations for several months, and the necessary maintenance visits to field mill installations can be expensive. As a result, the widespread deployment of DC electric field mills across the electrical grid is economically unfavorable. In recent years, several international research groups have explored micromachined electric field mills (MEFMs) as a means of improving the performance of field mills. Various MEFM technologies are discussed in Chapter 2.

A common technique employed by MEFMs involves the utilization of comb drives to induce lateral vibration in a perforated shutter positioned above sensing electrodes [21-25].

However, comb drive based vibrating shutter MEFMs have various disadvantages, including:

- Comb actuators often require large actuation voltages (20V-100V) which can interfere with the sense signal.
- Interference from the drive electrode can affect the measurement accuracy of MEFMs.
- High actuation voltages can lead to unreliable MEFM performance in the presence of high electric fields.
- Shutter lifting can occur in environments with electric fields exceeding 100 kV/m, leading to inaccurate measurements.
- Long-term ionic charging from weather effects or corona discharge can also cause charge build-up, leading to shutter lifting and unreliable MEFM performance.

Electrostatic force-based MEM-membrane actuators have been studied extensively as well, and they can solve some of the issues of vibrating shutter based MEFMs. These use a movable MEM platform which is deflected by an incident electric field [26-29,52-53]. The sensor utilized in this thesis for experimental work is an electrostatic force-based sensor. These systems have reported the following advantages and disadvantages:

- *High resolution:* These sensors can measure high electric fields without losing resolution, unlike other types of sensors.
- *No issues from ionic charging:* Electrostatic force-based MEM-membrane sensors do not suffer from issues caused by ionic charging.
- *Adjustable sensitivity:* The sensitivity of these sensors can be improved and adjusted by applying an AC voltage to the MEM-membrane to modulate force coupling from an incident DC field [52].

- *Compact size:* A compact version of these sensors has been developed, making them ideal for use in small spaces [13].
- *Wide measurement range:* These sensors can measure a wide range of electric field strengths, from 0.11 V/m to over 180 kV/m, with no saturation.
- *Works at atmospheric pressure:* Electrostatic force-based MEM-membrane sensors can be used at atmospheric pressure, eliminating the need for vacuum packaging which can be an issue for resonant MEFMs.
- *Ability to measure DC electric fields without a reference ground:* A design employing paired out-of-phase electrodes allows these sensors to measure DC electric fields without needing a reference ground [53].
- *Can be used on insulated platforms or as a hand-held insulated probe:* This new design offers the significant ability of being used on insulated platforms or as a hand-held insulated probe, making them versatile for a variety of applications.

Smart grid concept and HVDC transmission corridor

The increasing adoption of "smart grid" technology in the North American power industry has highlighted the need for innovative sensor technology that can evaluate the overall health of the power system. Manitoba Hydro, which relies on HVDC technology for over 75% of its generating capacity, requires continuous monitoring of the HVDC transmission corridor to ensure environmental safety. However, current technology used to monitor the electric fields of HVDC transmission lines is not suitable for remote and isolated locations typical of much of the HVDC corridor and requires extensive maintenance. The proposed MEM sensors, on the other hand, offer a low-power, long-term monitoring solution that could enable remote environmental monitoring initiatives that are currently not cost-effective.

Apart from environmental monitoring, MEMS sensors could also detect abnormalities in the electric fields surrounding DC transmission line insulators, thus helping in live-line maintenance by identifying defects and hazards. The sensors could also aid in developing better insulation systems, identifying faulty insulators, measuring line voltage remotely without bulky and expensive insulating structures, and serving other purposes. This would be beneficial not only to Manitoba Hydro but also to other Canadian operators of HVDC transmission systems in Quebec, BC, and Alberta. Moreover, as a leading province in HVDC, Manitoba is home to various consultants like Teshmont, Transgrid, and Electranix who could expand their services globally by incorporating MEMS DC electric field sensors.

1.2 Research goals and motivation

The research goals of this study are to provide innovation in the power systems industry, with a specific focus on developing instrumentation for HVDC infrastructure monitoring, ionic flux measurement, remote DC voltage probes, and worker safety systems. This research aims to develop electronic hardware and software to enable prototype evaluation, focusing optimized sensor enclosures to maximize sensor sensitivity, and systems suitable for all weather use.

Furthermore, the proposed MEM sensors offer the possibility of robust, low-power, long-term monitoring for environmental monitoring initiatives, aiding in live-line maintenance by identifying defects and hazards, and improving insulation systems. The successful development of sensor systems including packaging would also open the door to new applications and research, such as measurement of atmospheric charging and providing indications of blowing dust, sand, snow, or aerosols for environmental monitoring and predicting dangerous flashover situations near high voltage installations. These sensors could also be valuable to other industries requiring electric field or static charge monitoring.

The aim of the research project is to create a prototype of MEMS DC electric field sensors that are suitable for field testing by our industrial partner, Manitoba Hydro International (MHI). The testing conducted in my thesis will rely on a combination of relevant studies.

- Prototype sensor enclosures were developed and enhanced for optimal sensor sensitivity and all-weather functionality. The concept designs were refined to improve the aperture geometry and maximize the incident DC electric field on the sensor for improved sensitivity. The project focused on developing enclosures having a compact design, which would also be suitable for hand-held sensor use.
- A main objective of the DC electric field sensor research is to enable sensors to detect a wide range of electric fields, spanning from below 100 V/m to over 1 MV/m, which is especially relevant for monitoring HVDC infrastructure.

The surrounding environment of an electric field sensor is a crucial factor to consider for practical applications. Consequently, the enclosure that houses the sensor plays a significant role, as it can cause distortion of the incident electric field and reduce the sensor's sensitivity. The prior research of [52] and [53] investigated prototype housings for electric field sensors that incorporated electrically floating metal apertures. These enclosures provide complete protection to the sensor from the environment while allowing the DC electric field to pass through. However, additional research is required to optimize the enclosure designs to enhance the sensor sensitivity and enable its usage in outdoor (all-weather) and ionic environments.

Main objective of this thesis

A fundamental part of this project is the investigation of the correlation between the electric field that enters the sensor enclosure and the shape of the enclosure, as well as the geometric shape of the enclosure's electrically floating metal aperture. This thesis employs simulations (COMSOL Multiphysics software) to explore how the incident electric field can be potentially concentrated in proximity to the sensor electrodes, thereby increasing the sensor sensitivity.

Designs considered with be in accordance with the need for deployment of electric field sensors along an HVDC transmission lines. This will require the sensors to be packaged in sealed enclosures to avoid the influence of airflow and damage from bad weather conditions such as rain or snow. The enclosure should have an opening to allow the sensor to be influenced by the external field, which can be sealed by a dielectric material such as polymer [30] or a floating metal block [31]. Dielectric materials allow the electric field to pass, but they can suffer from charge accumulation, which leads to measurement errors during long-term operation. Floating metal covers can also allow an electric field to pass by redistributing surface charge, but the accumulation of free charges from the air onto the floating metal cover needs to be neutralized regularly.

Proposed DC electric field sensor enclosure

In this thesis, I present an enclosed MEMS electric field sensor that employs a grounded enclosure with a floating conductive metal plate on top assembly and a height-adjustable conducting pin extending into the enclosure. The pin is used to bring the sensed field into the interior of the enclosure and close to the sensor. Studies were undertaken to investigate the incident electric field on the sensor in relation to the capacitance of the interior enclosure and the capacitance of the pin that is observed by the sensor. Simulation and experimentation investigate the effect of pin height on sensor sensitivity.

These results are indicative of electric field variations on the micro-sensor surface, which can assist in the design of real sensor enclosures and explain the working principle of the sensor enclosure. Future studies of these enclosures aim to integrate them with other sensor types, such as field mills, to eliminate potential disadvantages.

1.3 Sensor capabilities and resolution

Sensitivity

In the context of a DC electric field sensor, sensitivity refers to the ability of the sensor to detect and measure small changes in the electric field strength.

Sensitivity is a key performance parameter of an electric field sensor, as it determines the smallest measurable electric field strength that the sensor can reliably detect. Generally, a more sensitive sensor will be able to detect smaller electric fields, which makes it more useful for detecting subtle changes in the environment.

Sensitivity is often expressed in terms of the minimum detectable electric field strength, or the voltage per unit distance that the sensor can detect. For example, a sensor with a sensitivity of 1 V/m could detect an electric field of 1 volt per meter.

To improve the sensitivity of an electric field sensor, several design considerations may be considered. These include increasing the size of the sensor's active area, reducing electrical noise in the sensor's circuitry, and optimizing the materials used in the sensor to maximize their sensitivity to electric fields.

In the context of DC electric field sensors that are intended to be used in high voltage direct current (HVDC) systems, sensitivity is a critical performance parameter that determines the ability of the sensor to accurately detect the electric field in the presence of high voltage and current levels. In HVDC systems, the electric field strength can be very high due to the presence of high voltage and current levels, which can cause electrical interference and noise in the sensor. This interference can affect the accuracy and reliability of the measurements, making it important to have a highly sensitive sensor that can detect even small changes in the electric field.

Resolution

In the context of a DC electric field sensor, resolution refers to the smallest detectable change in the electric field strength that the sensor can measure.

Resolution is an important performance parameter of an electric field sensor, as it determines the precision and accuracy of the measurements that the sensor can make. Generally, a higher resolution sensor will be able to measure smaller changes in the electric field strength, which makes it more useful for applications that require high precision and accuracy.

Resolution is often expressed in terms of the minimum detectable change in electric field strength, or the voltage per unit distance that the sensor can measure. For example, a sensor with a resolution of 0.1 V/m could measure a change in electric field strength of 0.1 volts per meter.

To improve the resolution of an electric field sensor, several design considerations may be considered. These include increasing the sensitivity of the sensor, reducing electrical noise in the sensor's circuitry, and optimizing the sampling rate and signal processing algorithms used to analyze the sensor's measurements. In addition, using high-precision instrumentation and calibration procedures can also improve the resolution of the sensor.

In the context of HVDC (High-Voltage Direct Current) electric field sensors, resolution refers to the smallest change in the electric field that the sensor can detect and measure accurately.

HVDC systems are used to transmit large amounts of electrical power over long distances with lower power losses compared to traditional AC (Alternating Current) systems. However, they also generate strong electric fields, which can be measured using sensors placed in the vicinity of the transmission lines.

The resolution of an electric field sensor is determined by its sensitivity, noise level, and dynamic range. The sensitivity of the sensor determines how much the output signal changes in response to a change in the electric field. The noise level of the sensor determines the smallest signal that can be detected above the background noise. The dynamic range of the sensor refers to the range of electric fields that can be measured accurately without saturating the sensor's output. Therefore, resolution is an important parameter for HVDC electric field sensors, as it determines the accuracy and reliability of the measurements. High-resolution sensors are required to accurately measure the electric field in HVDC systems and ensure their safe and efficient operation.

When considering E_{ac} of 2.2 equation in the Chapter 2, the measurement object is far, the sensitivity will be less since the E_{ac} electric field is inversely proportional to the distance. When the distance is far, to achieve the same sensitivity, the required procedure / solution can do one of the following: (1) increase the bias voltage, (2) move the pin closer, or (3) use higher gain in the measurement electronics. However, since noise will be amplified too, an additional filter circuit is needed.

Expected specifications on an electric field sensor, here are some key pieces of information that will experiment in this thesis

- *Measurement range:* What is the minimum and maximum electric field strength that the sensor is designed to measure?
- *Sensitivity:* What is the smallest change in electric field strength that the sensor can detect?
- *Resolution:* What is the smallest increment of electric field strength that the sensor can measure and display?
- *Accuracy:* How closely does the sensor's measured value match the true value of the electric field strength?
- *Operating frequency range:* What frequency range can the sensor measure?
- *Output signal:* What type of signal does the sensor produce (e.g., voltage, current, frequency)?
- *Operating temperature range:* What is the minimum and maximum temperature range in which the sensor can operate?
- *Physical size and weight:* What are the size and weight of the sensor, and how will it fit into the system or application you are using it for?
- *Power requirements:* What are the power requirements for the sensor, and can this system or application provide the necessary power?
- *Environmental considerations:* Will the sensor be exposed to any environmental factors that could affect its performance, such as humidity or vibration?

Bandwidth of a DC electric field sensor, there are a few things to consider

DC electric fields do not have a frequency in the traditional sense, as they are constant with time. As a result, the term "bandwidth" may not be directly applicable to a DC electric field sensor. Instead of bandwidth, one may want to consider the sensor's frequency response. The frequency response describes how the sensor's output changes as a function of frequency and can be used to determine the sensor's sensitivity to different frequencies.

To determine the frequency response of a DC electric field sensor, also, may need to perform a calibration or test using a known electric field source with a known frequency response. This can help you determine the sensor's sensitivity to different frequencies, even if the electric field itself is DC.

Enclosed DC electric field sensor

An enclosed DC electric field sensor is a type of sensor that is shielded or enclosed in some way, often with a metallic enclosure. However, when the sensor is enclosed, the electric field strength that it measures can be reduced due to a phenomenon known as electric field screening.

Electric field screening occurs when an electric field encounters a conductive material, such as the metal enclosure of an electric field sensor. The conductive material creates an opposing electric field that cancels out or reduces the electric field inside the enclosure. This effect can be particularly strong at high frequencies or for materials with high conductivity.

The phenomenon of electric field screening can be explained by the way that charges are distributed in a conductive material when it is exposed to an external electric field. When an electric field is applied, the charges in the conductor rearrange themselves to create an opposing electric field that cancels out the external field inside the material. The magnitude of the opposing field is proportional to the conductivity of the material, with highly conductive materials such as metals producing a stronger opposing field.

Therefore, when an electric field sensor is enclosed, the electric field strength that it measures can be reduced due to the screening effect of the enclosure. This reduction in electric field strength can be significant and can lead to inaccuracies in the measured field strength. To minimize this effect, it is important to design the enclosure and the sensor in such a way as to minimize the screening effect, for example by using materials with low conductivity or by designing the enclosure with openings or other features that allow the electric field to pass through.

If an electric field sensor is placed inside an electrically grounded enclosure, an aperture is required to enable the electric field to enter. If the sensor is deeply recessed inside the enclosure, a method is needed to bring the external electric field into the enclosure. To ensure accurate electric field measurements, it is essential to carefully consider the geometry and design of the enclosure system [39].

1.4 Research Contributions

Studies of sensor enclosure simulation and measurement results have been published in conference posters as follows.

- S. Isik, C. Shafai, "Simulation-based modeling of sensor enclosure to enhance dc electric field strength on MEMS-based sensors" MNE Eurosensors, Leuven, Belgium, 2 pages, 19 – 23 September (2022).
- T. Chen, B. Hill, S. Isik, C. Shafai, L. Shafai, "DC electric field sensor based on polyimide substrate", IEEE Sensors, 31 October – 04 November, 4 pages, Virtual Conference (2021).
- T. Chen, S. Isik, C. Shafai, L. Shafai, "MEMS Electric Field Sensor with Biased

Electrically Floating Cover to Measure Electric Field in Ionic Environments", CPEEE 2022 - International Conference on Power, Energy and Electrical Engineering, February 25-27, 4 Pages Shiga, Japan -Virtual, (2022).

1.5 Thesis Overview

The following chapters elaborate proposed enclosure for MEMS DC electric field sensors in detail.

- In Chapter 2, a brief background literature search for reported enclosed DC electric field sensors and mechanisms is presented.
- Chapter 3 includes the case-by-case electrical field strength analyses of the 2D enclosure structure using the COMSOL Multiphysics software. Appropriate boundary conditions along with the critical parameters analyses have been done for each case. The effect of parameters such as length, width, and thickness geometry on the electric field is studied and analyzed.
- Chapter 4 includes the case-by-case electrical field strength analyses of the 3D enclosure structure using the COMSOL Multiphysics software. Appropriate boundary conditions along with the critical parameters analyses have been done for each case.
- Chapter 5 is for the development of the experimental setup. This chapter includes the experimental test results. The experimental results are discussed and compared with a similar simulation model. The electric field strength for the capacitance model along with the equivalent circuit model for the sensor enclosure is studied.
- Chapter 6 is summaries of the thesis, and potential future works are further provided.

Chapter 2

Other DC electric field sensor technologies with enclosure

Chapter 1 discussed the background of DC electric field sensors, goals, motivation, and noted the importance of enclosures for DC electric field measurements. Chapter 2 will include brief background information about sharks' electric field sensing capability gifted by nature, widely used field mills without specific enclosures, and a few recently reported sensors with a protective enclosure. Moreover, background of designing and simulation using COMSOL Multiphysics also explained. Further extensive details on DC electric field sensors and mechanisms can be found in the references at the end of the thesis and in reference [31].

There are various types of electric field sensors available [45-49], each with their own advantages and disadvantages in terms of sensitivity and resolution. However, in general, the following types of sensors are known for their high sensitivity and good resolution:

***Capacitive electric field sensors*:** These sensors work by measuring changes in charge storage on a capacitor in response to changes in the electric field strength incident on one plate of the capacitor, in relation to the other plate held at a reference voltage. Capacitive sensors can be designed to be very sensitive and have high resolution, making them suitable for measuring electric fields in a variety of applications.

Electro-optic sensors: These sensors use materials that change their optical properties in response to changes in the electric field strength. The change in the optical properties can be measured using optical techniques such as interferometry or polarimetry, allowing for high sensitivity and good resolution.

Field mill sensors: These sensors use a rotating grounded metal plate over capacitive sensing electrodes, to create a changing electric field from a DC field. The rotation of the plates periodically electrically charges the sensing electrodes, with an electric current that is proportional to the electric field strength. Field mill sensors can have high sensitivity and resolution, but they are generally more complex and expensive than other types of electric field sensors [44].

It's worth noting that the choice of electric field sensor will depend on the specific application and requirements. Some applications may require higher sensitivity or resolution than others, while cost and complexity may also be factors to consider.

2.1 Shark's natural electric field sensing and mechanism [35]

Very sensitive electric field sensing is not new to nature. Some sharks have been proven to detect electric fields as small as 5 nV/cm, which is still a challenge for most advanced laboratories [32-34]. According to Douglas Fields' explanation on p.76 of the shark's electric sense, "Sharks and related species sense extremely weak electric fields generated by other animals in seawater thanks to hundreds or even thousands of specialized detectors in their snouts called ampullae of Lorenzini" [33]. Interestingly, in the shark, microtubes filled with conducting gel are used to enable the electric field to extend below the surface of the skin, closer to the sensing nerves [35]. In this thesis, I also employ a floating conducting pin to bring the electric field closer to the sensor body by extending it deeper into the enclosure box.

2.2 Traditional field mill rotating type DC electric field sensor [36]

In Chapter 1, it was explained that electric field mills are the most popular DC electric field sensors that have been commercially used for atmospheric sciences or measuring electric fields under HVDC lines for more than two decades. For instance, a traditional rotating-type field mill was used to measure the earth's quasi-static atmospheric electric field for the National Aeronautics and Space Administration (NASA) Marshall Space Flight Center (MSFC), and it is known to be one of the successful projects intended for use on aircraft [36]. The operating principle of a Rotating-Vane Electric Field Mill for Airborne Platforms [36] is explained below.

An external electric field is detected as the rotor electrode alternately covers and uncovers the sense electrodes. When the sense electrodes are uncovered, an electric charge is induced in them, resulting in an oscillating charge signal that varies in amplitude with the external electric field. This charge signal has an amplitude that is proportional to the vector component of the electric field normal to the plane of the modulator, a period that is related to the rotor's rotational velocity, and a phase that is related to the position of the rotor with respect to the sense electrodes.

Field mills are predominantly used for atmospheric field measurements. However, these devices require the turning of an "earthed" chopper to modulate the DC field into an AC one. Field mills operate by inducing an electric charge in the sense electrodes when they are uncovered.

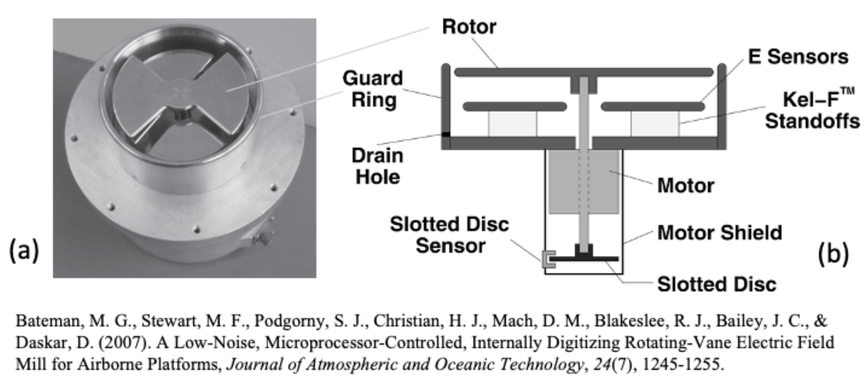

Bateman, M. G., Stewart, M. F., Podgorny, S. J., Christian, H. J., Mach, D. M., Blakeslee, R. J., Bailey, J. C., & Daskar, D. (2007). A Low-Noise, Microprocessor-Controlled, Internally Digitizing Rotating-Vane Electric Field Mill for Airborne Platforms, *Journal of Atmospheric and Oceanic Technology*, *24*(7), 1245-1255.

Figure 2.1: Field mill sensor - Lightning Instrument Package [36].

The problems with this design are that the chopper must be rotated by a motor, and an excellent electrical contact is needed with the rotating shaft. In practice, field mills require relatively large amounts of power and frequent maintenance due to the use of gold filaments that wear out quickly. Recently, field mill sensor technology has been developed to a greater extent by using MEMS-based small devices.

2.3 MEMS type DC electric field sensor [37]

MEMS-based sensors are miniaturized electric field sensor devices that can be used to measure power system voltages. MEMS DC electric field sensors have been studied by several groups [21-25]. In our group at the University of Manitoba, Wijeweera et al. [25, 50-51] designed a novel miniature micromachined electric field sensor was developed that can be used to measure both AC and DC voltages remotely by measuring the electric field. This was a micromachined thermally driven resonant shutter MEMS field mill electric field sensor. The minimum electric field detectable by the sensor was recorded as having a sensitivity of 200 (nV/(V/m)) and a 40 V/m resolution. Wijeweera also exhibited a prototype vacuum package to accommodate the sensor, indicating that the sensor could detect an external electric field from inside the package that consisted of a floating metal plate. While vacuum enclosures can be useful in protecting MEMS devices from environmental contaminants, they may not always be suitable for MEMS electric field sensors due to the potential issues with Electrostatic Discharge (ESD) damage, stress, temperature effects, sensitivity degradation, and reduced signal-to-noise ratio.

The operating principle of the sensor is illustrated in Figure 2.2(a). The sensor uses a moving electrically grounded shutter to periodically expose and shield the underlying electrodes from an incident electric field. In other words, when the shutter covers and uncovers the sensing electrodes in the presence of an electric field, an alternating current (or AC) is induced on the electrodes according to:

$$i = \varepsilon_0 \frac{d(EA)}{dt} \tag{2.1}$$

where ε_0 is the permittivity of free space, E is the component of the electric field normal to the electrodes and A is the effective area of the electrode. The illustration shows the sensing circuit where the induced AC currents on each electrode array are differentially measured and converted to a voltage.

A sensor package was developed for this DC electric field sensor, and the author describes the working principle as: “The sensor was placed inside a vacuum environment together with the sensing circuit. The proof-of-concept vacuum packaging developed to test the sensor is shown in Figure 2.2 (b). The body of the vacuum chamber was made from aluminum. The lid of the vacuum chamber possesses an electrically floating section (Metal B in), separated from the lower part of the vacuum chamber by Teflon spacing. The floating metal allows electric fields to enter the chamber. The lower body of the vacuum chamber was grounded, and the sensor was placed close to the floating lid by putting the sensor on support. In this proof-of-concept vacuum package, a pump was used to continuously pump out the air to maintain a constant vacuum pressure inside the chamber. However, a long-term operation of this sensor requires a self-contained vacuum package” [37].

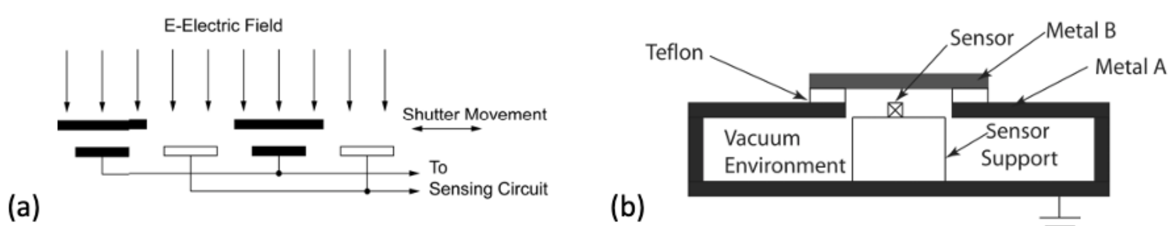

Wijeweera, G.; Shafai, C.; Rajapakse, A. Measuring power system voltage remotely using micromachined electric field sensor. In Proceedings of the 1st Microsystems and Nanoelectronics Research Conference, Ottawa, ON, Canada, 15 October 2008; pp. 209–212.

Figure 2.2: (a) Sensing circuit with sensing electrodes (b) Proof of concept vacuum package [37].

The vacuum packaging industry is well-developed today and the vacuum environment can be retained in a package for many years. Measuring both AC and DC fields of an unknown frequency is a significant advantage of this sensor in comparison to other sensors.

Electrostatic force-based sensors have been also explored by various researchers. An early work was done by Roncin [52], who investigated a micromachined optically interrogated deflected mass MEMS force electric field sensor. This demonstrated a sensitivity of 2000 (nV/(V/m)) and a resolution of 5000 V/m. Roncin also highlighted the significant advantage of the sensor over current technology, namely its compact size, single moving component, and the potential for low-cost yet durable manufacturing. However, the downside of the sensor is the need for environmental protection of the sensing element, which motivated me in this thesis.

In 2018, Liyanage [29] introduced a torsional moving MEMS DC electric field sensor capable of measuring a broad range of values with adjustable sensitivity in the 10s of V/m to MV/m range and a resolution of 3.2 V/m. Moreover, a portable, semi-automated measurement system was created to assess electric fields outdoors, surpassing the confinement of measurements to laboratory environments.

2.4 The Torsional micro-mirror sensor with adjustable sensitivity

MEMS DC electric field sensors are fabricated with a wide measurement range and adjustable sensitivity. The novel concept is applying two opposite voltages on the sensor surface that causes the sensor plate to tilt and enables the operation without any reference ground [39].

This sensor packaging consists of inner and outer boxes. The outer Al box has a window that is controlled by a stepper motor. The motor shaft can be moved back and forth to open and close the window. The inner box has an acrylic lid with a hole which is covered by an electrically floating Al metal plate the same size as the window. When the window is opened this Al metal plate is exposed to the outside electric field. When the window is closed, the floating Al metal plate is grounded through a metal spring connected to the window. The inner box is fixed to the outer Al box using wooden blocks. When the window is opened, an external electric field can pass through the opening and reach the sensor. The sensor is mounted on the Al base inside the inner box and this Al base is grounded. Therefore, most of the electric flux is engaged in the sensor area.

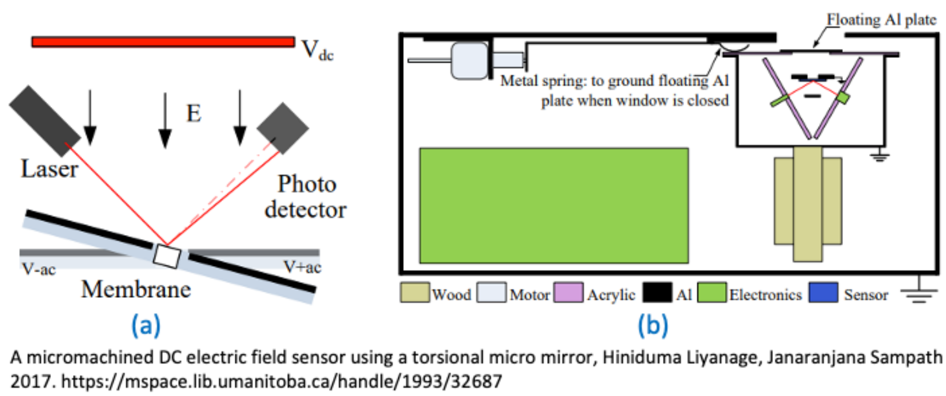

Figure 2.3: (a) Sensor working principle (b) Cross section of the portable enclosure box [39].

In a DC electric field, the electrostatic forces on each side of the mirror are [43]:

$$F_+ = -\frac{1}{2}\varepsilon A(\frac{V_{dc} - V_{ac}}{d})^2 = -\frac{1}{2d^2}\varepsilon A(V_{dc}^2 - 2V_{dc}V_{ac} + V_{ac}^2) \quad (2.2)$$

$$F_- = -\frac{1}{2}\varepsilon A(\frac{V_{dc} + V_{ac}}{d})^2 = -\frac{1}{2d^2}\varepsilon A(V_{dc}^2 + 2V_{dc}V_{ac} + V_{ac}^2) \quad (2.3)$$

where ε is the permittivity of the air, A is the area of the electrodes, d is the distance to the voltage source V_{dc}, and V_{ac} is the bias voltage on the electrodes. The middle term on the right-hand side is comprised of $V_{ac}V_{dc}$ component, at the frequency of V_{ac}, but the directions are opposite to each other on each electrode. This results in a rotational vibration of the mirror at the frequency of V_{ac}, as shown in equations (2.4) and (2.5):

$$F_{+} = \frac{\varepsilon_0 \varepsilon_r}{d^2} V_{dc} V_{ac} \tag{2.4}$$

$$F_{-} = -\frac{\varepsilon_0 \varepsilon_r}{d^2} V_{dc} V_{ac} \tag{2.5}$$

Due to the differential bias technique, the sensor does not need a ground reference for sensor operation. This is an advantage because it enables easy measurements and resolves the grounding-related problems of the current state-of-the-art sensors. Furthermore, the sensor response can dynamically change according to the electric field situation.

To reduce the cost of fabrication, normal Si wafers were used instead of SOI wafers. Also, to reduce the complexity of fabricating the sensors the bulk micro-machining technique was used. A new, low-stress fabrication process was developed to design the reflective mirrors.

The developed torsional mirror sensors are capable of measuring DC fields from 10's of V/m to MV/m range. The portable sensor box, which is powered by 6V batteries, is capable of visualizing and storing data, changing frequency and sensor bias voltage, and changing the sampling frequency of the sensor measurement. The sensor was tested under a mock DC line, with and without the presence of corona discharge effect and it effectively identified changes in the environment due to the space charges in a field with corona presence. The added calibration voltage plate in the measuring system can be used to calibrate the sensor before measuring the incident field making the measurement more reliable and accurate. The electric field drops down with different sizes of floating Al plates. The reach of the electric field to the sensor depends on a few parameters including the window size, floating Al plate size, distance to the sensor from the window and distance to the nearest ground from the window. In this study floating metal plate sensor enclosure placed inside environmental enclosure below the open.

2.5 Microsensor with a package taper shape cap structure [31]

The summary of “Resolution-Enhancing Structure for the Electric Field Microsensor Chip,” Micromachines, 2021 research paper consists,

- Electrostatic voltage is crucial for industrial production lines to reduce electrostatic discharge harms and improve yields.
- Previously reported electric field microsensors have drawbacks such as package shielding and low resolution, making them unsuitable for industrial static monitoring applications.
- The paper introduces a newly designed microsensor package structure that enhances the field strength inside the package cavity remarkably.
- The magnification effect was studied and optimized by theoretical calculation and ANSYS simulation.
- A compact signal processing circuit for the packaged microsensor was developed using digital synthesizer and digital coherent demodulation methods.
- The meter prototype was calibrated above a charged metal plate, and the electric field resolution was measured to be 5 V/m, with a measuring error of less than 3 V, from -1 kV to 1 kV in a 2 cm distance.
- The meter was installed into a production line and showed good consistency with, and better resolution than, a traditional vibratory capacitance sensor.

Figure 2.4 shows the electric field microchip and Package design with a taper shape package cap for the electric field microchip.

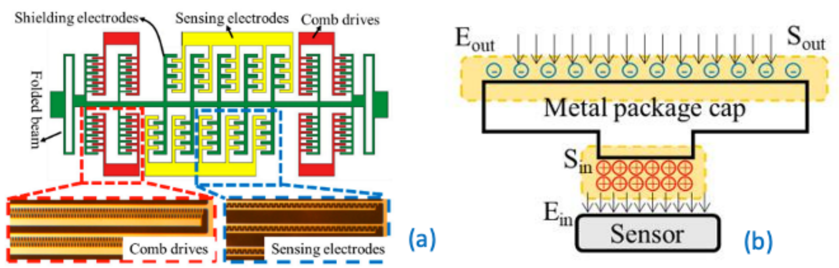

X. Wen, P. Yang, Z. Zhang, Z. Chu, C. Peng, Y. Liu, S. Wu, B. Zhang, and F. Zheng, "Resolution-Enhancing Structure for the Electric Field Microsensor Chip," Micromachines, vol. 12, 936, 2021.

Figure 2.4: (a) Sketch and pictures of the electric field microchip (b) Package design with a taper shape package cap for the electric field microchip [31].

Y. Yan et al. [31] provides the relationship between the electric field inside and outside the package cavity. The equation is stated as follows in his paper:

$$E_{in} = c.E_{out} \tag{2.6}$$

And for the design with a taper shape package cap for the electric field microchip:

$$E_{in} = \frac{S_{out}}{S_{in}} E_{out} \tag{2.7}$$

The equation indicates that the amplification coefficient $'c'$ is determined by the ratio of the two surface areas. In the previous flat cap structure, $'c'$ was equal to one ($c=1$). However, upon considering and calculating the support for the cap, it was found that the amplification coefficient was less than one ($c<1$). To develop a high sensitivity packaged microsensor, a new package structure was proposed using the equation. Unlike the simple flat structure, the new design features a tapered package cap, where the outer surface is large enough to collect the induced charge, while the inner surface is small enough to concentrate the opposite induced charge. This design allows for enhancement of the electric field within the package cavity.

The author has pointed out a drawback of the sensor, which is the limited measurement range that results from its magnified sensitivity. Thus, in cases where a larger measurement range is needed, the sensor would have to be positioned farther away from the object, thereby decreasing its sensitivity.

The author also noted that the package cap structure is sensitive to accumulated electrostatic charge, which can be transferred during the installation process. Since this sensor neglects the accumulated charge and considers the package cap as an electroneutral conductor, it is not easy to maintain neutrality during actual testing. The author also reported that it can take hours, or even days, for the accumulated charge to dissipate.

The author indicated that some advantages of the newly proposed package structure are also applicable in other circumstances. For example, in a dusty atmosphere, traditional vibrating capacitor meters or field mills are prone to be destroyed by particles. The thermally sealed package can protect the sensor's mechanical structure. Furthermore, the packaging method can also be used to improve the resolution of other electric field sensors, such as vibrating capacitors, optical-type electric field sensors, and other types of MEMS-based electric field microsensors.

2.6 MEMS Electrostatic Sensor [54]

This application uses an electric field sensor that operates based on a micro-mirror supported by two S-shaped micro-springs. Both the mirror and springs are coated with a thin layer of aluminum. The aluminum coating on the mirror is divided into two electrodes, with each electrode linked to an external AC bias voltage through the supporting springs. This setup effectively demonstrates the operational principle of the electric field sensor used in the application. The complete details of the operating principle of this sensor can be found in the reference list [42]. The study conducted by Hill developed a MEMS DC electric field sensor, as depicted in Figure 2.5, which was utilized in my thesis. The complete specifications and operation of the sensor can be found in Chapter 3 of his thesis [54].

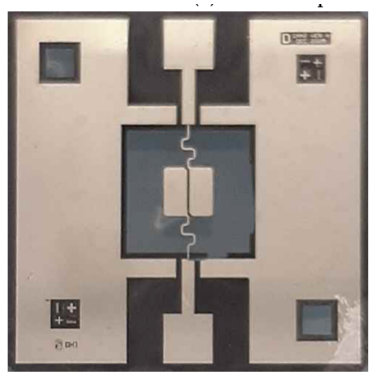

Figure 2.5: Si-MEMS Sensor DC electric field sensor [54].

The MEMS sensor chip designed by Hill [54] as shown in Figure 2.6 (a) in his thesis work by suspending a small flat membrane with springs that allow it to rotate around a central axis. The membrane has conductors that can be charged to different potentials and acts as a mirror for a laser beam. When exposed to an external field, the membrane rotates, causing a deflection in the reflected laser beam and a difference in current produced by the split photodiodes. The differential current can be used to measure the electrostatic field. The torsion springs provide a restoring force, and resonant operation increases the sensor's sensitivity.

The sensing system of [54] and this thesis uses an optical method of interrogation, which allows the distance between the MEMS mirror and receiving photodiodes to magnify the mirror's movement. However, factors such as beam divergence, apparent radius of origin, and spot size on the photodiodes can affect the signal per degree of tilt. The sensitivity of the device depends on the beam width, focusing, distance from the mirror, quality of the reflective surface, flatness, and dispersion in the reflected light.

In [54], it was also mentioned that the noise limited resolution of a sensing system depends on the sampling frequency, and it is important to state it in terms of bandwidth to avoid ambiguity. A complete noise spectrum can accurately calculate the resolution for any measurement bandwidth, while a single figure for resolution without indication of the bandwidth is ambiguous. The resolution of a sensing system is limited by noise factors, and a longer integration period may yield high resolution but be impractical in many scenarios. Higher sampling rates may have poorer resolution.

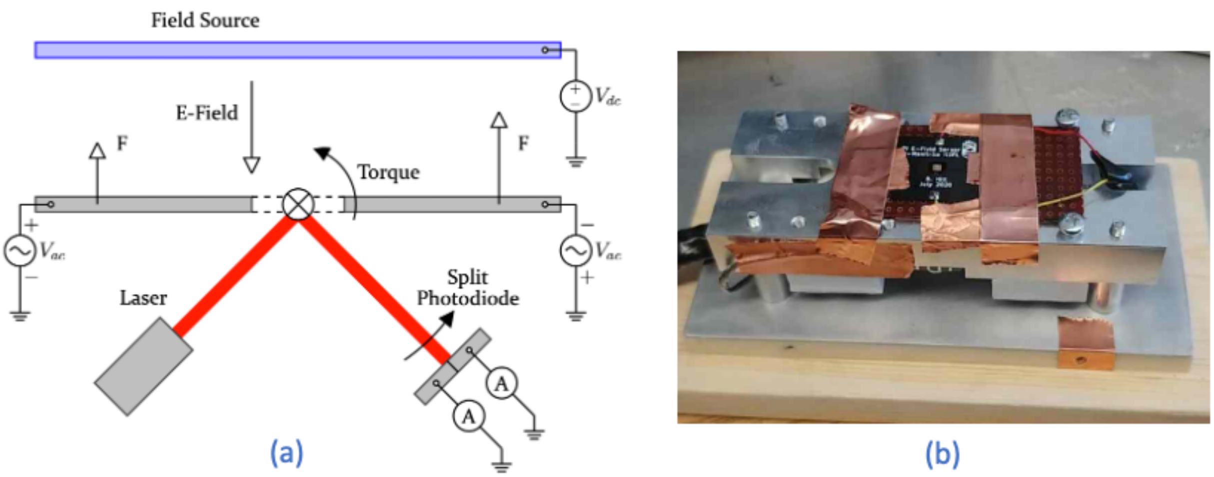

Investigation of a Flexible Printed Circuit Board MEMS Electrostatic Field Sensor, Brandon Hill, 2023.
https://mspace.lib.umanitoba.ca/bitstream/handle/1993/37089

Figure 2.6: (a) Operating principle (b) Electric field sensor mounted on the stage [54].

2.7 Finite element models

COMSOL Multiphysics is a powerful software package that can solve a wide range of physics problems using a variety of numerical methods. When it comes to solving for the DC electric field in 2D or 3D, the software uses the finite element method (FEM) to solve the governing partial differential equations (PDEs) that describe the electric field.

To solve for the DC electric field in a 2D or 3D domain, COMSOL Multiphysics first discretizes the domain into a mesh of small elements. Each element is assigned a set of equations that describe the electric field within that element. The equations consider the material properties of the region, including the conductivity and permittivity of the materials present.

The software then solves the resulting set of equations using the FEM, which involves approximating the electric field within each element as a linear combination of basic functions. By using the Galerkin method, the software can determine the coefficients of these basis functions, which in turn provide a numerical approximation to the electric field within the domain.

COMSOL Multiphysics is a software that can solve for the electric field using numerical methods. The software uses the finite element method to discretize the solution domain into small elements and then solves the governing equations of the electric field within each element. To solve for the electric field, COMSOL Multiphysics uses the following steps:

- Define the geometry of the problem, including the boundaries, material properties, and sources of electric field.
- Set up the governing equations that describe the behavior of the electric field, including Maxwell's equations for the electromagnetic fields and the continuity equation for the electric charge.
- Set up the governing equations that describe the behavior of the DC electric field, including

the Poisson equation for the electrostatic potential and the continuity equation for the electric charge.

- Choose appropriate boundary conditions for the problem, such as specifying the electric potential or electric field on the boundaries.
- Discretize the problem domain into a mesh of small elements, which allows for the numerical solution of the governing equations.
- Solve the discretized problem numerically, obtaining a numerical approximation of the electric field in the problem domain.
- Visualize and analyze the results of the simulation to gain insight into the behavior of the electric field in the problem.
- The electric field can be solved for in both DC and time-varying scenarios. For time-varying problems, additional considerations may be necessary, such as specifying the time-varying sources of the electric field or incorporating the effects of electromagnetic waves.

COMSOL Multiphysics solves for the DC electric field using physics equations related to electrostatics. The main physics equations involved in solving for the DC electric field are the Poisson equation and the continuity equation. The Poisson equation relates the electric potential to the electric charge density and is given by:

$$\nabla^2 V = -\rho/\varepsilon_0 \tag{2.8}$$

where V is the electric potential, ρ is the electric charge density, ε_0 is the electric constant, and ∇^2 is the Laplacian operator. The continuity equation relates the electric current density to the electric charge density and is given by:

$$\nabla \cdot J = -\partial\rho/\partial t \tag{2.9}$$

where J is the electric current density and t is time.

To solve for the DC electric field within a bounded region, the above equations are coupled and solved using the finite element method. The software discretizes the solution domain into small elements and then numerically solves a system of linear equations to determine the overall solution.

COMSOL Multiphysics is a finite element code which allows solving partial differential equations (PDEs) in 2D and 3D domains. There are predefined application modes where the governing PDEs are pre-set, but one can as well freely define the PDEs.

After defining boundaries and domains the mesh must be generated. This includes the selection of the basis functions' order and the choice of the order of the curved mesh elements. Orders higher than one mean curved element. They are used for a better approximation of curved boundaries. The COMSOL Multiphysics Reference Guide recommends using the same order for the curved elements as for the basis functions. There is an automatic option for the order of the curved elements which is meant to ensure that the order is set to the maximal order of the used basis functions. Nonetheless it was found that this option malfunctions sometimes. Best control over the solution process is achieved by manually setting the order of the curved elements. Another way to influence the meshing is to specify the number of nodes and their distribution on each edge of the model.

As a third step the system of equations must be solved. COMSOL Multiphysics offers a wide variety of solvers for this purpose. There are direct solvers which are suitable for smaller problems and iterative solvers which should be used for larger problems. If there is enough memory available on the computer, the direct algorithms can be applied to larger problems as well. This is desirable because they give a more accurate solution than the iterative solvers.

The last task is to visualize or further process the solution. COMSOL Multiphysics allows for 2D and 3D plots. Depending on the selected application mode one usually disposes of variables for the electric field and magnetic field. They can be plotted as vector plots and field intensity plots. The from the electromagnetic field derived quantities like Poynting vector, energy and energy loss are as well available as predefined variables. In cases where there is no predefined variable which suits, one can define customized quantities based on the solution vector.

For the general simulation models defined in this thesis, the surrounding air box, sensor enclosure, and elements dimensions of the geometries are between 1 mm to 1 m. Therefore, to obtain accurate results, COMSOL's specified 'normal mesh' size is generally sufficient. Due to non-curvature surfaces, triangular shaped mesh was selected. The convergence study showed that the result converges and that finer meshes can be quite expensive in terms of computation time. Thus, the normal meshing is used for all further computations. If wanting to model the real sensor, due to the smaller size of some objects in the design, a finer mesh would be ideal.

In the general simulation models, a square shape enclose is simulated, which allows to employ the advantage of symmetry to speed up computation time, while to keep parameters constant and consistence along with the variable. However, the interior of the real sensor enclosure is not symmetrical (for example it has a laser integration system in its interior as shown in Figure 2.7), so symmetry could not be used.

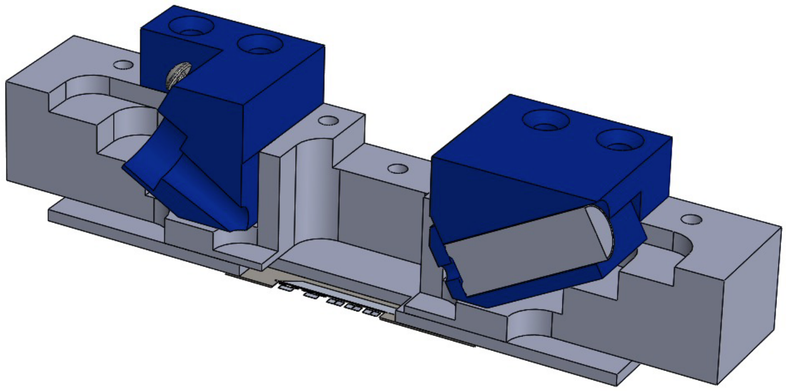

Figure 2.7: Rectangular shape Sensor stage (Designed by Hill [54] using SolidWork software).

To allow simplification of the structure and run different simulation rapidly to explore the changing of different parameters, initial simulations were done using 2D model to reduce computation time and memory. In order to ignore the omitted 3rd dimension, any influence like adjacent boundaries must be far enough away. Later models used 3D simulations and boundaries.

For both 2D and 3D models, the boundary of the air box is modelled to be 50 cm x 100 cm to better represent a distant field source, compared to the size of the sensor, such as an overhead HVDC line, and to ensure that the approaching 0 Hz electric field approaches the ground. The distribution of mesh density is larger in the air box, which would make the simulation faster but less accurate.

In COMSOL Multiphysics, 2D and 3D meshes are generated using a variety of techniques, including triangular and quadrilateral elements in 2D and tetrahedral, pyramid, prism, and hexahedral elements in 3D. The choice of mesh element depends on the geometry and the physics being modeled.

In 2D simulations, the mesh is generated by dividing the domain into a set of 2D triangles or quadrilaterals, with each element having three or four nodes respectively. The size and shape of the elements can be adjusted to optimize the simulation accuracy and computational efficiency.

In 3D simulations, the mesh is generated by dividing the domain into a set of 3D tetrahedral, pyramid, prism, or hexahedral elements, with each element having four, five, six, or eight nodes respectively. The size and shape of the elements can be adjusted to optimize the simulation accuracy and computational efficiency.

COMSOL Multiphysics also provides a variety of meshing options, including structured and unstructured meshes, as well as adaptive mesh refinement techniques. Structured meshes are generated using a regular pattern of nodes and elements, which can be more efficient and accurate for certain types of problems. Unstructured meshes, on the other hand, allow for more flexibility and can better handle complex geometries. Adaptive mesh refinement techniques dynamically adjust the mesh size and element shape based on the solution, allowing for increased accuracy in areas of interest while minimizing computational resources.

To solve the simulation using the mesh, COMSOL Multiphysics uses finite element analysis (FEA) techniques to discretize the governing equations into a system of algebraic equations that can be solved numerically. The accuracy and efficiency of the FEA solver depend on the mesh quality, with finer and more uniform meshes generally leading to more accurate results. Therefore, generating an appropriate mesh is an important step in achieving accurate and efficient simulations in COMSOL Multiphysics.

In COMSOL Multiphysics, the mesh density is a measure of the number of elements per unit volume or unit area in the mesh, while the mesh size is a measure of the physical length or distance between the nodes in the mesh. The reason why COMSOL Multiphysics uses mesh density rather than mesh size is because the mesh density provides a more accurate measure of the number of elements per unit volume or area, which is important for accurately capturing the solution in areas of high variation or complexity. Mesh size, on the other hand, is a more simplistic measure of the distance between nodes and does not consider the variation in geometry or solution that may require different element sizes in different parts of the domain.

By using mesh density, COMSOL Multiphysics can dynamically adjust the size and shape of the elements based on the local solution variation and geometry complexity, which can lead to a more accurate and efficient simulation. Additionally, COMSOL Multiphysics allows the user to specify the maximum and minimum mesh density, as well as the target mesh density, which provides a way to control the overall size and quality of the mesh.

Simulation considerations:

When undertaking the COMSOL simulations, some of the assumptions that need to be made are:

- The simulation is being done in two dimensions only, which means that the properties and behavior in the third dimension are neglected.
- The simulation assumes that the system under study is uniform in the third dimension, which means that variations in the third dimension are ignored.
- The simulation assumes that the properties and behavior of the system under study do not change with time or that the changes are slow enough to be ignored.
- The simulation assumes that the boundary conditions are well-defined and that the system behaves as expected at the boundaries.
- The simulation assumes that the physical laws and equations used to model the system are valid and applicable to the system under study.

It's worth noting that these assumptions may not always hold, and the accuracy of the simulation may be limited by these assumptions. Therefore, it's essential to carefully consider the assumptions made and their implications when performing a 2D simulation.

In COMSOL Multiphysics simulations, the choice of mesh size and refinement is critical for obtaining accurate results. Generally, the finer the mesh, the more accurate the simulation results. However, using a fine mesh can also significantly increase the computational time and memory requirements of the simulation.

- In 2D simulations, the geometry is simplified, and the mesh is much simpler to generate. As a result, the difference between the normal, fine, and finer mesh may not be very significant.
- In 3D simulations, however, the complexity of the geometry and the mesh is significantly increased. 3D simulations often involve curved surfaces and complex geometries, which can require more elements to accurately represent the geometry. Additionally, 3D simulations involve a larger volume of space, which requires more elements to accurately represent the solution. Therefore, using a finer mesh in 3D simulations can lead to significant improvements in the accuracy of the results.

However, it is important to note that using a finer mesh in 3D simulations can also significantly increase the computational time and memory requirements of the simulation. Therefore, it is important to balance the need for accuracy with the practical limitations of the simulation hardware and software.

Chapter 3

DC electric field sensor enclosure modeling (2D)

Chapter 2 summarized presently available DC electric field sensors with enclosures. This chapter will extensively discuss the new type of structure developed in this thesis, modeling for the localizing DC electric field at the sensor vicinity. These simulation models are done in 2D for faster computation and to gain general understanding. 3D simulation shown in Chapter 4 are more indicative of real sensor situations.

When conducting a 2D simulation of a static electric field, there are several assumptions that are typically made, including:

- *2D geometry*: A 2D simulation assumes that the system being analyzed has planar symmetry and can be reduced to a two-dimensional cross-section without significant loss of accuracy.
- *Axisymmetric or planar symmetry*: In some cases, the geometry may have additional symmetry, such as axisymmetric or planar symmetry. These additional assumptions can simplify the simulation by reducing the amount of data that needs to be input and simulated.
- *Quasi-static conditions*: A quasi-static approximation assumes that the time-varying electric and magnetic fields can be neglected compared to the static field. This is valid when the system is operating at low frequencies, such as in the case of electrostatics.
- *Linear materials*: The simulation assumes that the materials in the system are linear,

meaning that the relationship between the applied electric field and the resulting polarization or electric displacement is linear and time-invariant.

- *Steady-state conditions*: The simulation assumes that the system is in steady-state, meaning that the electric field and other parameters do not change with time. This assumption is valid for systems that are not subject to significant time-varying perturbations.
- *Uniform or homogeneous materials*: The simulation assumes that the materials in the system are uniform or homogeneous, meaning that they have the same properties throughout the system. This simplifies the simulation by eliminating the need to model material variations.

These assumptions are designed to simplify the simulation and reduce the number of computational resources required. However, it is important to recognize that these assumptions may not always hold true in practical situations, and the accuracy of the simulation should be carefully evaluated against experimental data or more complex numerical simulations if available.

3.1 Introduction

Employing a protective enclosure surrounding a DC electric field sensor can easily affect the measurement conditions and sensor performance. The characteristic of DC electric fields is that they can interact with the enclosure and negatively affect the sensor performance and its practical use. Section 2.3, 2.4, and 2.5 previously presented work on DC sensors that were tested with protective enclosures, and the conclusion was that the enclosures can impact the sensor's performance. These studies introduced an electrically floating metal plate on the enclosure body, which allows the electric field to pass into the enclosure and onto the sensor. However, those studies did not completely analyze the critical design parameters and mechanism to optimize the developed enclosure, which would be needed in practical applications.

Therefore, this chapter will provide background information on successfully modeling the enclosure to enhance the DC electric field strength upon the sensor. This chapter will cover the theoretical information needed to build the simulation model of the electric field sensor enclosure used in the experimental testing of Chapter 4.

3.2 Structure of the enclosure

The basic developed sensor enclosure model is shown in Figure 3.1. It is a square-shaped box suitable for a portable handheld device. This enclosure is large enough to provide room for the delicate micromachined MEMS based sensor, supporting electronics, and other peripheral elements including the mechanically support sensor platform.

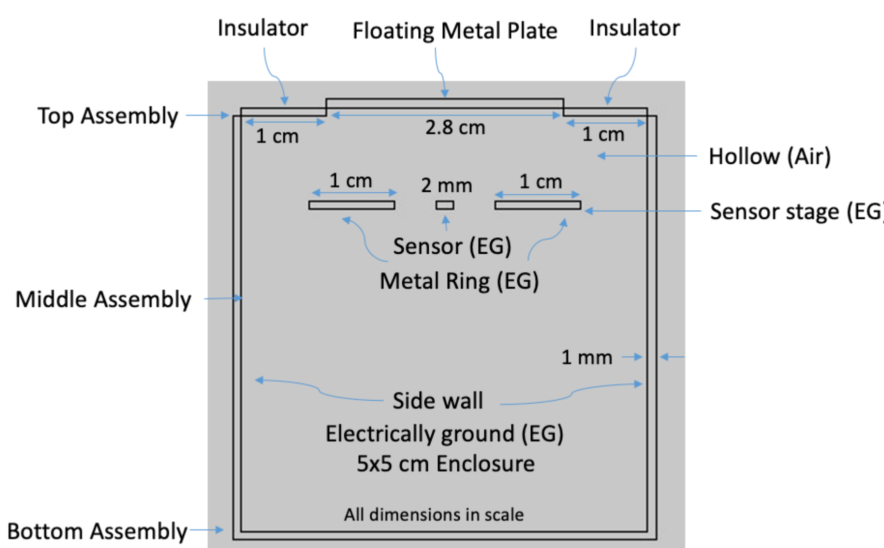

Figure 3.1: The enclosure box (sketched in scale).

The simulated enclosure measures 5 cm wide x 5 cm tall and has two main parts. The top part is the top assembly of the enclosure. The middle part of the top assembly is made of a floating metal plate (FMP), which is supported by an insulating material. The FMP allows the electric field to get into the enclosure while the insulating layer helps to electrically isolate the metal plate. The sensor is placed 1 cm below the FMP, within the hollow cavity of the enclosure, and positioned along the center of the FMP. The sensor is mounted on a support, which is surrounded by a grounded metal ring. The walls and floor of the enclosure are made of aluminum and electrically grounded.

The insulating support for the FMP is made of either acrylic or Teflon. Teflon better withstands harsh conditions. This insulating material:

1. Provides mechanical support to the floating metal plate
2. Isolates the FMP from the electrically grounded walls
3. Protects the sensor from harsh environmental conditions

Physics behind the enclosure structure:

The capacitance between the floating metal plate and the sensor will depend on the geometry and separation distance between the two, as well as the dielectric constant of any material that is between them. By carefully designing the geometry and separation distance between the floating metal plate and the sensor, it is possible to optimize the capacitance and sensitivity of the sensor. However, it is important to ensure that other the conductive objects do not interfere with the accuracy of the measurement by creating unwanted noise or distortion in the electric field being measured. In this setup, the floating metal plate with the conductive pin employs the pin to guide the external electric field into the enclosure, and so increase the sensitivity of the MEMS DC electric field sensor.

3.3 Simulation of the basic enclosure and simulation environment (2D)

COMSOL Multiphysics [40] was the software used to simulate the electric field environment. This software solves the physics equations over the simulated geometry numerically by iteration towards minimizing a converging error function [41]. The simulation model included an airbox space around the enclosure as shown in Figure 3.2. The Electrostatics (es) interface was employed to simulate the electrostatic physics and compute the electric field, electric displacement field, and potential distributions in dielectrics. When this physics interface is added, the parameters that are also added to the model builder include charge conservation, zero charge (the default boundary condition), and initial values.

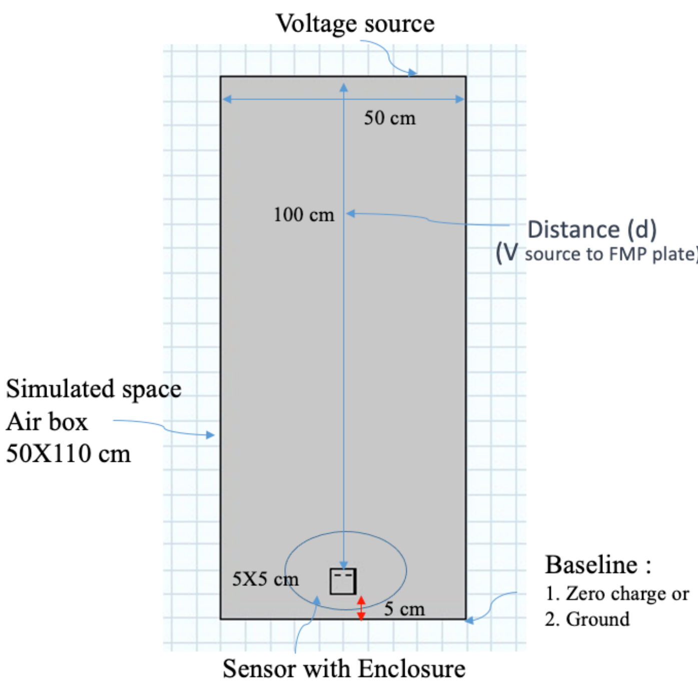

Figure 3.2: Schematic of the electric field simulation environment.

The simulation environment model included an airbox space around the enclosure. COMSOL's Electrostatics interface was included to simulate electrostatic physics that is used to compute the electric field, electric displacement field, and potential distributions in dielectrics under conditions where the electric charge distribution. When this physics interface is added, these default nodes are also added to the model builder - charge conservation, zero charge (the default boundary condition), and initial values.

When simulating an air box, having a large box can also help to create a uniform electric field environment inside the box. This, in turn, can enhance the accuracy of the simulation. The larger the box, the more uniform the electric field environment becomes, resulting in more accurate and reliable measurements. The size of the air box used in the simulation is 50 x 110 cm, which is also the maximum possible area size for taking measurements in the indoor lab setup.

Using a large box for simulating an electric field sensor under a DC power line helps to block external electromagnetic fields, create a uniform electric field environment, and enhance the accuracy of the simulation. There can be several limitations when designing a large air box in a simulation environment, including:

- *Computational resources*: Simulation of large air boxes can require significant computational power and memory, especially if high fidelity models and mesh resolutions are used. This can limit the size and complexity of the simulations that can be performed.
- *Modeling accuracy*: To accurately simulate air flow in a large air box, it is important to use appropriate turbulence models, boundary conditions, and mesh resolutions. However, these models can be computationally expensive and can also be limited in their accuracy for certain flow conditions.
- *Geometry complexity*: large air boxes may have complex geometries that can be difficult to accurately model in a simulation environment. For example, irregular shapes, sharp edges, and corners can cause flow separation, vortices, and other flow phenomena that can be challenging to capture in a simulation.

- *Uncertainty in boundary conditions*: The accuracy of simulation results is highly dependent on the accuracy of the input boundary conditions. However, it can be difficult to obtain accurate boundary conditions for large air boxes, especially in real-world applications where wind and temperature conditions can vary widely.
- *Validation and verification*: Simulation results must be validated and verified against experimental data to ensure accuracy and reliability. However, this can be challenging for large air boxes, especially if experimental data is not readily available or if the simulation results are sensitive to small changes in boundary conditions or modeling parameters. Overall, designing a large air box in a simulation environment requires careful consideration of these limitations.

Electrostatic domain is applied to simulate electrostatics. The top line of the airbox (2D) or top surface of the airbox (3D in Chapter 4) is assigned as a voltage source (power line). Side walls of the airbox and the baseline (2D) or ground surface (3D) are assigned zero charge distribution. The sensor enclosure was placed 1 m below the voltage source (power line). For the FMP at the top of the enclosure, a floating potential node is defined when modeling this metallic electrode. It applies a constant voltage V_0 on the boundary (for domain features, this is the boundary enclosing the selected domain), such that the total normal electric displacement field D equals a specific charge Q_0.

Different design cases were studies for the enclosure placement and the enclosure design itself. A parametric sweep study was performed to find the solution for each studied case. These are discussed in the sections below for each case study.

3.4 Case 1: Open enclosure, variable sensor width and depth within the enclosure

Figure 3.3 shows the 2D geometry model that was used for simulating the electric field distribution setup in the model builder for an open enclosure with no top surface. The setup includes the sensor, the supporting metal ring (electrically grounded), and the enclosure walls (1 mm thick) and bottom surface (electrically grounded). The enclosure box is in the center of the simulation space from side to side and located Y = 5 cm from the bottom of the simulation space (see Figure 3.2). This sensor enclosure is raised 5 cm above the bottom of the simulation region to add room for an environmental enclosure in later cases.

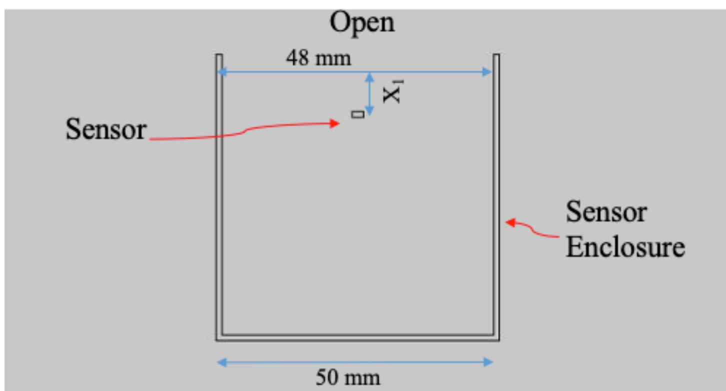

Figure 3.3: The enclosure box without roof.

The sensor (2 mm wide and 1 mm thick) is placed in the center of the enclosure between two side walls. The voltage on the voltage source at the top of the air box is 11 V. This case studied the changes to the electric field observed by the sensor, due to variation of the sensor depth (X_1) in the enclosure (X_1 was varied from 5 mm to 45 mm). The average simulated electric field at the top surface of the sensor is plotted in Figure 3.4 (black line), and the electric field at top of the airbox on the voltage source is the red line. The electric field distribution around the sensor is shown in Figure 3.5.

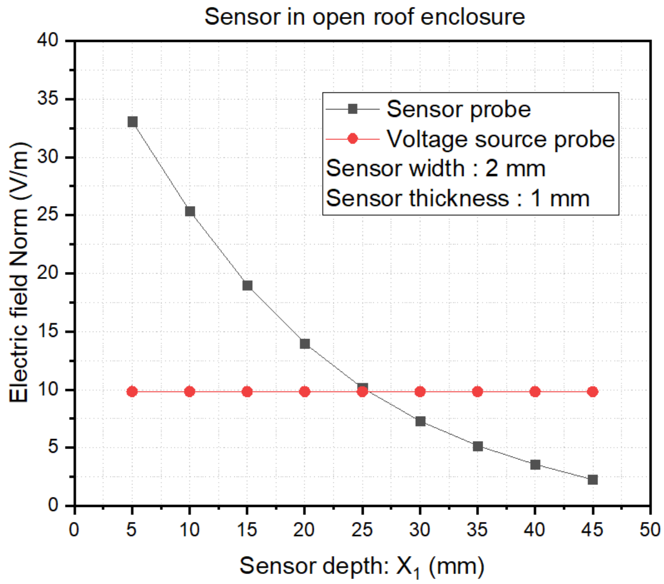

Figure 3.4: Electric field on sensor surface vs depth inside enclosure X_1.

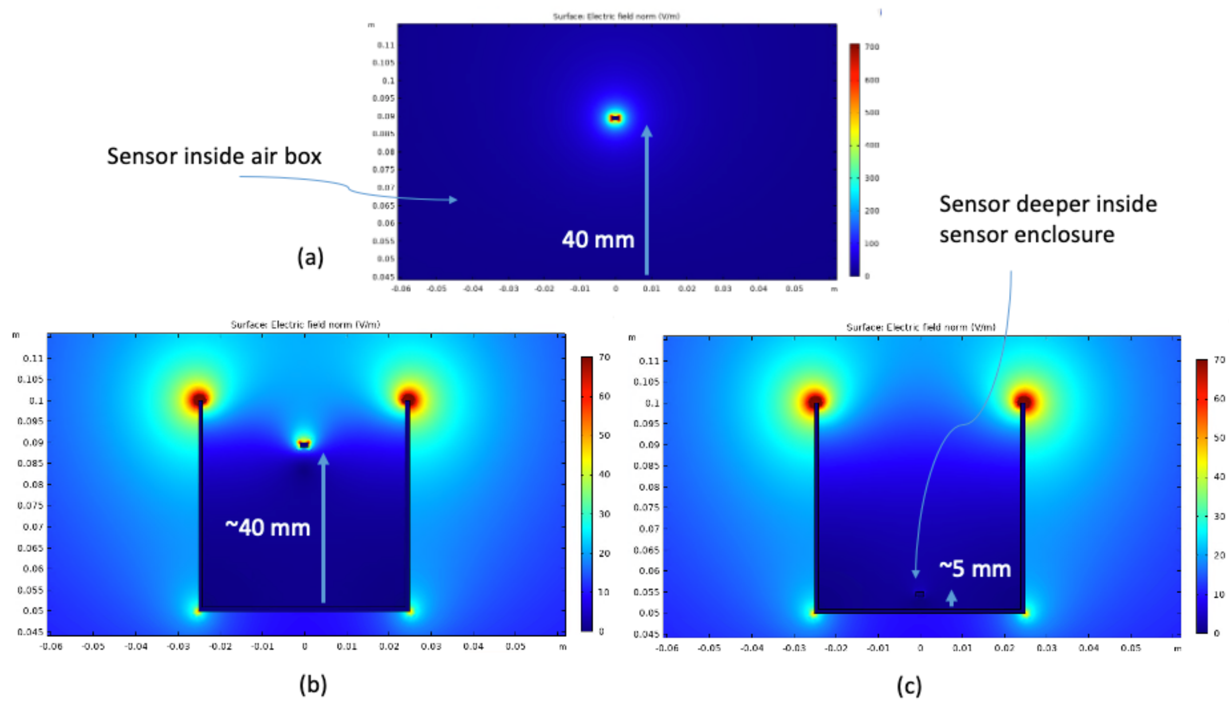

Figure 3.5: distribution around the sensor for Case 1. (a) Sensor in simulated airbox without enclosure. (b) Sensor 1 cm below top of enclosure. (c) Sensor 1 mm above bottom of enclosure.

From this study we observe that as the sensor moves vertically deeper in the enclosure, the electric field strength decreases. Therefore, sensor should be placed close to the top of the enclosure. From figure 3.5, we observe that the electric field strongest at the corners of the sensor, due to the sharp edge in the simulated geometry.

Figure 3.6 simulates the situation for the sensor width (X_{ws}) changed from 1 mm to 10 mm. In this model sensor placed 1 cm deep into enclosure. From this result, we can see that a smaller sensor will have a larger average electric field. Therefore, sensor should be made smaller if possible. The small size of the micromachined sensor is therefore beneficial for this.

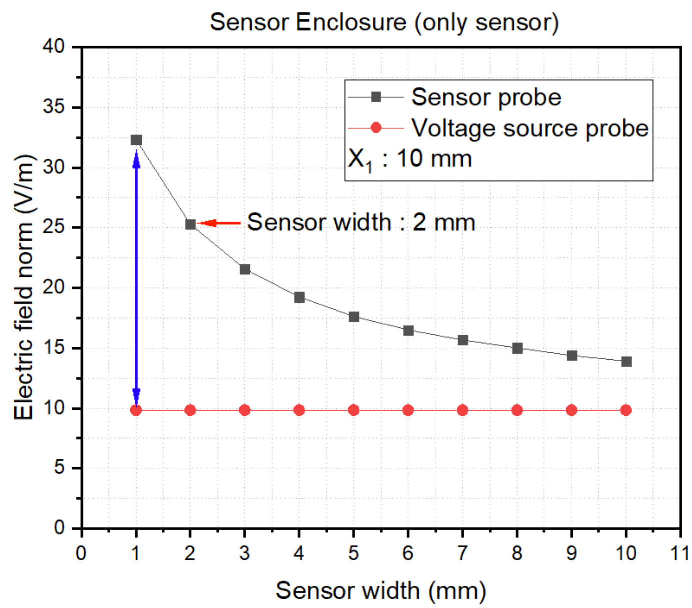

Figure 3.6: Electric field on sensor surface vs sensor width X_{ws}.

3.4.1 Effect of mesh size in simulations

Different simulations were carried out for different mesh sizes to analyze the effect on the simulated solution. The option for a physics-controlled mesh selection was used in COMSOL Multiphysics. The result of the second data point in Figure 3.6 (for 2 mm sensor width) was re-simulated for different mesh sizes ranging from extremely coarse to extremely fine and is plotted in Figure 3.7 with respect to element size mesh density. We can see that for mesh densities above "Coarser", all solutions are similar. In the plot of Figure 3.6 and all other simulation plots in this chapter, a mesh density of "Normal" was used. Figure 3.8-3.10 show the different mesh sizes and density surrounding the sensor elements.

In simulation, the mesh density refers to the number of mesh elements used to discretize the simulation domain. The mesh density can affect the accuracy and computational cost of the simulation. If the mesh density is too low, the simulation may be inaccurate due to lack of detail, and if the mesh density is too high, the simulation may become computationally expensive and take a long time to complete.

The goal is to use an appropriate mesh density that balances the accuracy and computational cost of the simulation. Using a mesh density that is too high (i.e., a fine mesh) may result in a more accurate simulation, but it can also significantly increase the computational cost and make the simulation much more time-consuming to run. On the other hand, using a mesh density that is too low (i.e., a coarse mesh) may result in a simulation that is fast to run but not very accurate.

For this reason, a normal mesh density is used in simulation, which provides a good balance between accuracy and computational cost. If it is necessary to further increase the accuracy of the simulation, a fine mesh density can be used, but this will come at the cost of increased computational cost. The appropriate mesh density for a given simulation will depend on the specific requirements of the simulation and the available computational resources.

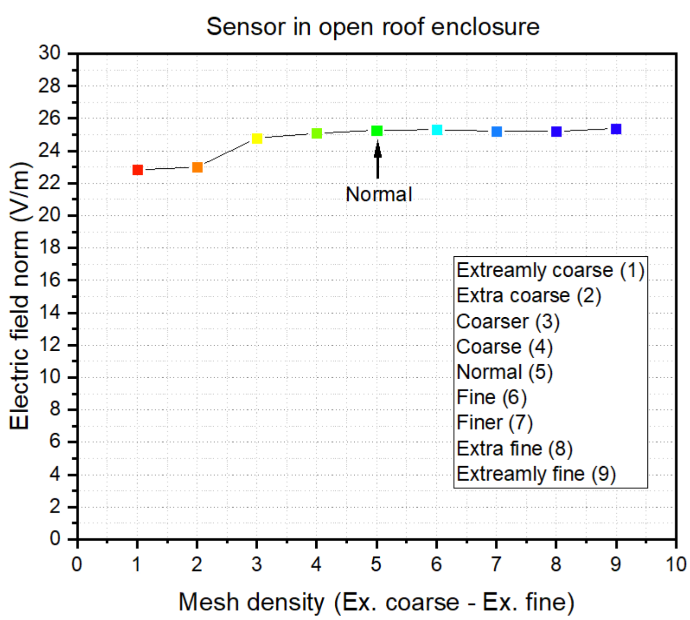

Figure 3.7: 2D electric field simulation of 2 mm wide sensor in the open enclosure of Figure 3.3 as a function of mesh density.

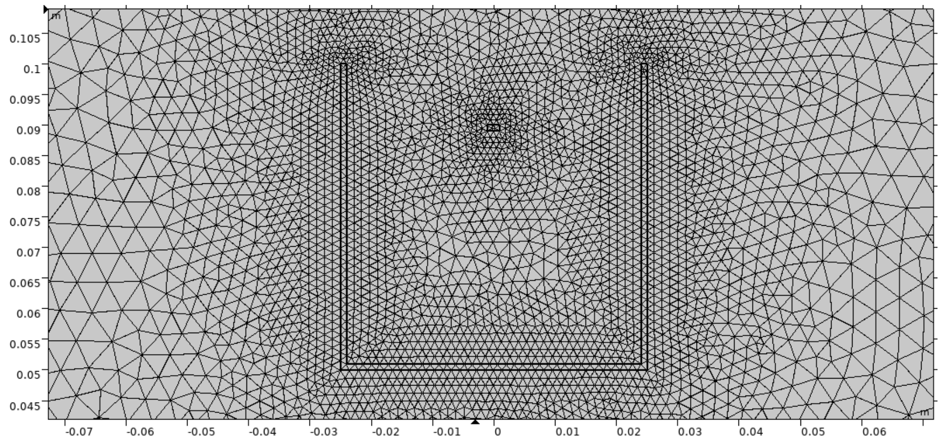

(a)

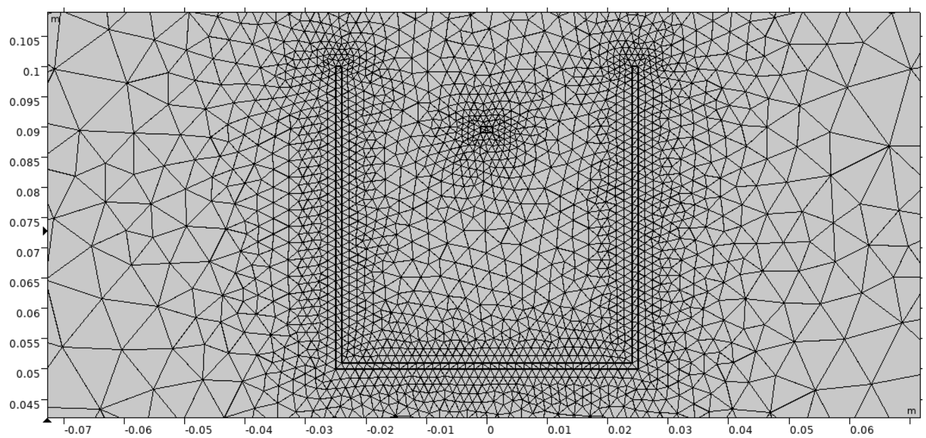

(b)

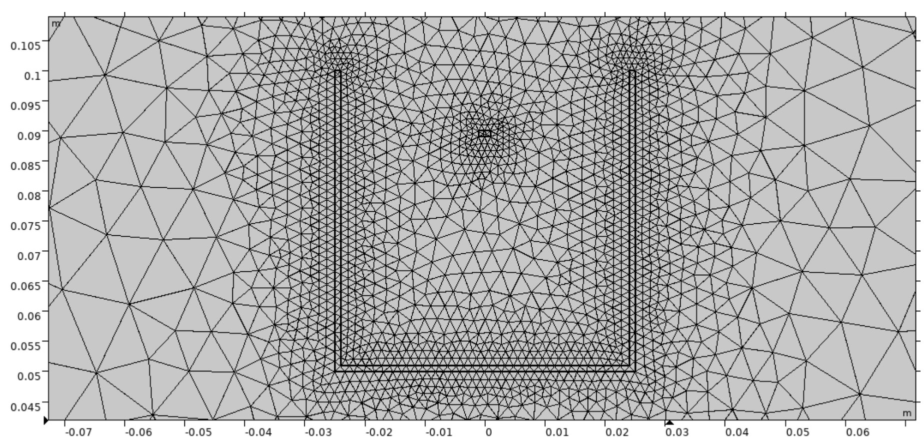

(c)

Figure 3.8: Mesh densities of (a) Extremely fine, (b) Extra fine, (c) Finer.

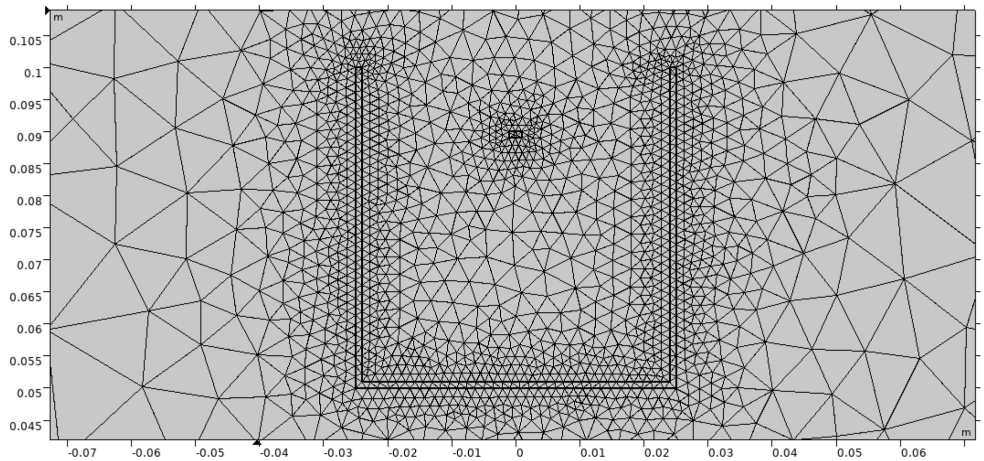

(a)

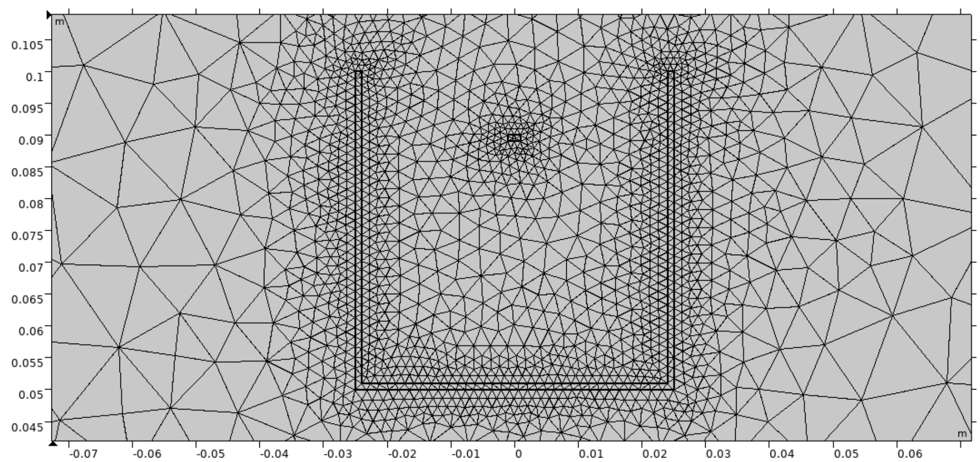

(b)

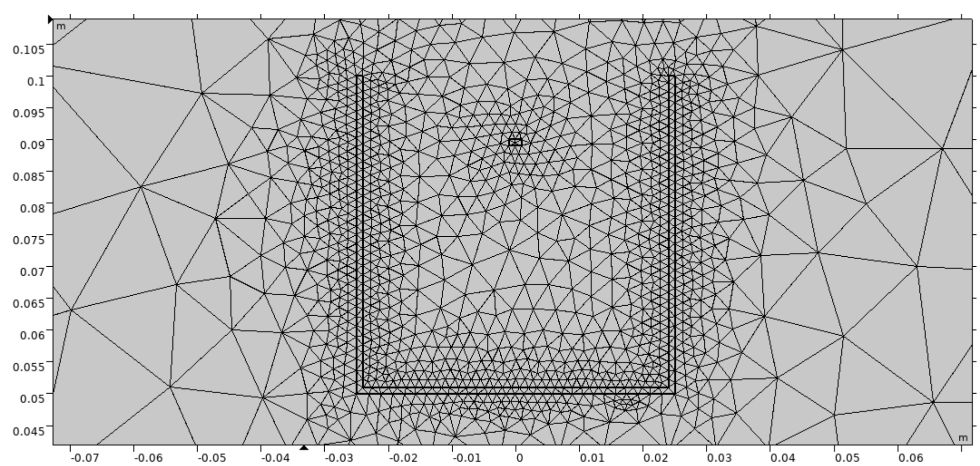

(c)

Figure 3.9: Mesh densities of (a) Fine, (b) Normal, (c) Coarse.

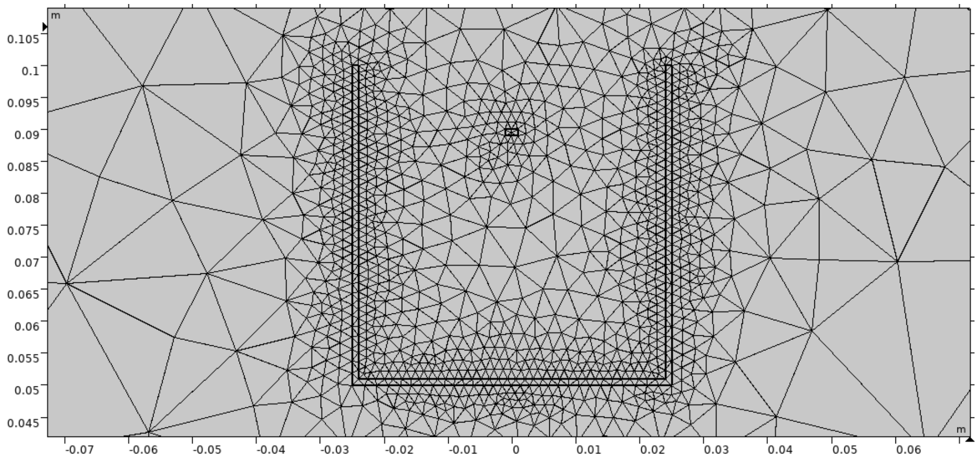

(a)

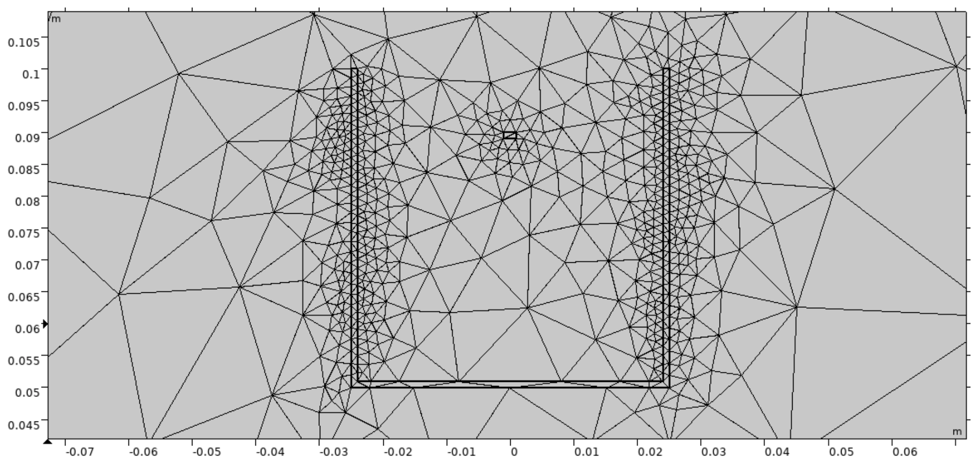

(b)

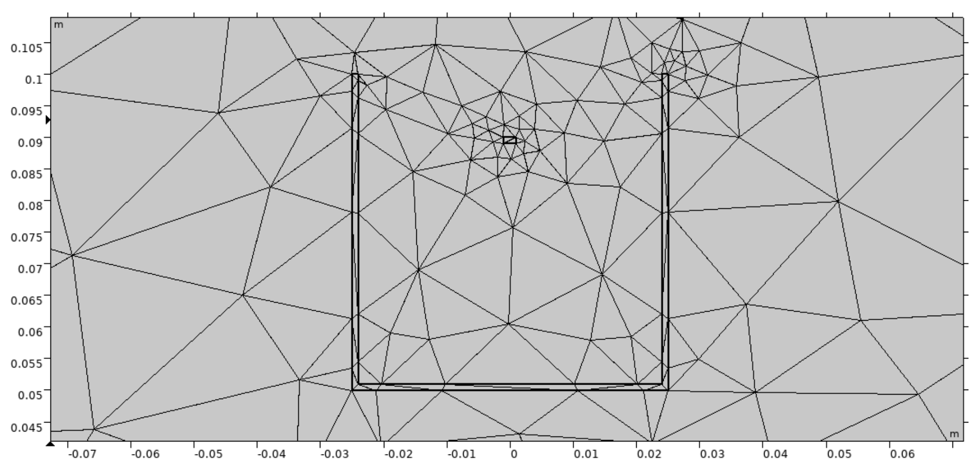

(c)

Figure 3.10: Mesh densities of (a) Coarser, (b) Extra Coarse, (c) Extremely Coarse.

3.5 Case 2: Open enclosure, sensor surrounded by metal ring

Figure 3.11 illustrates the 2D geometry model adding a grounded metal ring surrounding the sensor to the situation of Case 1. The setup includes the sensor, the supporting electrically grounded metal ring (of width X_{mr}), and the enclosure walls and bottom surface (1 mm thick and electrically grounded). The metal ring gives mechanical support for the sensor. The sensor and metal ring are both placed a distance X_1 below the enclosure opening and on the horizontal axis. The gap between sensor and the metal ring (X_g) is also studied.

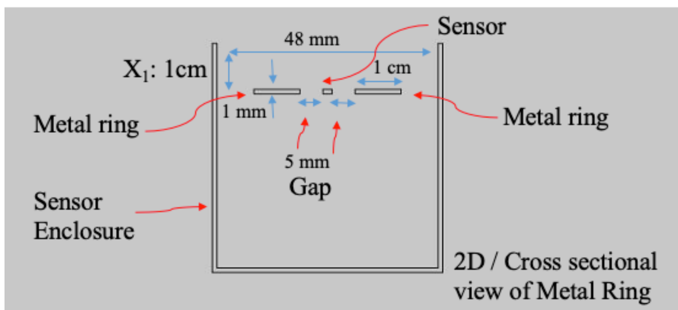

Figure 3.11: The enclosure box without roof and with metal ring.

Figure 3.12 simulates the situation for the metal ring width (X_{mr}) changed from 1 mm to 16 mm. In this model sensor placed X_1 = 1 cm deep into enclosure as Case 1. From this result, we observed that when the width of the metal ring increases the electric field decreases, but after ~ 8 mm it starts to become constant.

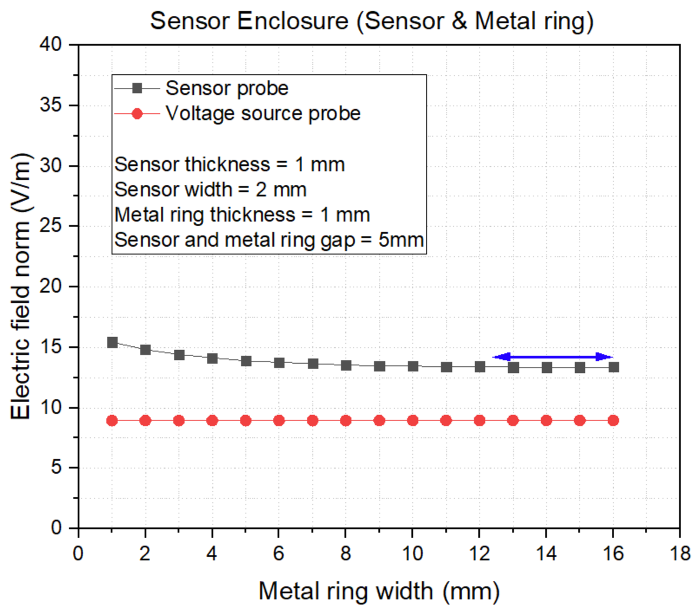

Figure 3.12: Electric field on sensor surface vs metal ring width X_{mr}.

Next, the gap spacing between the sensor and metal ring (X_g) was varied from 1 mm to 10 mm, while keeping all other parameters constant. The observed simulated result is shown in the Figure 3.13. We can see that when metal ring is closer to the sensor, the electric field decreases.

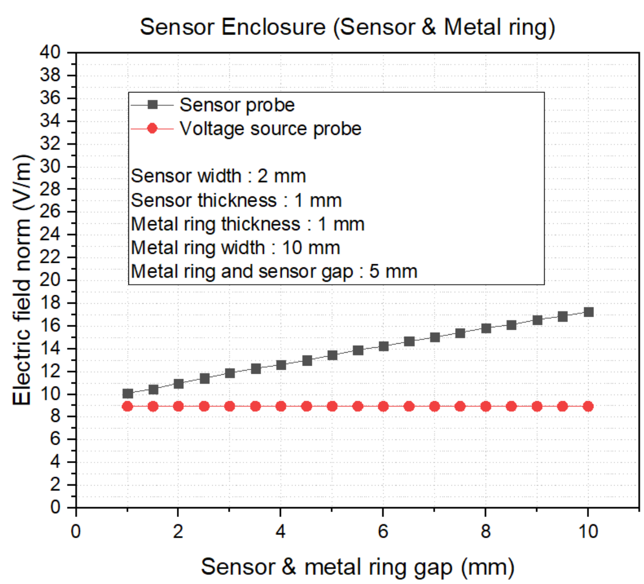

Figure 3.13: Electric field on sensor surface vs Gap between sensor & metal ring Xg.

Figure 3.14 shows the simulation for the metal ring thickness (X_{mrt}) varied from 0.5 mm to 5.5 mm while sensor located at center of metal ring thickness. The metal ring width is X_{mr} = 10 mm, and the gap between the metal ring and the sensor is X_{mr} = 5 mm. All other parameters are the same as for Case 1.

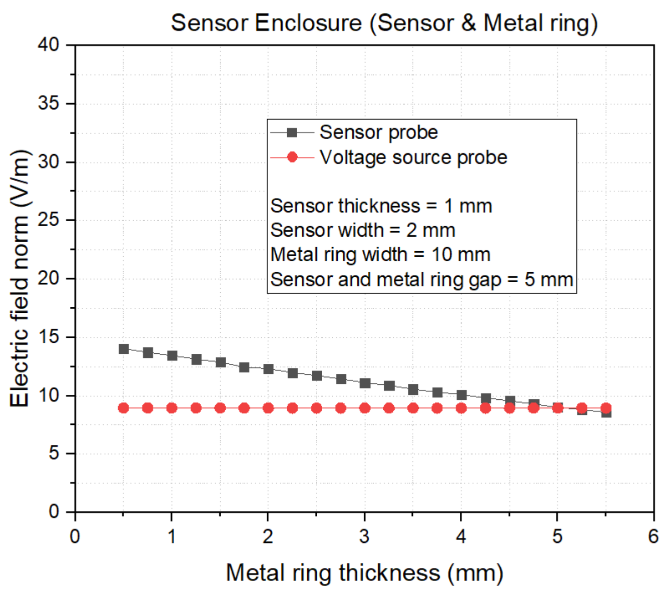

Figure 3.14: Electric field on sensor surface vs metal ring thickness X_{mrt}.

Figure 3.15 shows the electric field distribution around the metal ring and sensor. It is evident that when metal ring thickness becomes larger, the electric field strength decreases sharply on the sensor surface. Therefore, the sensor should be placed above the metal ring to ensure a stronger electric field on the sensor.

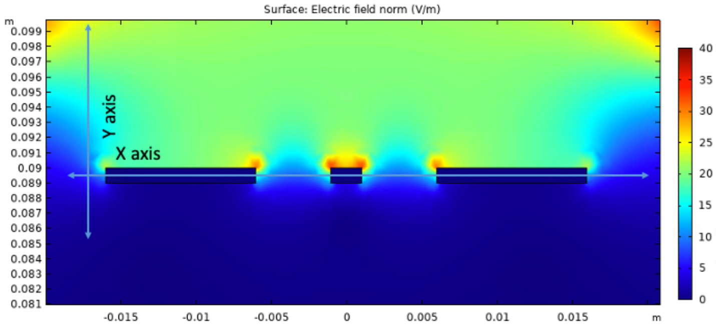

Figure 3.15: Electric field distribution around the sensor for Case 2.

3.6 Case 3: Closed enclosure with acrylic insulator supporting the floating cover

Figure 3.16 represents sensor enclosure covered with the electrically floating metal cover and supported by the acrylic insulator. Figure 3.16 on the left side shows the floating metal cover in position 1 which is in line with the acrylic support. The right side of Figure 3.16 shows the floating metal plate in position 2 located just above the acrylic insulator.

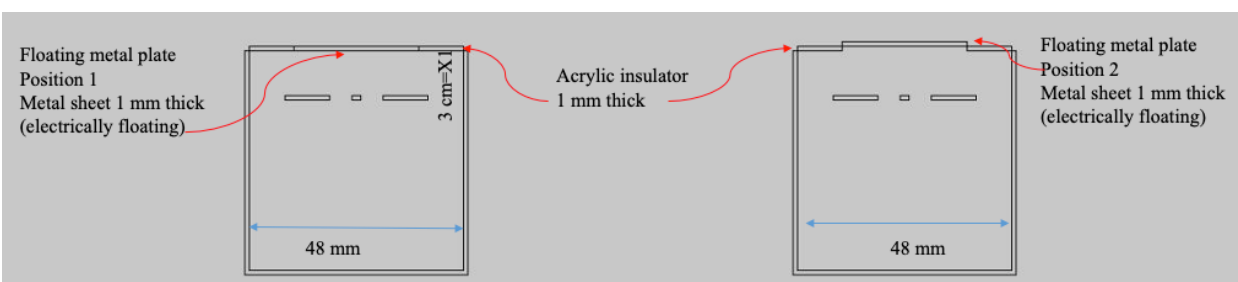

Figure 3.16: The sensor enclosure with cover.

Figure 3.17 demonstrates the impact of varying the dimension of the acrylic insulator width and the width of the floating metal cover. The acrylic width (W_{ac}) for 2D model was varied from 1 mm to 23.5 mm. The width of the floating metal plate is then 48 mm – 2(W_{ac}) in the 2D model. All other dimensions are as Case 2.

It is evident from Figure 3.17, that when the floating metal cover is in position 2, the signal is slightly higher for small sizes of the acrylic width. It can be observed that the electric field increases as the W_{ac} increases, until about $W_{ac} = 1$ cm where it becomes nearly constant. This trend is similar for positions 1 and 2.

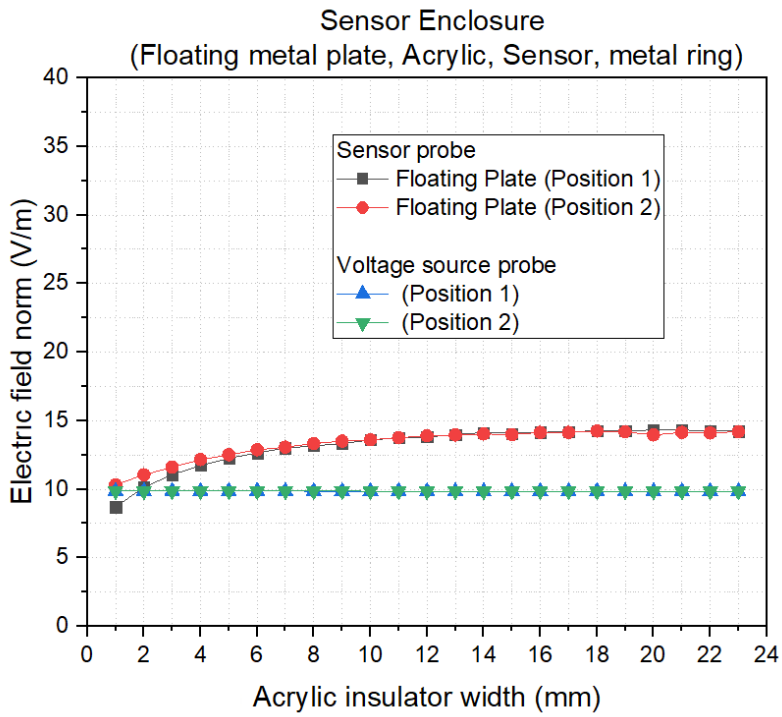

Figure 3.17: Electric field on sensor surface vs width of acrylic insulator and floating metal.

3.7 Closed enclosure, conducting pin extending downwards from cover

Figure 3.18 introduces the main structure of the sensor enclosure for this thesis. This study simulates the Case 3 situation for the enclosure that is covered with an acrylic insulator and a floating metal (Al) cover, and a conducting pin (Al) that extends from the floating metal plate towards the sensor. The sensor and conducting pin are located along the vertical center line, and all other dimensions remain the same as before. The conducting pin varies in length from 1 mm to 9 mm and has a width of 2 mm in the 2D model, giving it the same width as the sensor to ensure symmetry and uniformity. The sensor enclosure with the pin is labeled as (a), while the parameters attributed to the sensor enclosure are labeled as (b). The electric field distribution around the sensor and pin is labeled as (c), and the sensor enclosure with the environmental enclosure is labeled as (d). The electrical grounded surfaces and aluminum surfaces are indicated in (d) of Figure 3.18.

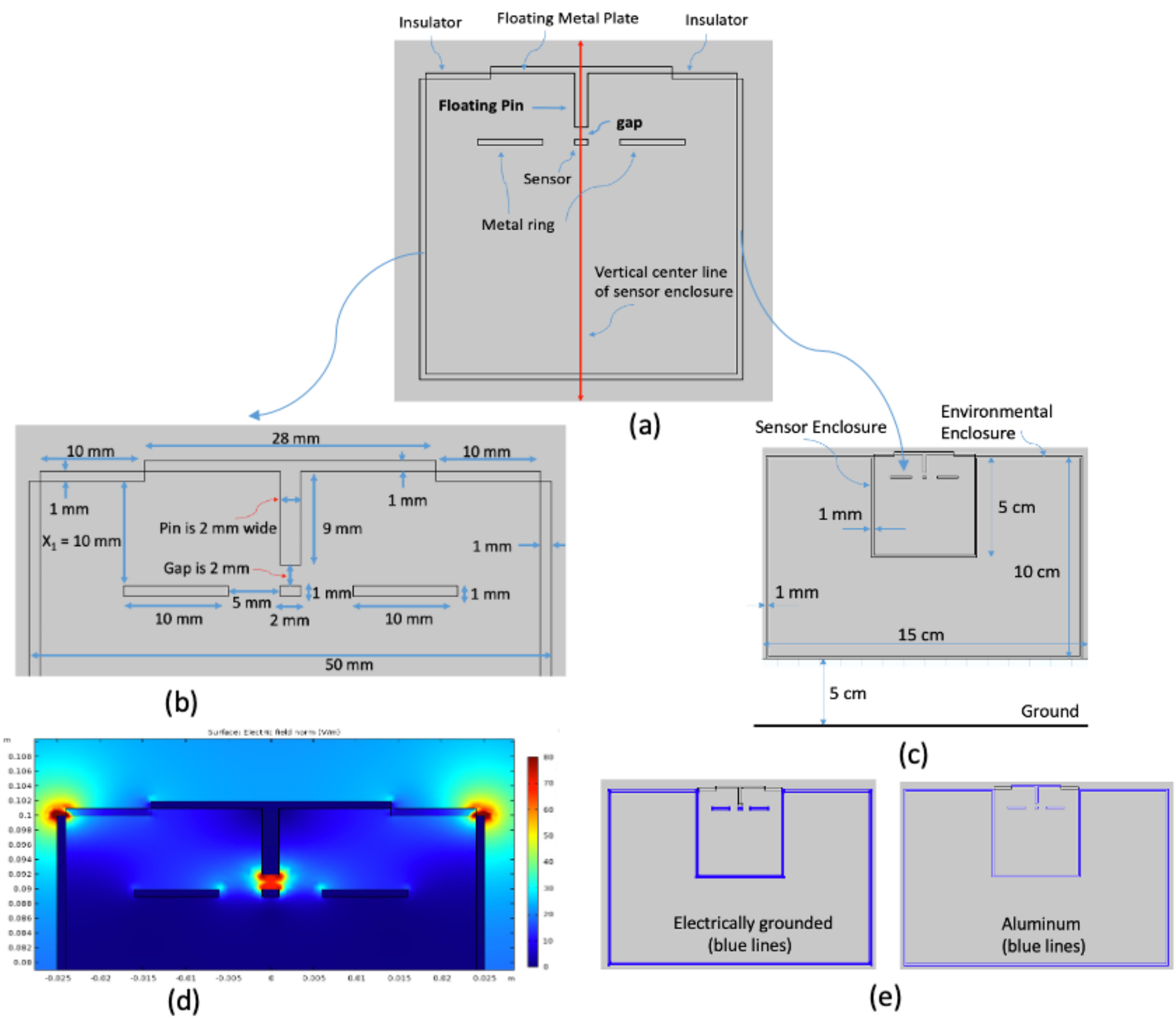

Figure 3.18: Design of sensor system. (a) The enclosure box with conducting pin. (b) Parameters for sensor enclosure. (c) Electric field distribution around the sensor and conducting pin. (d) The sensor enclosure enclosed by an outer enclosure (environmental enclosure) parameter. (e) Grounded surfaces and aluminium surfaces.

Figure 3.19 illustrates all the sensor enclosure variations that will be studied based on this design. Each of these cases are simulated separately in the air box 1 m below the voltage source / powerline. Case 4 is sensor enclosure itself with pin extending downwards. Case 5a is the sensor enclosure further enclosed in an environmental enclosure with the bottom of the enclosure 5 cm above the ground. Case 5b is sensor enclosure enclosed by an environmental enclosure sits on the ground. The Case 6 is Case 5 buried in the ground. Case 7 is Case 6 but with the acrylic insulator extended so that the floating metal plane is elevated 1 cm above the ground. Case 8 is Case 7 but with the floating metal plate formed into an angled roof shaped.

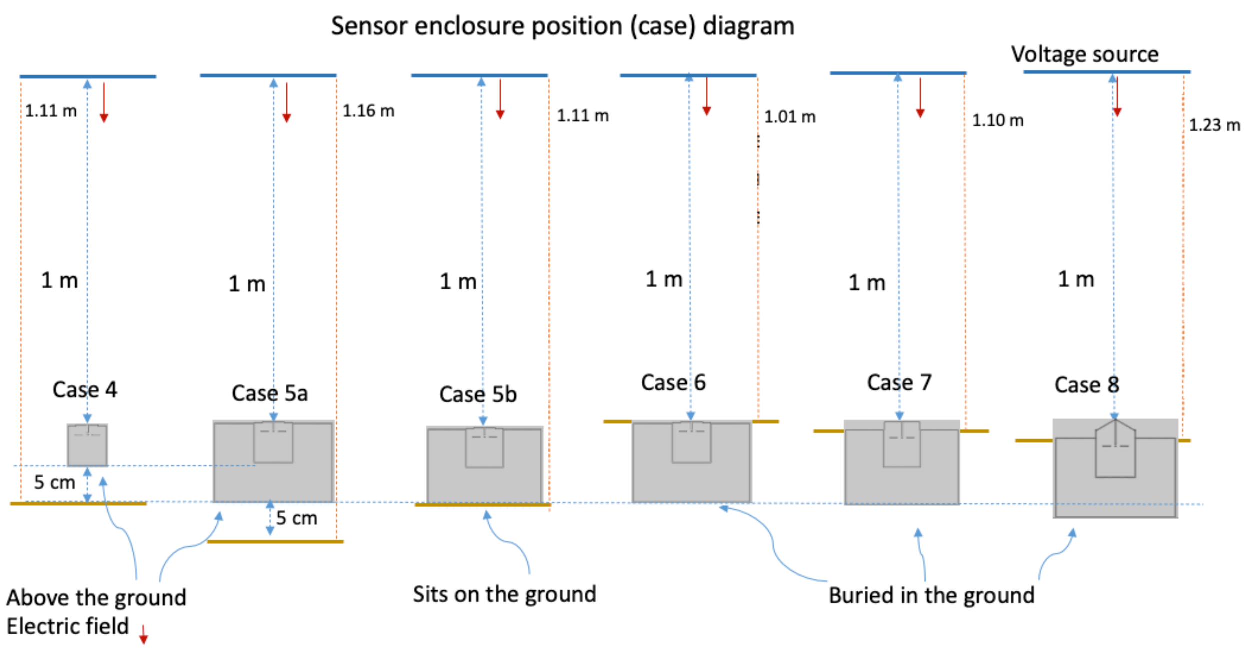

Figure 3.19: Sensor enclosure variations in the simulated environment.

The position and details of the different cases are summarized at Table 3.1.

Table 3.1: Summary of different cases studied (position and details).

Case	Detail of enclosure	Figure	Study
Case 4	Sensor enclosure itself	3.20	Case 4
Case 5a	Case 4 with outer Environmental Enclosure	3.26	Case 4 vs Case 5a
Case 5b	Case 5a sits on the ground	3.27	Case 5a vs Case 5b
Case 6	Case 5a buried in the ground	3.29	Case 5b vs Case 6
Case 7	Elevated insulator sensor enclosure with environmental enclosure buried in the ground	3.30	Case 7 $f(x_1)$ {1cm / 2cm}
Case 8	Angled elevated insulator sensor enclosure with environmental enclosure buried in the ground	3.36	Case 8 vs Case 4

3.7.1 Case 4 - Closed enclosure, conducting pin extending downwards from cover

For the basic closed enclosure situation, with the conducting pin extending downward to the sensor, Figure 3.20 demonstrates how varying the length of the conducting pin improves the electric field distribution on the sensor. In this situation, the pin length is changed from 1 mm to 9 mm keeping other dimensions as normal. This situation favorably increases electric field strength when conducting pin comes closer to the sensor.

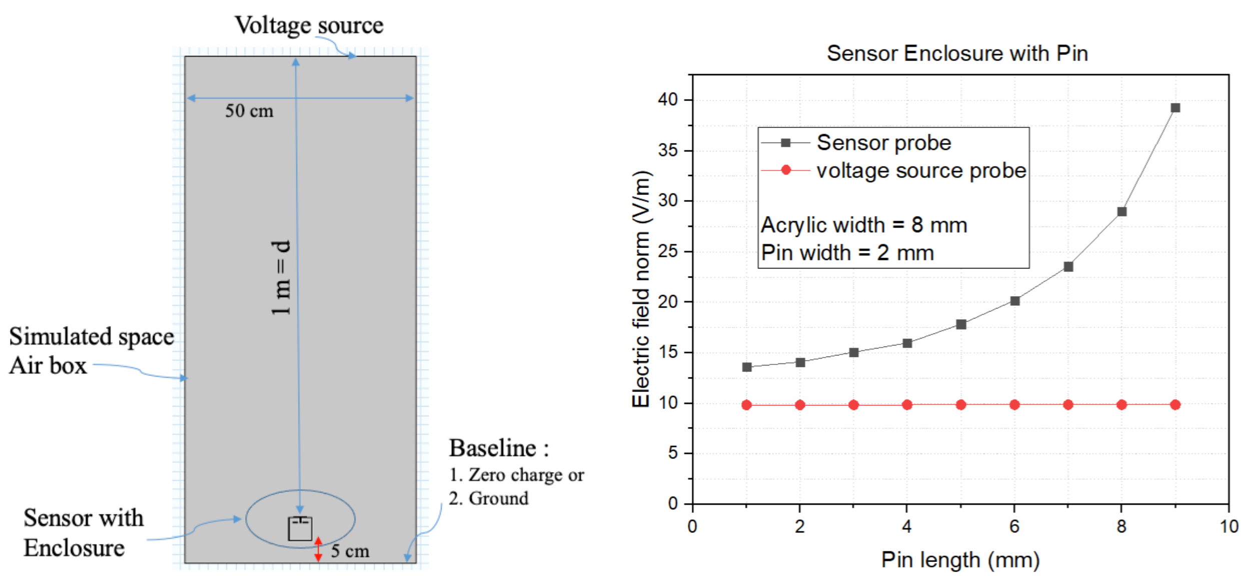

(a) (b)

Figure 3.20: (a) Schematic of the electric field simulation environment: Case 4. (b) Electric field on sensor surface vs conducting pin length.

In Figure 3.21, the 2D geometry model is presented to understand the effect of varying the acrylic width (W_{ac}) from 1 mm to 23.5 mm, with changes made to the floating plate width to be 48 mm – 2(W_{ac}). The study considered pin lengths of 5 mm, 7 mm, 8 mm, and 9 mm, with a pin width set to 2 mm and other dimensions remaining normal. A notable peak in the electric field can be observed for each situation of acrylic width. For all cases, a width of approximately 1 cm for the acrylic insulator is suitable. The highest electric field is observed for the 9 mm pin length and ~ 8 mm for the supporting acrylic insulator (32 mm floating metal plate).

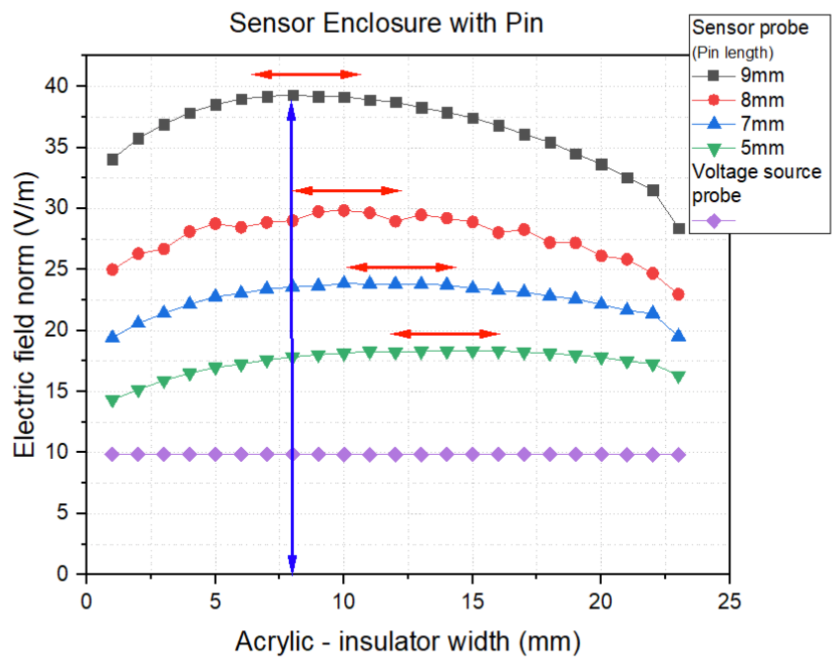

Figure 3.21: Average electric field on sensor surface vs varying the length of pin and width of acrylic insulator, and with pin width set to 2 mm.

Figure 3.22 studies the situation for changing the pin width from 1 mm to 4 mm, and for a 9 mm long pin. We can see that for 2 mm, 3 mm, and 4 mm pin widths the signals are similar to each other. Basically, pin width should be at least the width of the sensor. The peak signal is again when the acrylic width is about 8 mm wide.

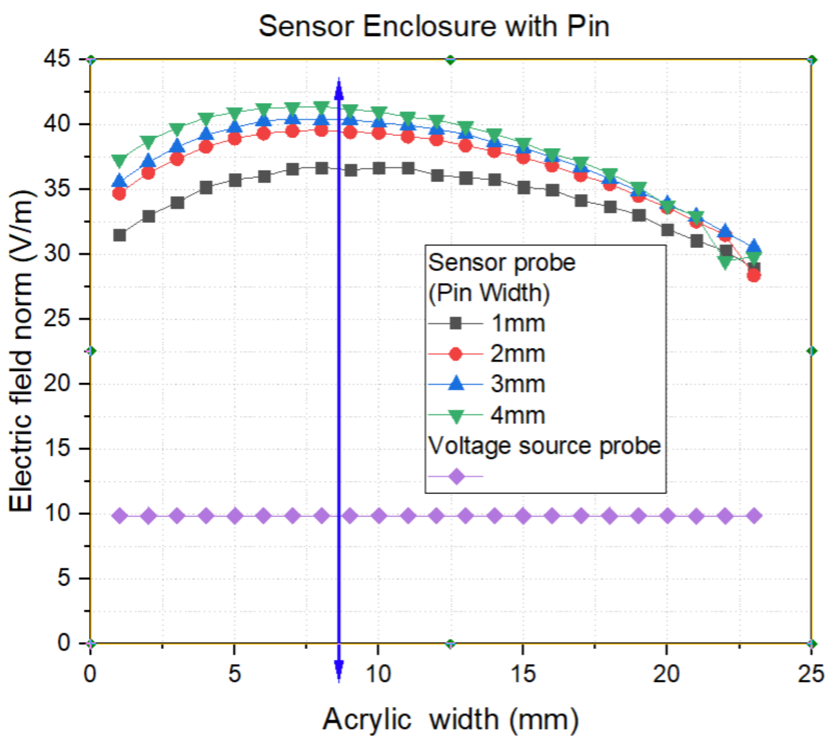

Figure 3.22: Average electric field on sensor surface vs varying the width of acrylic insulator and width of pin, with pin length set to 9 mm.

Figure 3.23 shows another simulation for Case 4, now moving the sensor deeper in the box, and with an accordingly longer pin. The acrylic width (W_{ac}) is 8 mm, and floating plate width is 32 mm. Two situations are explored. First, the sensor is located a distance X_1 = 1 cm, and pin length of 1 mm - 9 mm is studied. Second, the sensor is located a distance X_1 = 2 cm, and pin length of 1 mm - 19 mm is studied. All other dimensions are as before, and with the pin width of 2 mm. We observe that the average electric field is similar for both situations when the pin extends to a similar distance from the sensor. Therefore, this shows that the pin can compensate for a sensor located deeper in the enclosure box.

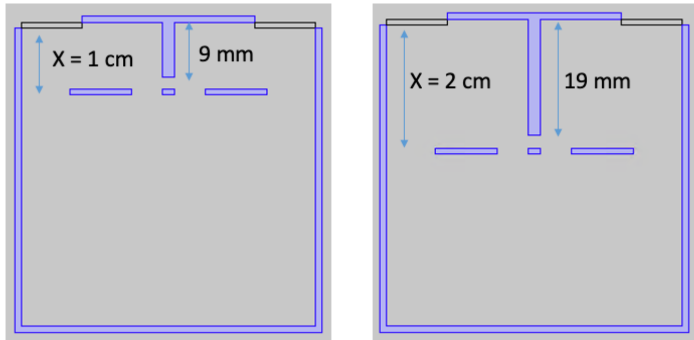

(a)

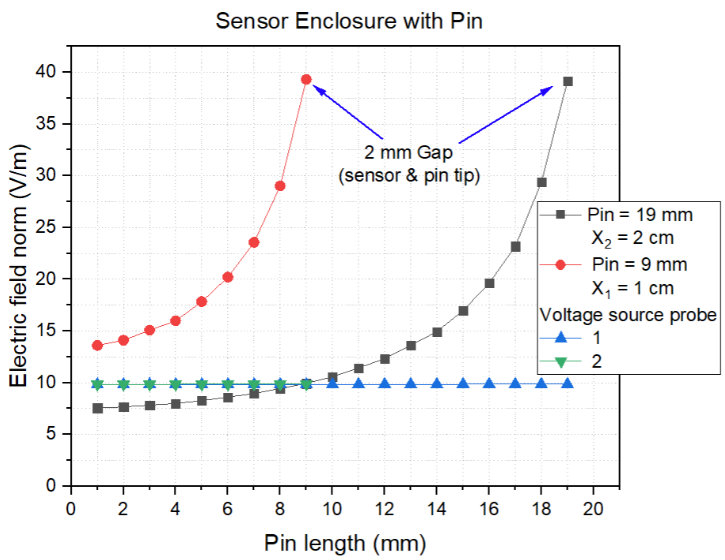

(b)

Figure 3.23: Study of sensor location in the enclosure and extending pin. (a) Simulation schematic. (b) Average electric field on the sensor surface vs varying sensor depth in the box and with pin length.

3.7.2 Case 5: Sensor enclosure further enclosed in an outer environmental enclosure

Case 5 illustrates the 2D geometry for the sensor enclosure (Case 4) placed in another outer enclosure (Case 5), acting as an environmental enclosure. It is expected that in outdoor applications, a secondary weatherproof environmental enclosure would be used. This outer enclosure has length of 15 cm, and the sensor enclosure (Case 4 design) is placed in the middle of the outer enclosure as shown in Figure 3.24. Case 5a is the situation with the outer enclosure located 5 cm above the ground. Case 5b is with the enclosure sitting on the ground. The outer enclosure along with the sensor enclosure are electrically grounded. The outer enclosure walls are made of Al and 1 mm thick.

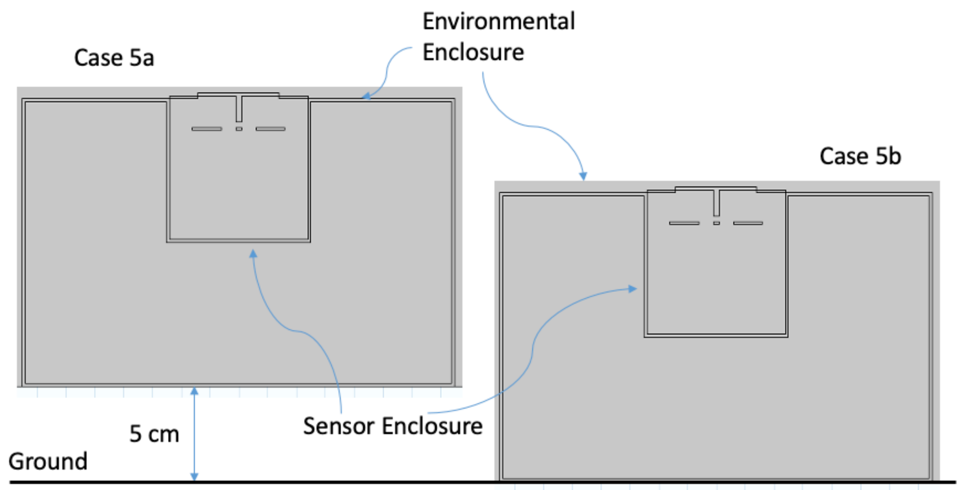

Figure 3.24: The sensor enclosure enclosed by an outer enclosure (environmental enclosure).

Figure 3.25 illustrates the simulation models used to consider this case. Figure 3.25a shows the situation with the outer environmental enclosure raised 5 cm above the ground (Case 5a). Figure 3.25b shows the situation with the environmental enclosure sitting on the ground (Case 5b). In the situation of Case 5b, the inner sensor enclosure is located at the same height in the simulation space, as in Cases 1-4.

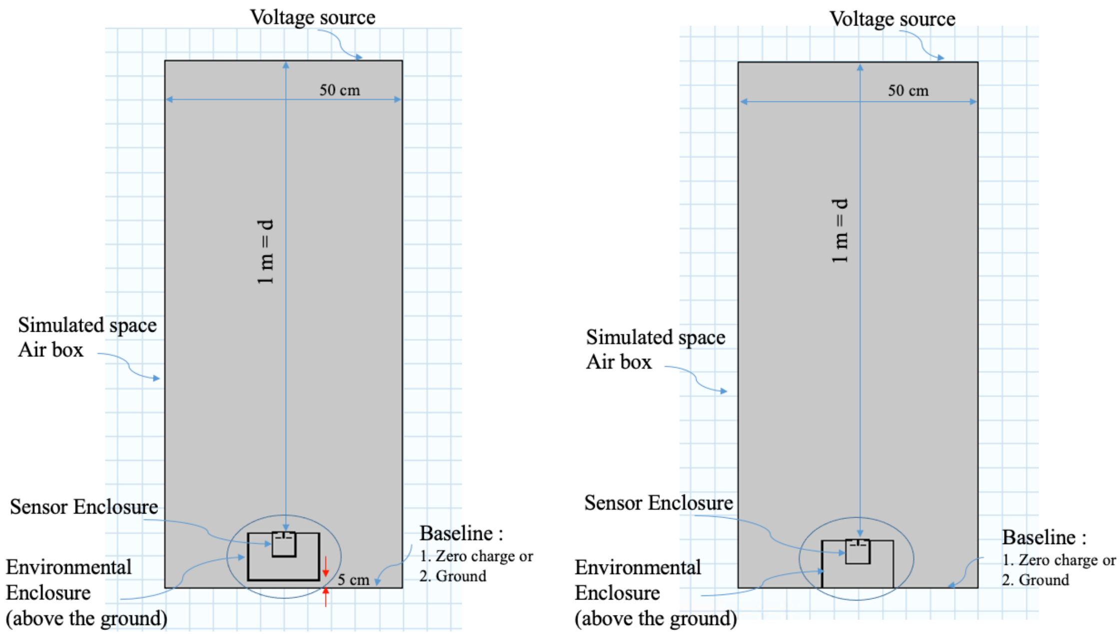

(a) (b)

Figure 3.25: Schematic of the electric field simulation environment. (a) Case 5a with outer enclosure raised 5 cm above the ground. (b) Case 5b with outer environmental enclosure sitting on the ground.

Figure 3.26 shows the effect of the outer environmental enclosure. Figure 3.26(a) is the result for Case 4 (Figure 3.19). Figure 3.26(b) is Case 5a showing the effect of the outer environmental enclosure around the sensor box. Simulated results show that having the outer enclosure, reduces the electric field to about 1/2 of the sensor enclosure alone (Case 4).

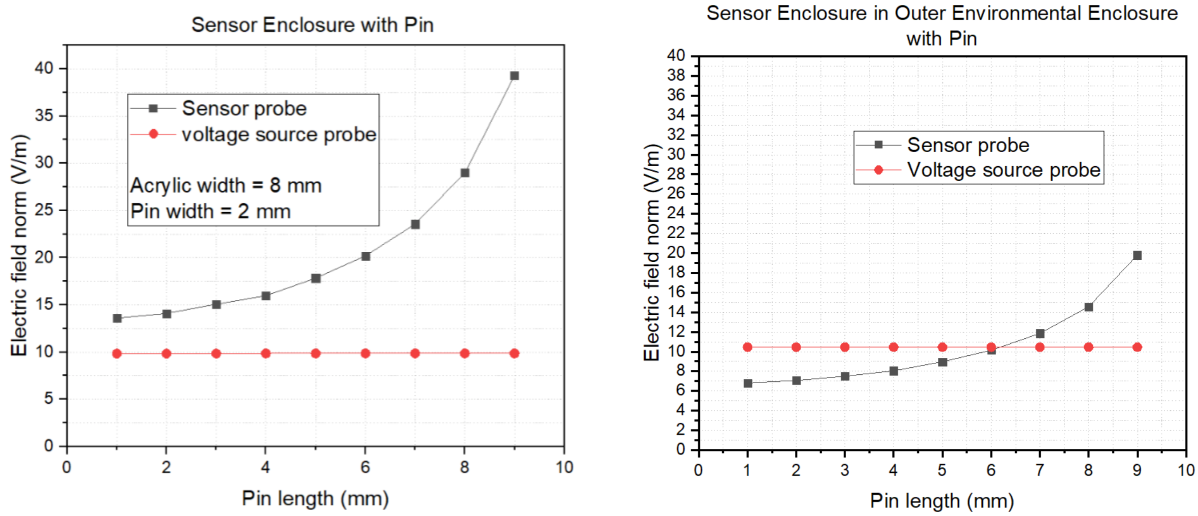

(a) (b)

Figure 3.26: Electric field on the sensor surface vs pin length. (a) Situation without the outer enclosure (Case 4). (b) Situation with the outer environmental enclosure (Case 5a) and elevated 5 cm above the ground.

Figure 3.27 compares the effect of the outer environmental enclosure sitting on the ground (Case 5b) vs elevated 5 cm above the ground (Case 5a). We can see that elevating the enclosure reduced the measured electric field signal by about 10%.

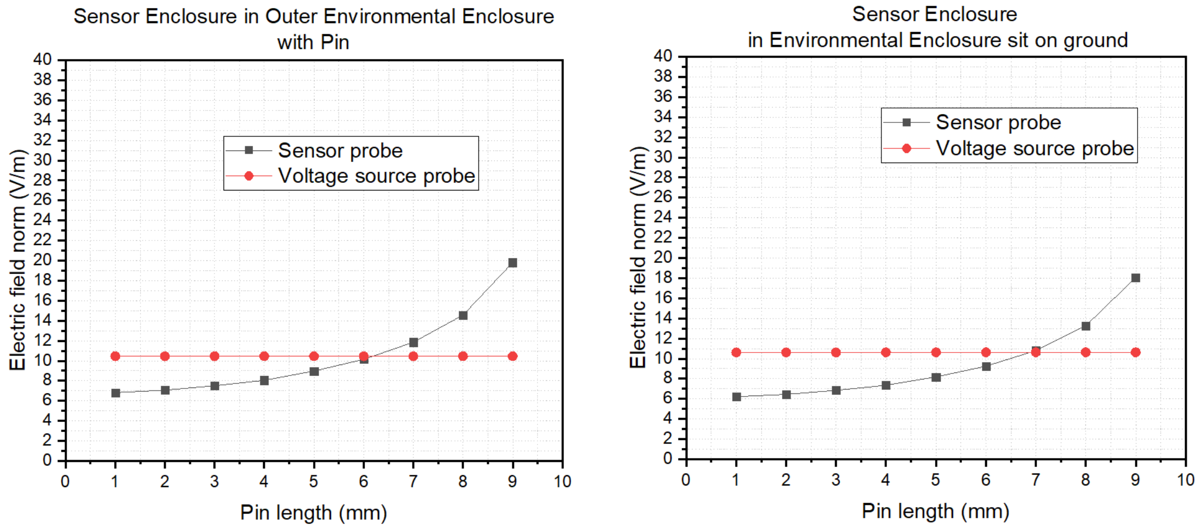

(a) (b)

Figure 3.27: Electric field on the sensor surface inside environmental enclosure for (a) elevated 5 cm above the ground (Case 5a), and (b) sitting on the ground (Case 5b).

3.7.3 Case 6: Outer enclosure buried in the ground

Figure 3.28 illustrates the schematic view of two situations, first with the outer enclosure sitting on the ground (Case 5b), and then buried in the ground (Case 6). All the blue lines represent electrically grounded surfaces. Figure 3.26 shows that the electric field signal is reduced about 20-25% for the sensor on the surface vs buried in the ground.

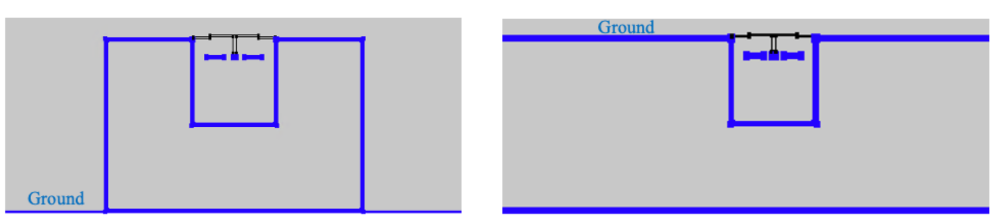

Figure 3.28: The enclosure box in the outer box on the ground (Case 5b) and buried in the ground (Case 6).

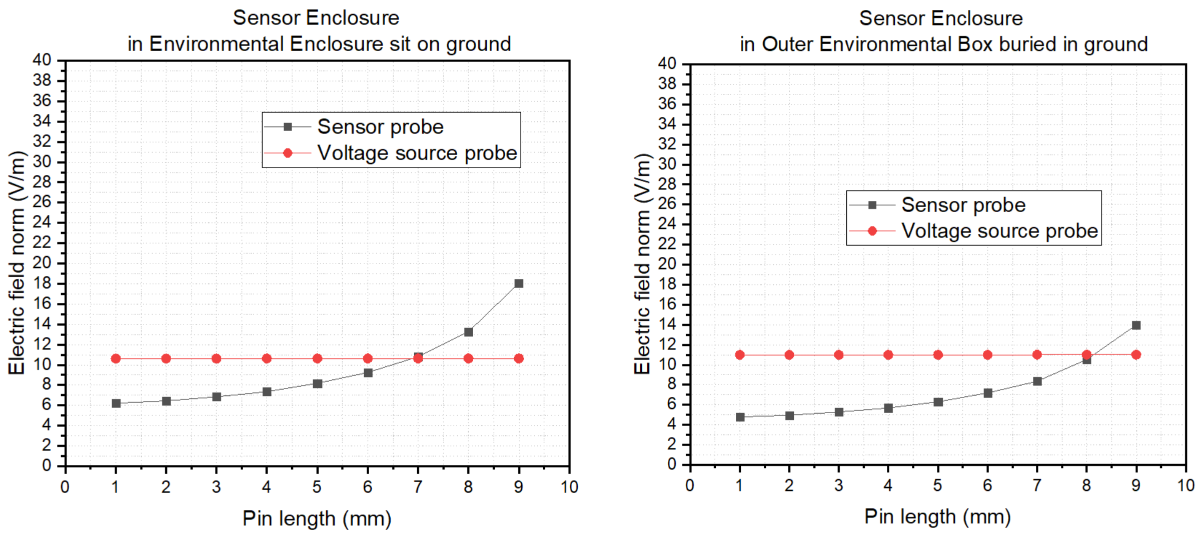

(a) (b)

Figure 3.29: Electric field for the sensor environmental enclosure for (a) Case 5b sitting on the ground, and (b) Case 6 buried in the ground.

3.7.4 Case 7: Elevated metal floating plate

This situation involves raising the metal floating plate above the sensor enclosure. The goal is to investigate if this better interacts the with the electric field. The simulation model included an airbox space around the sensor enclosure box as shown in Figure 3.30. The distance from the voltage source to floating metal plate and the ground surface is 1 m.

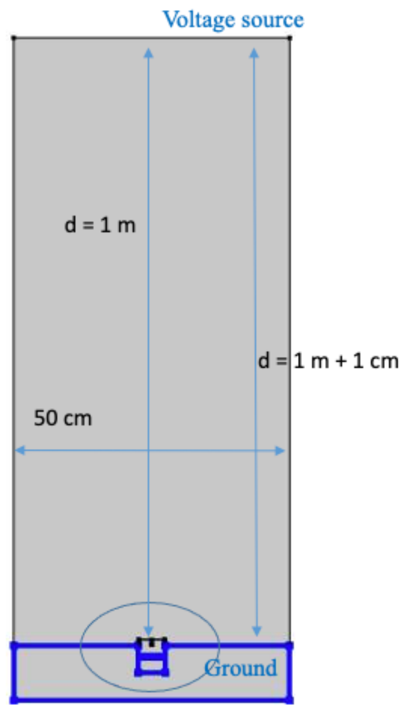

Figure 3.30: Schematic of the Electric Field Simulation Environment: Airbox 2 (elevated floating metal plate).

Figures 3.31 represent the model schematics for the simulations of Case 7. The floating plate is elevated and is the full size of the enclosure opening less the acrylic support on the edge (46 mm wide), replacing the area previously covered by the acrylic insulator. The floating metal plate is supported by a 1 mm thick and 1 cm long acrylic insulator at its edges. Figure 3.31(a) shows the case with the sensor a distance of X_1 = 1 cm below the ground surface, and Figure 3.31(b) shows the case with the sensor a distance of X_1 = 2 cm below the ground surface. The pin length is 19 mm in Figure 3.31(a) and 29 mm in Figure 3.32(b), so that in either case, the pin end 1 mm above the sensor as before. Figure 3.32 shows electric field distribution around the sensor for the situation of Figure 3.31(a).

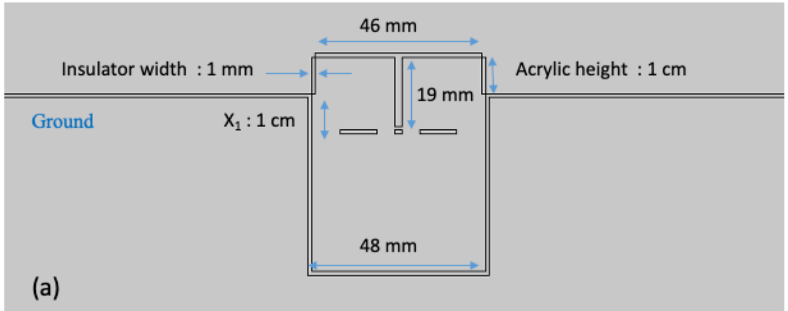

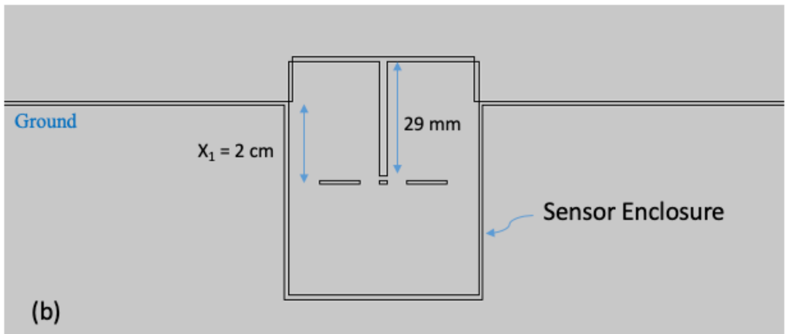

Figure 3.31: The enclosure box with elevated floating metal plate. (a) Sensor located 1 cm below the ground. (b) Sensor located 2 cm below the ground.

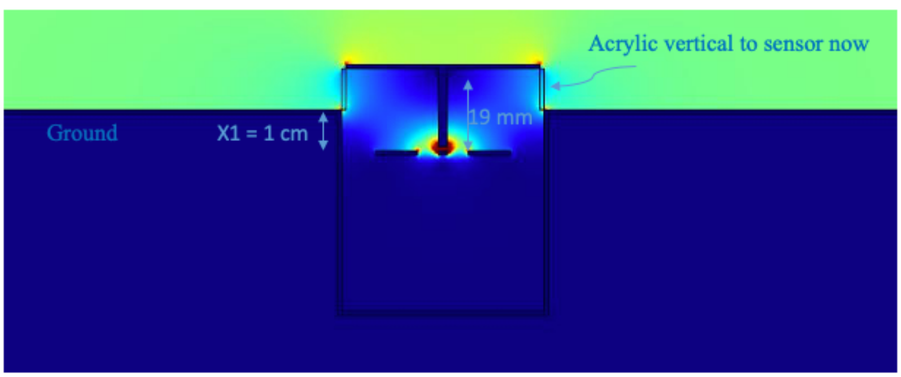

Figure 3.32: Electric field distribution around the sensor for figure 3.31(a).

Figure 3.33 is the graph for electric field on the sensor surface for Figure 3.31, as function of pin length. The blue line illustrations the result for Case 6 with the outer box buried in ground, and the green line for the sensor moved 1 cm deeper in box. The red line shows the result for Figure 3.31(a), with 19 mm pin length, with the sensor moved downward 1 cm below the ground level, so that distance from power to floating plate is common to earlier cases (in the air box simulations with the sensor located d = 1.01 m below the voltage source). Finally, the black line is for Figure 3.31(b) with the sensor 2 cm below ground level.

We can see from Figure 3.33 that the outcome of elevating the floating metal plate 1 cm increases the signal ~ 2.5x (red line vs. blue line).

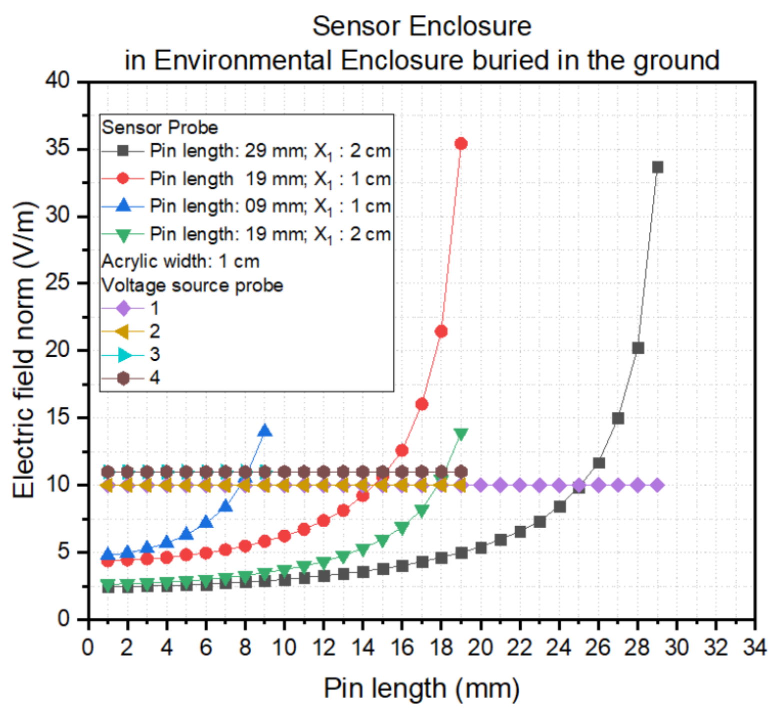

Figure 3.33: Electric field on the sensor surface vs pin length change.

3.8 Case 8: Sensor enclosure with various angled roof shape floating metal plate

These case studies explore the effect of having a sloped floating metal cover (angled roof shaped) to reduce any precipitation like snow or water collecting on the floating metal plate. This would be a more suitable in an outdoor environmental usage. Figure 3.34(a) shows detail the enclosure variations studied for Case 8, and Figure 3.34(b) shows the schematic of the electric field simulation environment. Figure 3.35 show a design with the pin extending downward towards the sensor a distance of 31 mm, and the distance between sensor and pin tip is 1.9 mm.

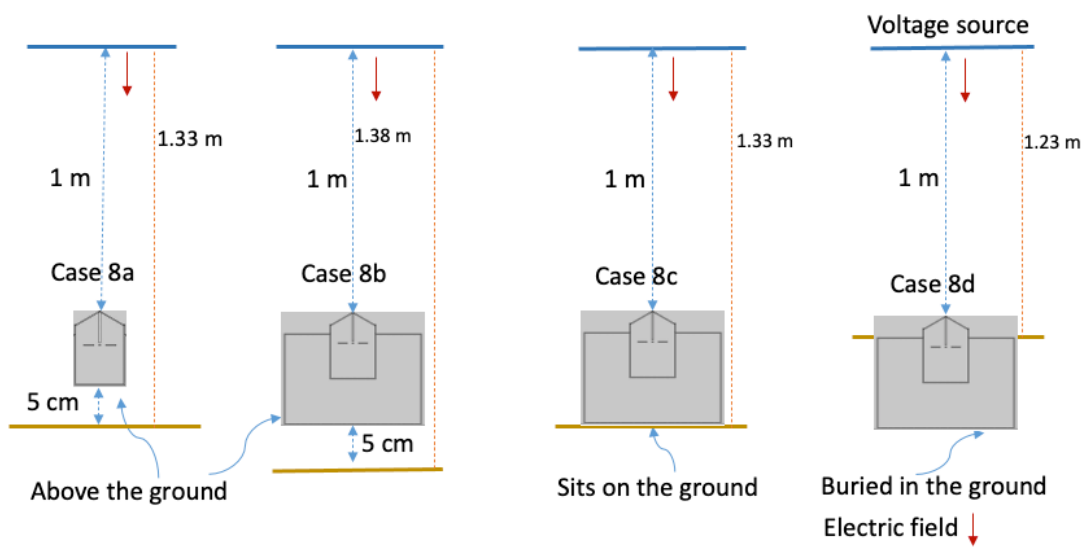

Figure 3.34: Variations of Case 8 studied.

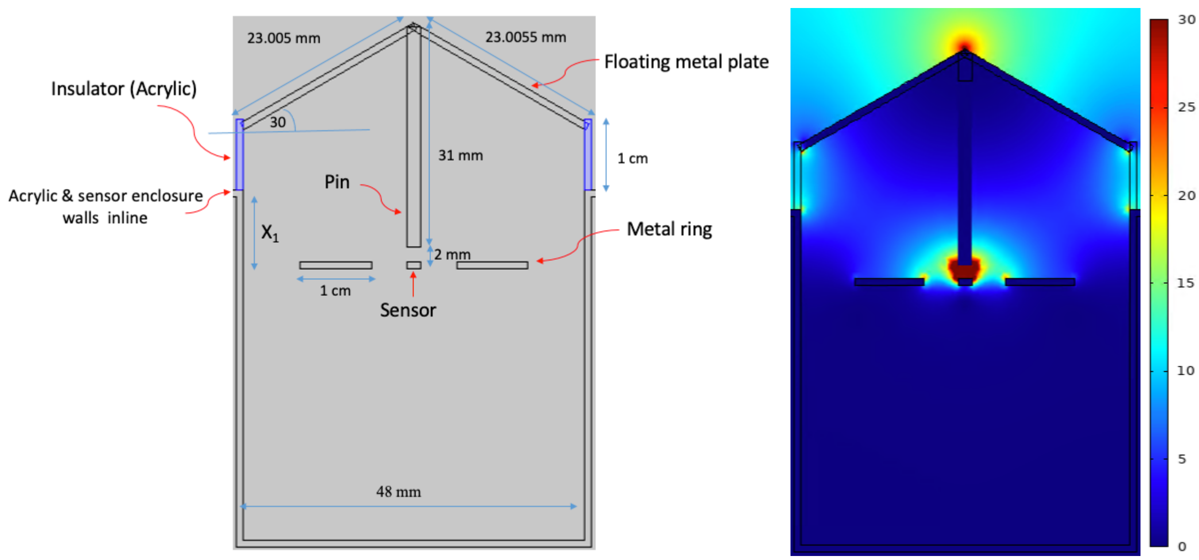

(a) (b)

Figure 3.35: Roof shape sensor enclosure. (a) Illustration of the design schematic. (b) Illustration of the electric field distribution.

Table 2 provides the details of the elevated insulator (acrylic) for this angled roof shaped floating metal plate situation. All these situations have the air box located a fixed distance of 1 m below the voltage source.

Table 3.2: Summary of different cases studied for Case 8 (position and details).

Case 8 detail of enclosure	Figure	Study
Case 8a	3.36	Case 8a vs Case 4
Case 8b	3.38	Case 8a vs Case 8b
Case 8c	3.39	Case 8b vs Case 8c
Case 8d	3.40	Case 8c vs Case 8d
Case 7 vs Angled elevated sensor enclosure with environmental enclosure buried in the ground	3.42	Case 7 vs Case 8d (adjusted height to match Case 7)

3.8.1 Case 8a: Sensor enclosure with angled roof shape floating metal plate

Figure 3.36 compares Case 8a with Case 4 as a function of varying the length of the conducting pin. We observe that having an angled floating plate extending into the airbox above the enclosure approximately doubled the electric field strength on the sensor.

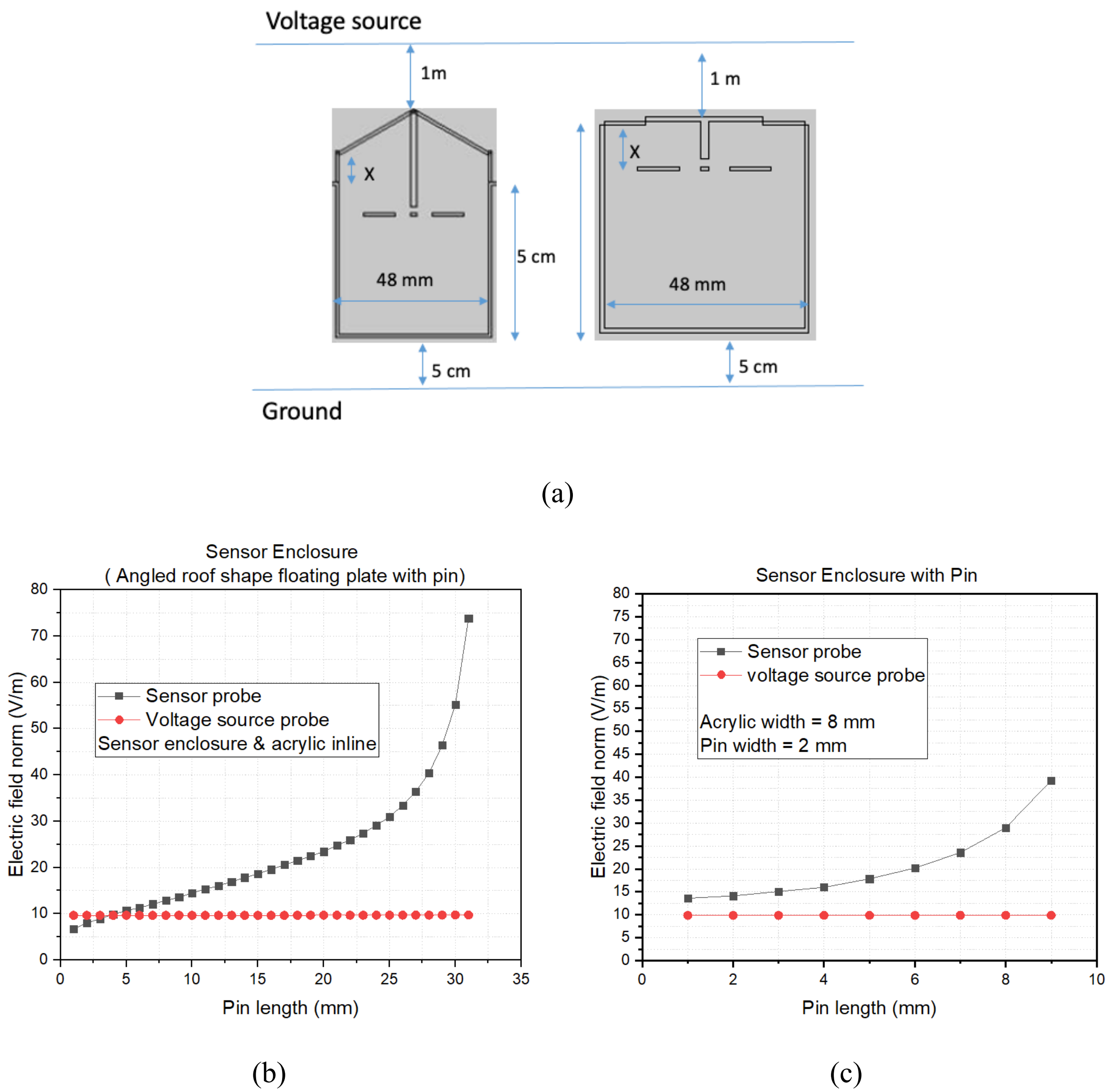

Figure 3.36: (a) Case 8a vs Case 4 schematic illustration (not to scale). (b) Electric field on sensor vs pin length for Case 8a. (c) Electric field on sensor vs pin length for Case 4.

3.8.2 Case 8b: Sensor with angled roof shape in environmental enclosure

Figure 3.37(a) shows a schematic illustration of Case 8b. Figure 3.37(b) shows the electrically grounded surfaces. Figure 3.38 plots the simulated electric field on the sensor as a function of pin length and compares to the situation without the environmental enclosure. We see that having the outer environmental enclosure reduces electric field to about 1/2. This result is consistent with the result of Case 5, which studied the effect of the outer environmental enclosure.

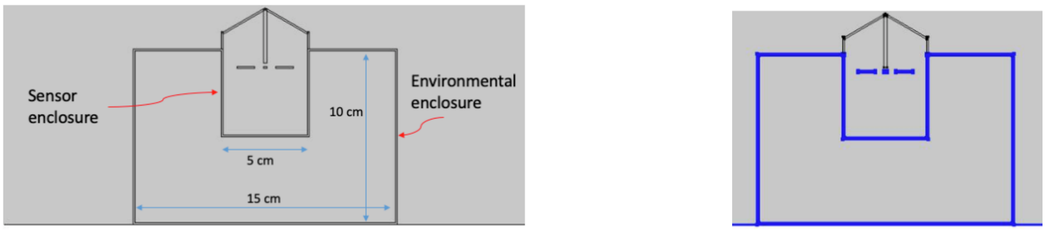

(a) (b)

Figure 3.37: Angled roof shape sensor enclosure used with the outer environmental enclosure. (a) Schematic geometry illustration. (b) Electrically grounded surfaces.

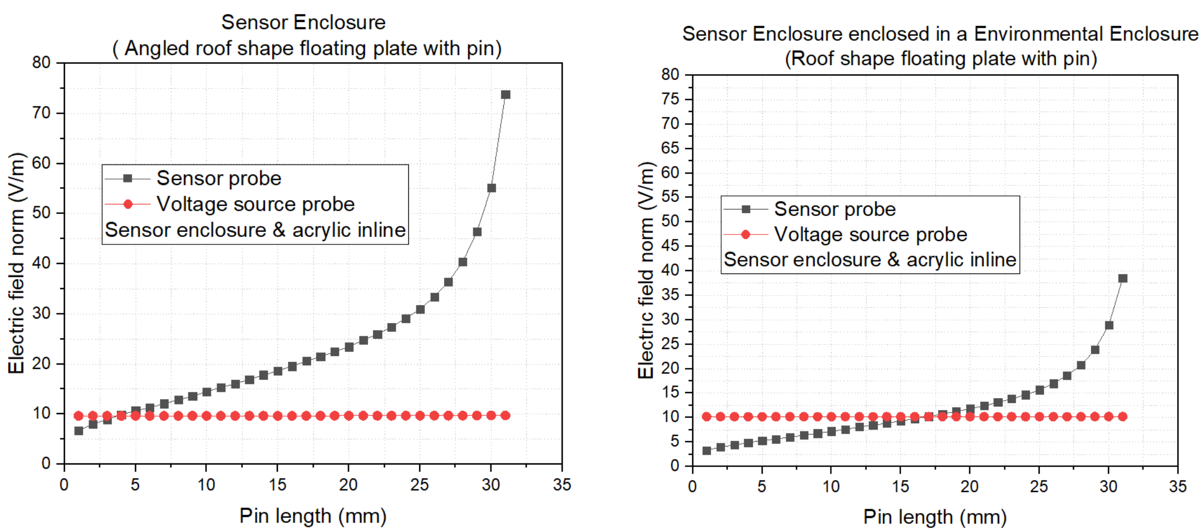

(a) (b)

Figure 3.38: Electric field on sensor vs pin length change. (a) Case 8a for the angled roof shape sensor enclosure. (b) Case 8b of angled roof shape with environmental enclosure of Case 5.

3.8.3 Case 8c: Sensor with angled roof in environmental enclosure on the ground.

Figure 3.39 compares Cases 8b and 8c. In both designs, the sensor distance to the voltage source is constant. The graph indicates that with the outer box sitting on the ground (Case 8c), the measured electric field is slightly elevated about 10%.

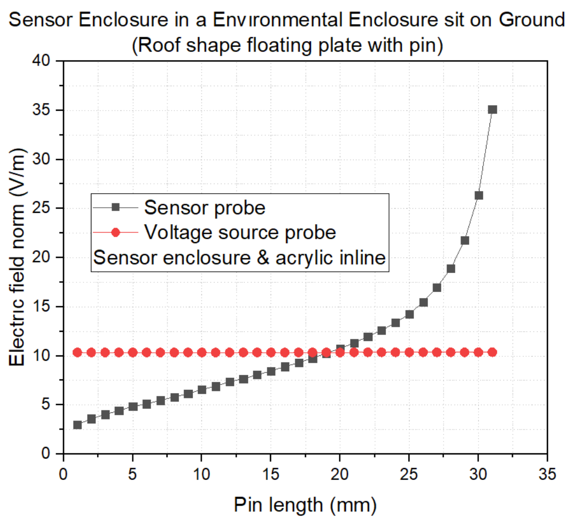

(a)

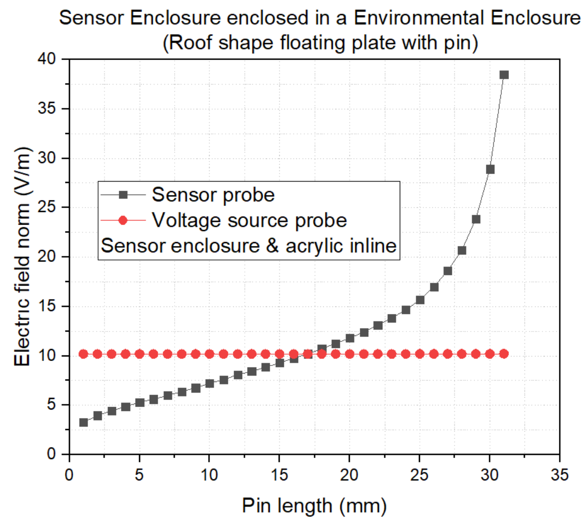

(b)

Figure 3.39: Electric field on the sensor surface for (a) Case 8b and for (b) Case 8c.

3.8.4 Case 8d: Sensor with angled roof in environmental enclosure buried in the ground

Figure 3.40 compares Cases 8c and 8d. We can see that the signal is reduced about 20-25% for the environmental enclosure buried in the ground (case 8d), and this result is consistent with the Case 6.

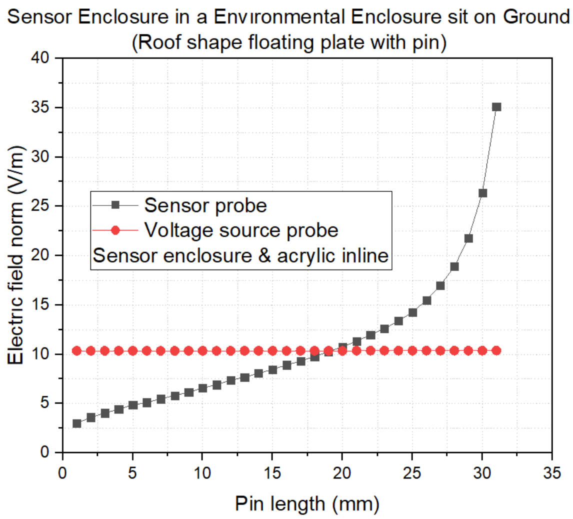

(a)

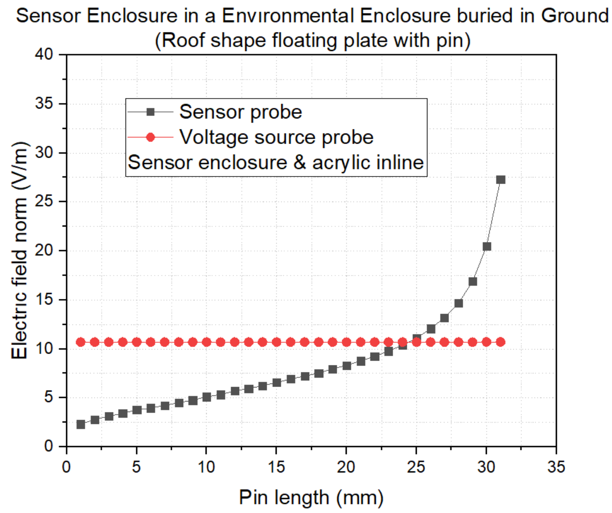

(b)

Figure 3.40: Electric field on the sensor surface for (a) Case 8c and for (b) Case 8d.

3.9 Comparison of elevated angled vs flat roof floating metal plate

Figure 3.41 compares the sensor enclosure with angled roof shape metal plate with flat metal plate. Both models are adjusted so that the pin is 31 mm long, and with a gap from the pin tip to sensor of 1.9 mm. The distance between the top of the floating plate and the bottom of the acrylic insulator height is 22.9 mm in both cases.

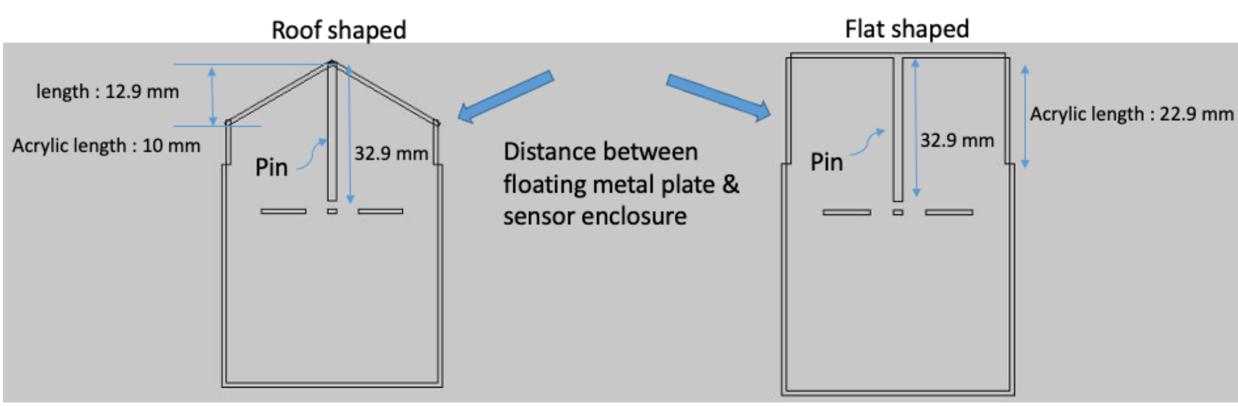

Figure 3.41: Schematics of Case 8a and Case 7.

Figure 3.42 compares Case 7 and Case 8a. We can see that Case 7 has a slightly higher measured signal than Case 8a.

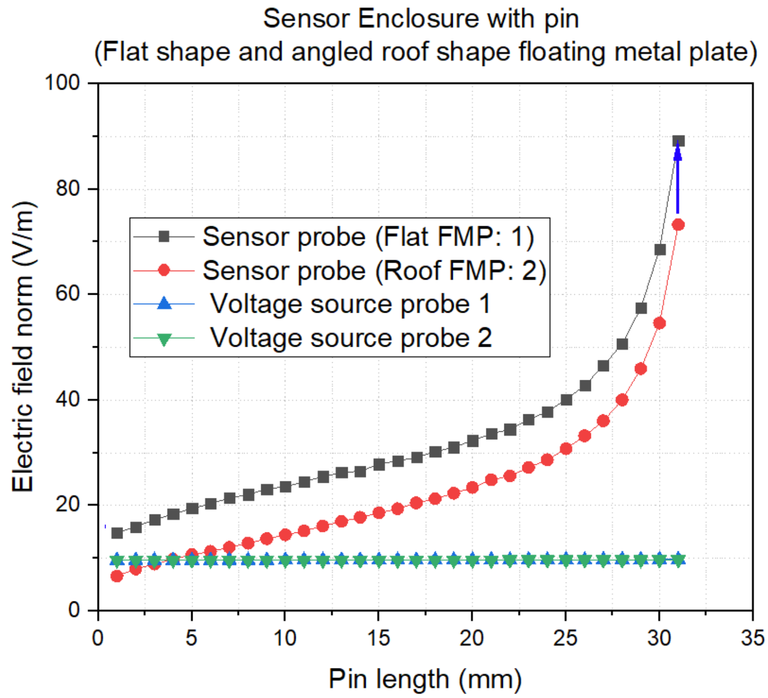

Figure 3.42: Electric field on the sensor surface vs pin length change for angled roof shape (Case 8a) and flat shape (Case 7) floating metal plate.

3.10 Summary

The table below summaries some of the main results that were observed in the 2D simulation models of this Chapter.

Table 3.3: Summary of main results observed in the 2D enclosure simulation models.

Case	Situation	Comments
Case 1	Sensor in enclosure with no cover plate. Enclosure 5 cm above ground.	Electric field reduces as sensor is placed deeper in enclosure. 2 mm sensor shows ~ 25V/m.
Case 2	Sensor surrounded by metal ring.	Reduced signal from Case 1. 2 mm sensor shows ~ 10-17 V/m.
Case 3	Enclosure with floating metal cover.	Similar result as Case 2.
Case 4	Pin extending downward from floating metal cover.	Signal increases with approaching pin to sensor and negates sensor depth inside box. At 1 mm spacing ~ 40 V/m.
Case 5a	Sensor enclosure placed inside environmental enclosure, 5 cm above ground.	Electric field about ½ that of case 4.
Case 5b	Environmental enclosure sitting on ground.	Slightly higher field than Case 5a.
Case 6	Sensor environmental enclosure buried in the ground.	Slightly reduced field vs Case 5b.
Case 7	Sensor enclosure having 1 cm elevated floating metal plate.	Electric field ~ 2.5x higher than Case 6.
Case 8	Sensor enclosure with angled roof floating metal plate.	Electric field ~ 2x higher than Case 4.

Case 1: Electric field reduces as sensor is placed deeper in enclosure. 2 mm sensor shows ~ 25V/m.

Case 2: Reduced signal from Case 1. 2 mm sensor shows ~ 10-17 V/m.

Case 3: Similar result as Case 2.

Case 4: Signal increases with approaching pin to sensor and negates sensor depth inside box. At 1 mm spacing ~ 40 V/m.

Case 5a: Electric field about ½ that of case 4.

Case 5b: Slightly higher field than Case 5a.

Case 6: Slightly reduced field vs Case 5b.

Case 7: Electric field ~ 2.5x higher than Case 6.

Case 8: Electric field ~ 2x higher than Case 4.

The given cases indicate that placing the sensor in an enclosure without a cover plate, 5 cm above the ground, shows a reduced electric field as the sensor is placed deeper in the enclosure. Surrounding the sensor with a metal ring or enclosing it with a floating metal cover yields similar results. However, extending a pin downwards from the floating metal cover increases the signal as it approaches the sensor and negates the sensor depth inside the box. Placing the sensor enclosure inside an environmental enclosure on the ground slightly reduces the electric field. However, an elevated floating metal plate or an angled roof floating metal plate can significantly increase the electric field.

Chapter 4

DC electric field sensor enclosure 3D modeling

Chapter 3 extensively studied 2D modeling for DC electric field sensor enclosure, and the purpose of simulation was to understand the presented model and to find the critical parameters needed for modeling. These simulation results indicate that the enclosure successfully allow electric field to pass to the sensor surfaces, and the extension pin can further increase electric field. Chapter 4 will further simulate the sensor enclosure using 3D modeling for the local DC electric field at the sensor vicinity. The 3D simulation more appropriately explores the effect of the sensor enclosure parameters for floating metal plate, insulator (acrylic), opening size, and extending pin.

4.1 Introduction

COMSOL Multiphysics is a software package that uses finite element analysis (FEA) to solve partial differential equations (PDEs) that describe various physical phenomena. The software divides the geometry into small elements and applies the PDEs to each element to obtain a system of equations that are solved simultaneously to obtain the overall solution. The 3D modelling solutions more fully solve the electric field solutions, by considering all dimensions of the problem. The result will be better understood and much closer to real world situation. The trend of how the electric field varies on the sensor vicinity in 2D modelling will be compared with 3D modeling.

4.2 Structure of the 3D model enclosure

The basic developed sensor enclosure model is shown in Figure 4.1 in 3D situation and based on the 2D model of Figure 3.1. The sensor enclosure is a rectangular-shaped box suitable for a portable handheld device. This enclosure is large enough to provide room for the delicate micromachined MEMS based sensor, supporting electronics, and other peripheral elements including the mechanical support of the sensor platform.

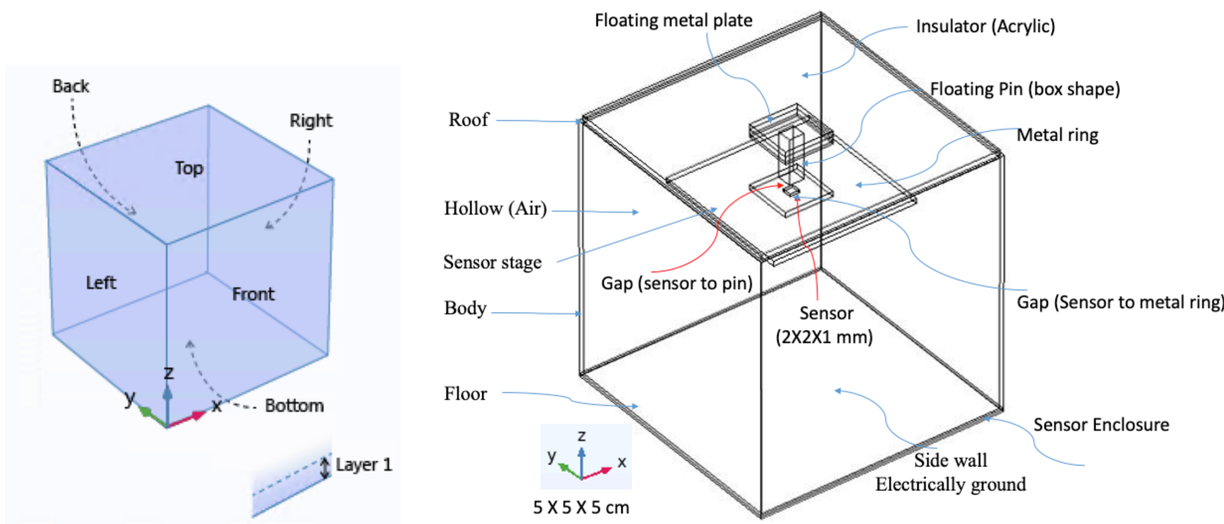

Figure 4.1: 3D Schematic illustration of sensor enclosure.

4.3 Effect of mech size on simulations

Different simulations were carried out for different mesh sizes to analyze the effect on the simulated solution for the 3D situation. The option for a physics-controlled mesh selection was used in COMSOL Multiphysics. The result of the 2D Case 1 model was re-simulated for different mesh sizes ranging from extremely coarse to extremely fine and is plotted in Figure 4.2 with respect to element size mesh density. We can see that for mesh densities above “Normal”, there is a noticeable change jump in the data obtained. For all simulation plots in this chapter a mesh density of "Normal" was used. Figure 4.3, 4.4, 4.5 shows the 3D meshing surrounding the sensor elements.

The selection of mesh density in 3D simulations is like the selection of mesh density in 2D simulations, in that a balance must be struck between accuracy and computational cost. A finer mesh will generally provide more accurate results, but at the cost of increased computational time and memory usage.

The selection of mesh density in 3D simulations is a complex and problem-specific process that requires careful consideration of the balance between accuracy and computational cost. It is important to perform appropriate validation and verification studies to ensure that the selected mesh density is sufficient to provide accurate and reliable results for the specific problem being simulated. Here are several reasons why a normal or moderate mesh density might be selected over an even finer mesh density in 3D simulations:

- *Adequacy for this problem*: In many cases, a moderate mesh density is sufficient to capture the important features of the problem being simulated. If the solution is not significantly affected by small changes in the mesh density, then a coarser mesh can be used without significantly affecting the accuracy of the results.
- *Memory and computational resources*: 3D simulations require significantly more memory and computational resources than 2D simulations, and this cost increases with mesh density. Therefore, if the simulation needs to be completed in a reasonable amount of time, a more moderate mesh density may be preferred.
- *Convergence of the solution*: As with 2D simulations, it is important to ensure that the

solution has converged and is not affected by numerical artifacts or errors resulting from the discretization of the domain. This requires performing a mesh convergence study, which involves gradually refining the mesh until the solution converges. Once convergence is achieved, there may be little benefit in further refining the mesh.

- *Geometric complexity*: In 3D simulations, the geometric complexity of the problem can be a significant factor in determining the appropriate mesh density. In general, a finer mesh is required in regions of high geometric complexity or where there are sharp gradients in the field being simulated. However, a coarser mesh may be sufficient in regions of low complexity or where the field gradients are relatively small.

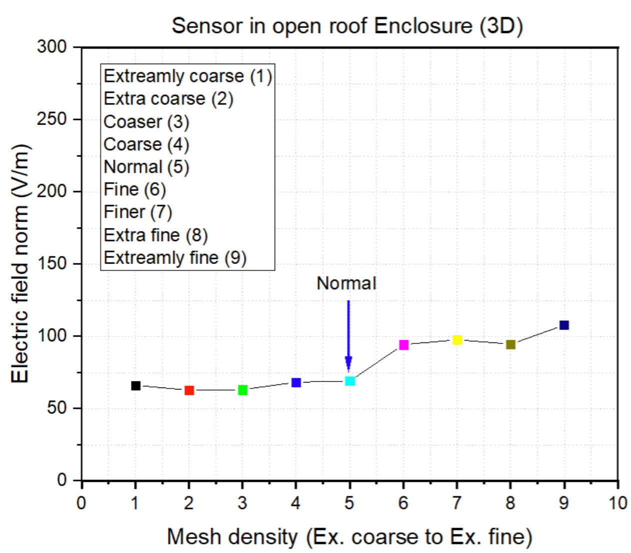

Figure 4.2: 3D electric field simulation of 2x2x1 mm wide sensor in the open enclosure of Figure 3.3 as a function of mesh density.

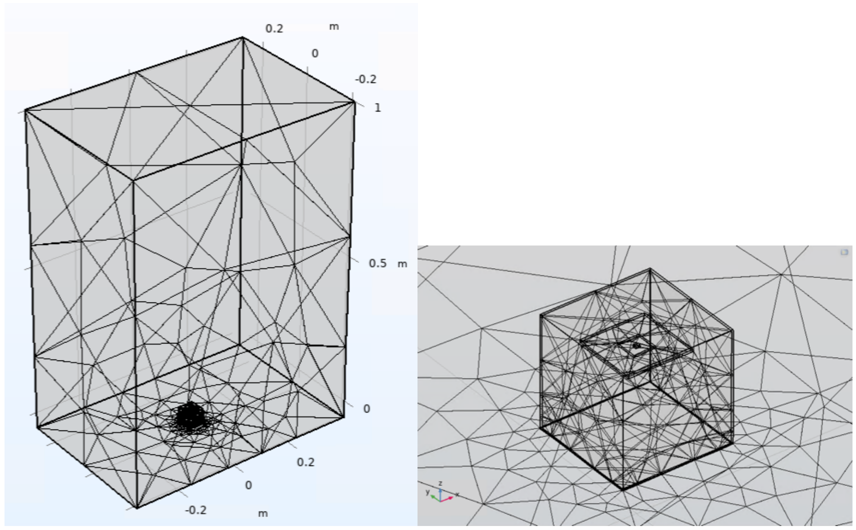

(a) (b)

Figure 4.3: Mesh densities of simulated environment. Extremely Coarse (a) air box (b) Sensor enclosure.

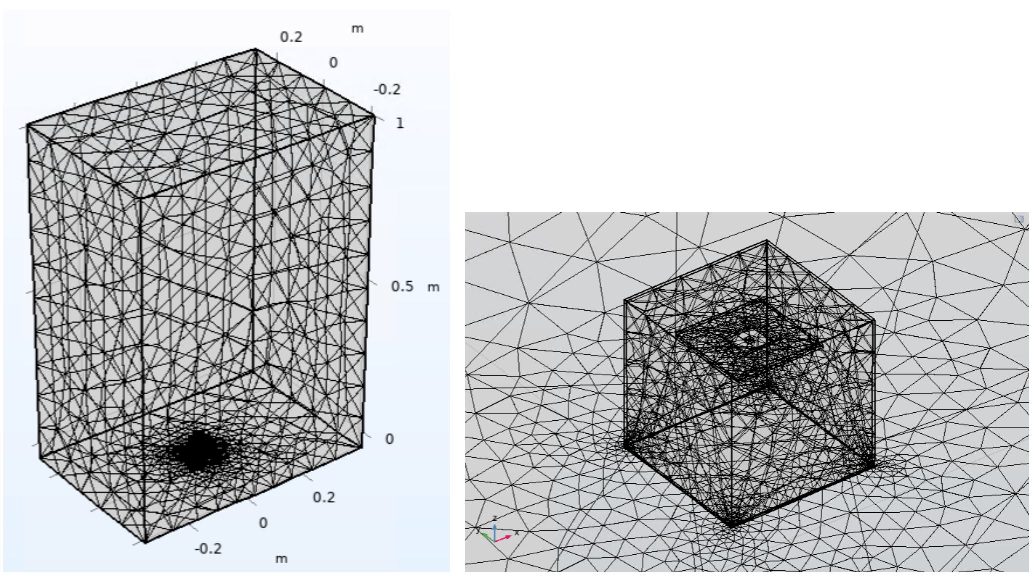

(a) (b)

Figure 4.4: Mesh densities of simulated environment. Normal (a) Air box (b) Sensor enclosure.

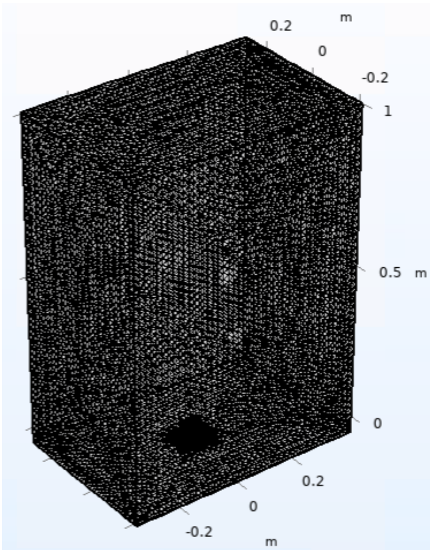

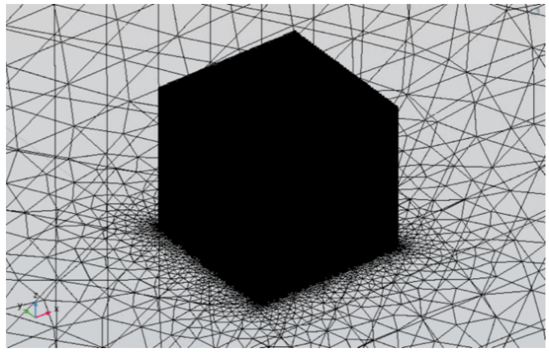

(a) (b)

Figure 4.5Mesh densities of simulated environment. Extremely Fine. (a) Air box (b) Sensor enclosure.

Figure 4.6 shows case 4 as a 3D design with the floating metal plate perspective view of sensor enclosure in 3 directions. XY, YZ and XZ. YZ and XZ parameters are identical due to the symmetry.

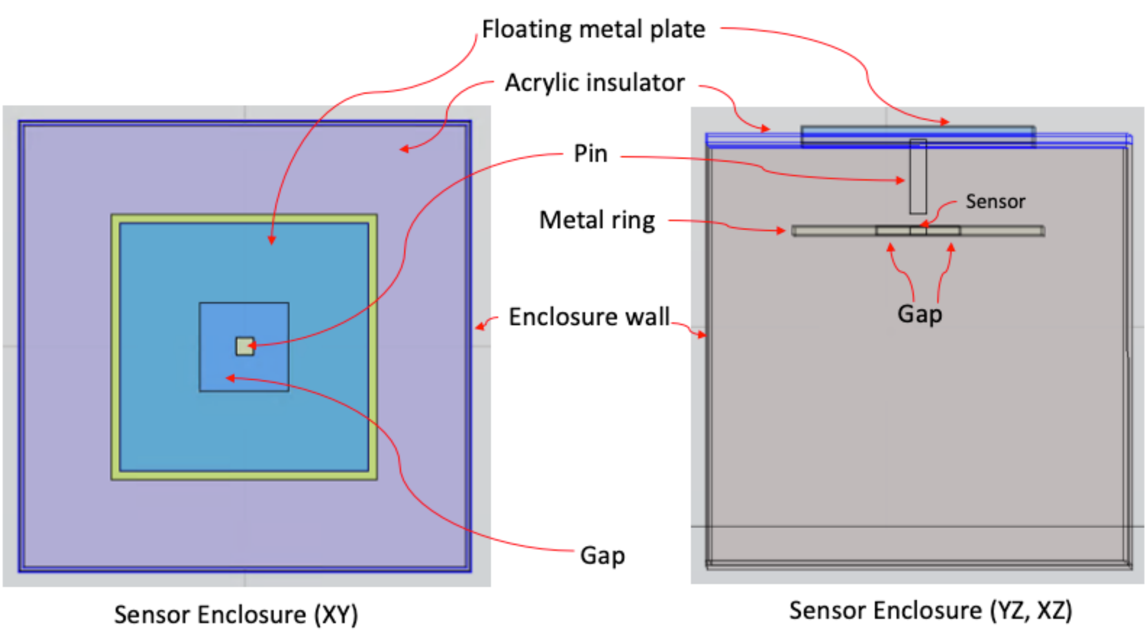

Figure 4.6: (a) Schematic Sensor Enclosure faces. (Left) XY direction. (Right) YZ and XZ direction.

4.4 Simulation of the basic enclosure and simulation environment (3D)

Figure 4.7 shows the 3D model of Figure 3.2 illustrating the airbox space around the enclosure. This is a 75 x 50 x 111 cm size large rectangle space gives enough room to include more studies such as the environmental enclosure.

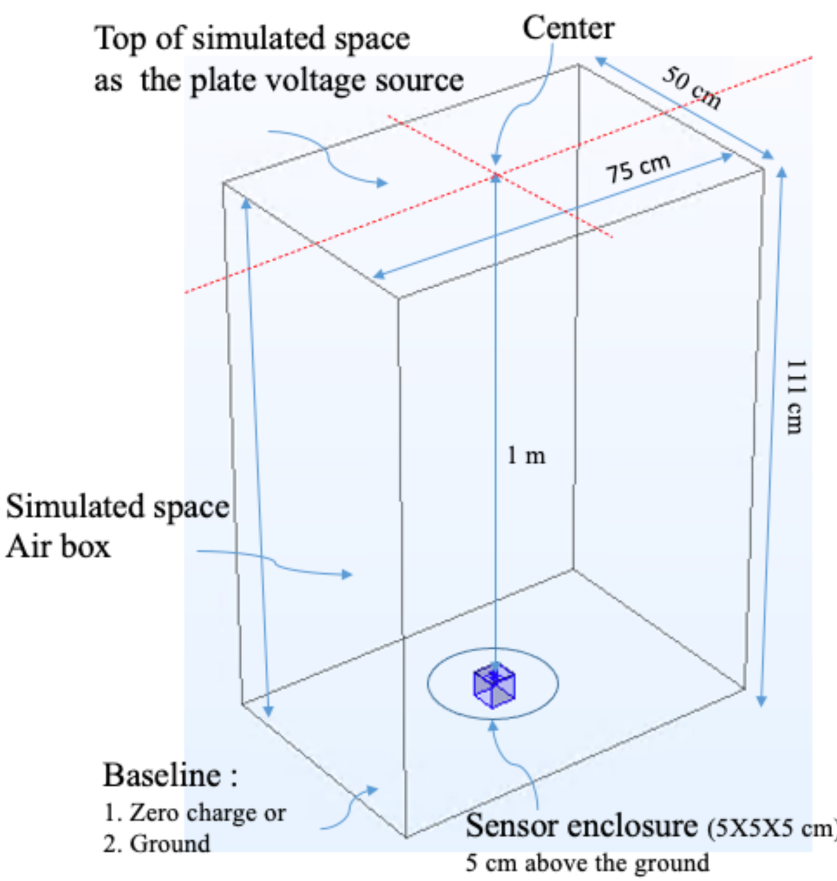

Figure 4.7: 3D schematic of the electric field simulation environment.

Figure 4.8 illustrates the electric field distribution throughout the air box and sensor enclosure in 3D under the plate voltage source and under the power line source. The color scheme shows the electric field strength varying when 3D Case 4 and Case 6 are placed in the air box, and how these parameters can influence the strength of the electric field on the sensor.

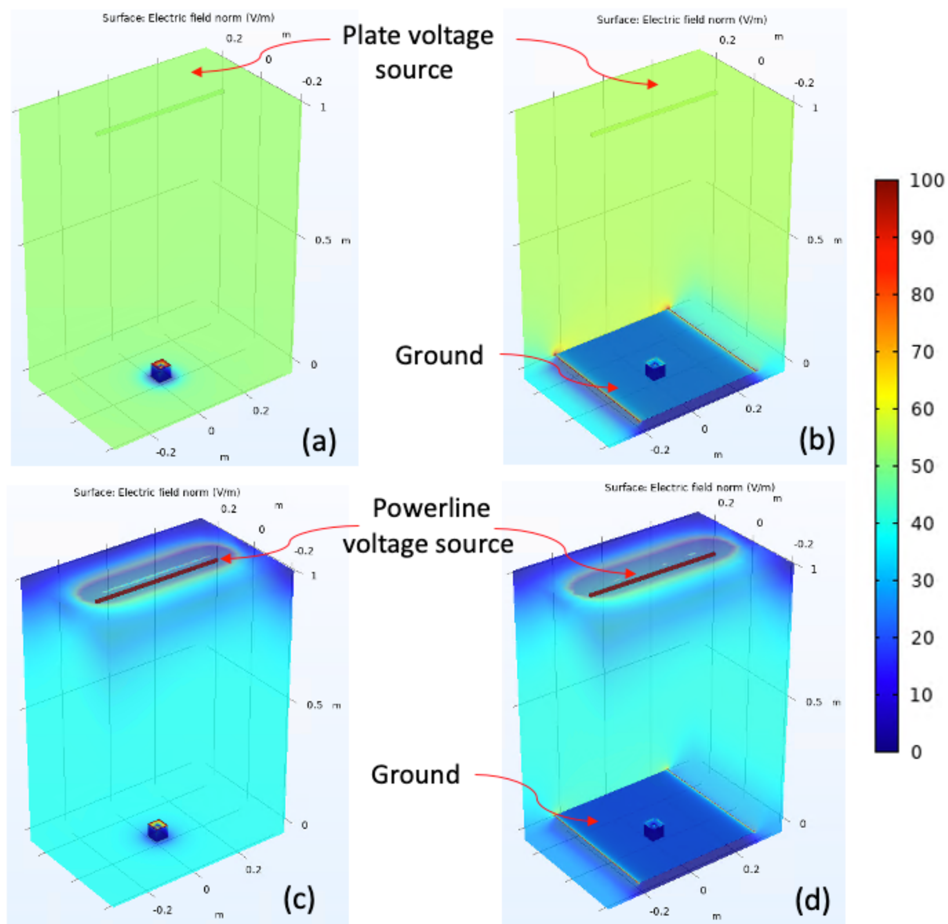

Figure 4.8: 3D electric field distribution for the air box. (a) Case 4 under plate voltage source. (b) Case 6 under plate voltage source. (c) Case 4 under powerline. (d) Case 6 under powerline.

Figure 4.9 shows the 3D electric field distribution for Case 4. Color scheme best displays electric field strength to be strongest in the corners, and that deeper inside the enclosure the electric field diminishes. This figure illustrates the electric field distribution on the sensor, metal ring under the floating metal plate, and floating pin. Other elements are hidden in this figure, to better view the electric field strength variation inside the enclosure.

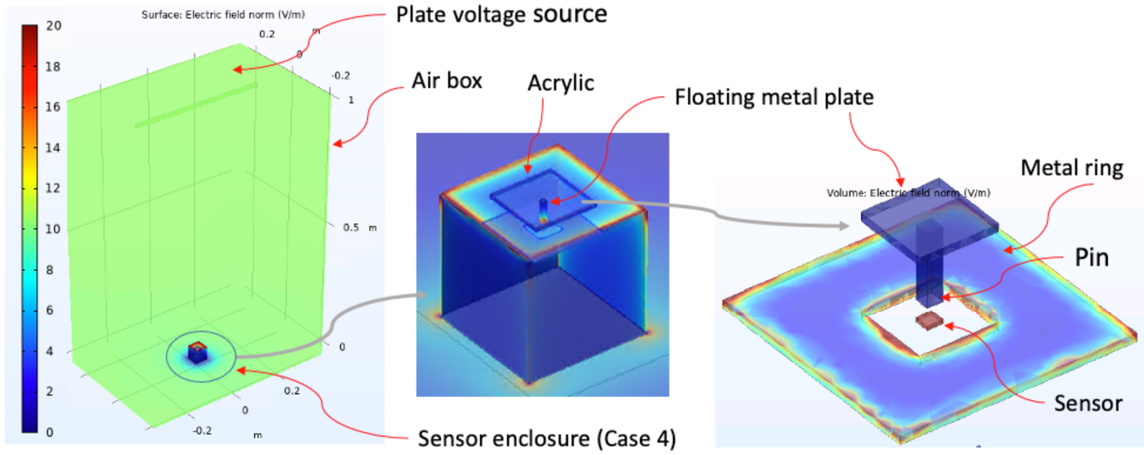

(a) (b) (c)

Figure 4.9: 3D electric field distribution for (a) air box, (b) sensor enclosure, and (c) on the sensor and metal ring.

Figure 4.10 illustrates Case 4 sensor enclosure variations that will be studied based on this design. Each of these cases are simulated separately in the air box 1 m below the voltage source (powerline or plate). Case 4 is the sensor enclosure itself with pin extending downwards. Case 7a is with the extended acrylic insulator supporting the floating metal plate (In the 2D model of Chapter 3, Case 7 was simulated with the enclosure buried in the ground).

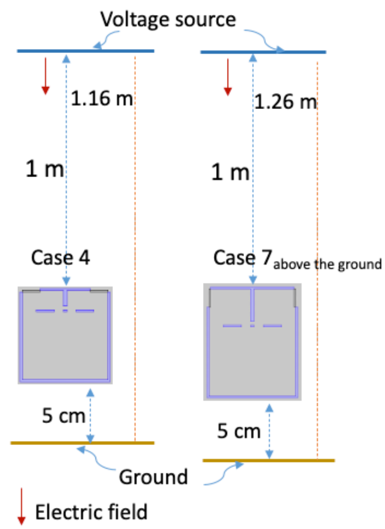

Figure 4.10: Sensor enclosure variations in the simulated environment.

4.5 3D Simulation of the basic enclosure with extending pin (Case 4 in 3D)

Figure 4.11 shows 2D (left) and 3D (right) simulation comparison for the Case 4. The graph shows the varying electric field on the sensor surface as function of pin length. The black line illustrates the result for Case 4. The red line is Case 5b that has environmental enclosure. The black line illustrates the result for Case 6 with the outer box buried in ground.

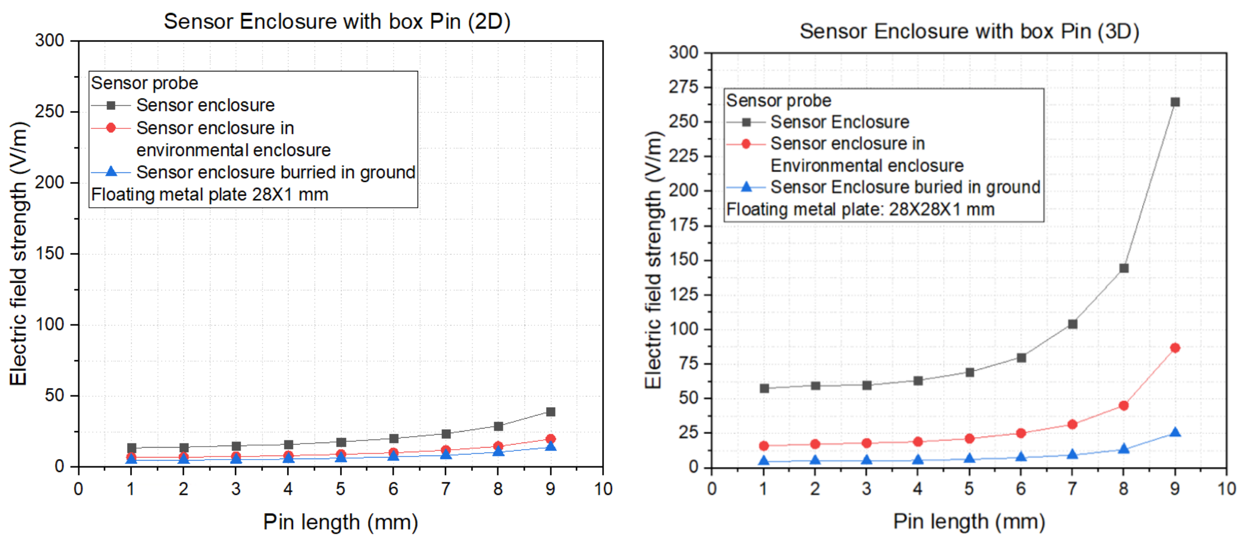

(a) (b)

Figure 4.11: Electric field on the sensor surface vs pin length change for sensor enclosure (Case 4), sensor in environment enclosure (Case 5a), sensor environmental enclosure buried in the ground (Case 6). (a) Results of 2D simulation. (b) Results of 3D simulation.

Comparing the 2D and 3D results, we can see that the 3D result shows a much higher electric field on the sensor. This is due to the 2D model not considering the third dimension of the floating metal plate and pin, that directs the electric field upon the sensor. We also see from the simulated results that having the outer enclosure, reduces the electric field to about 1/2 of the sensor enclosure alone (Case 4) for the 2D, and the 3D model shows nearly 6 times reduction.

4.6 3D Elevated metal floating plate (Case 7a)

Figure 4.12 shows a design with the floating metal plate having elevated acrylic wall on top and around sensor enclosure side walls. The pin extends downward towards the sensor is modelled with length of 14 mm, 19 mm, and 24 mm, and the distance between the sensor and pin tip is 1 mm.

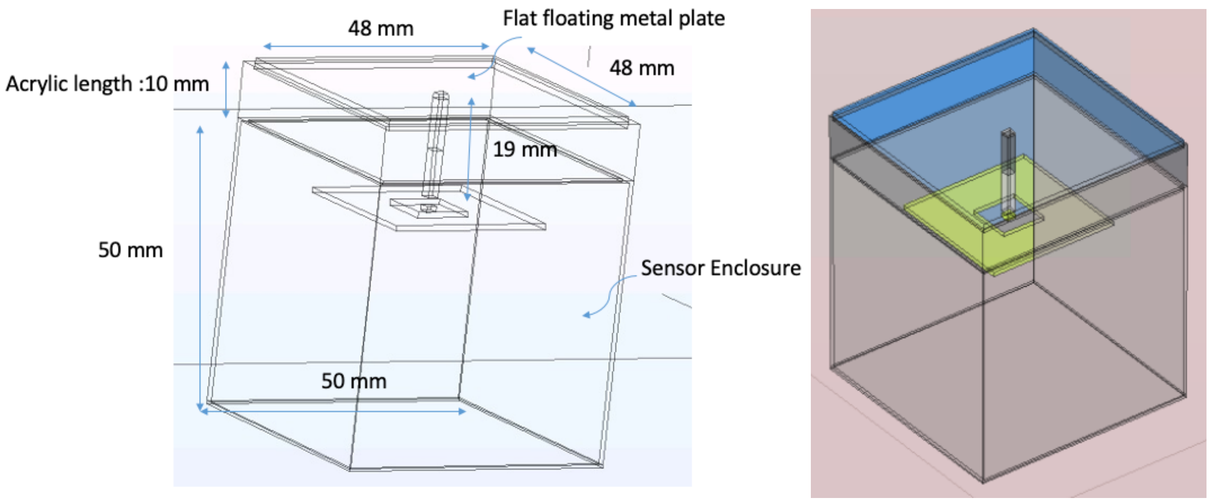

Figure 4.12: 3D Elevated Floating metal plate with increased height of acrylic.

Figure 4.13 shows Case 7a as a 3D design with the floating metal plate perspective view of sensor enclosure in 3 directions. XY, YZ and XZ. YZ and XZ parameters identical due to the symmetry. Figure 4.14 illustrate the electric field distribution in the space.

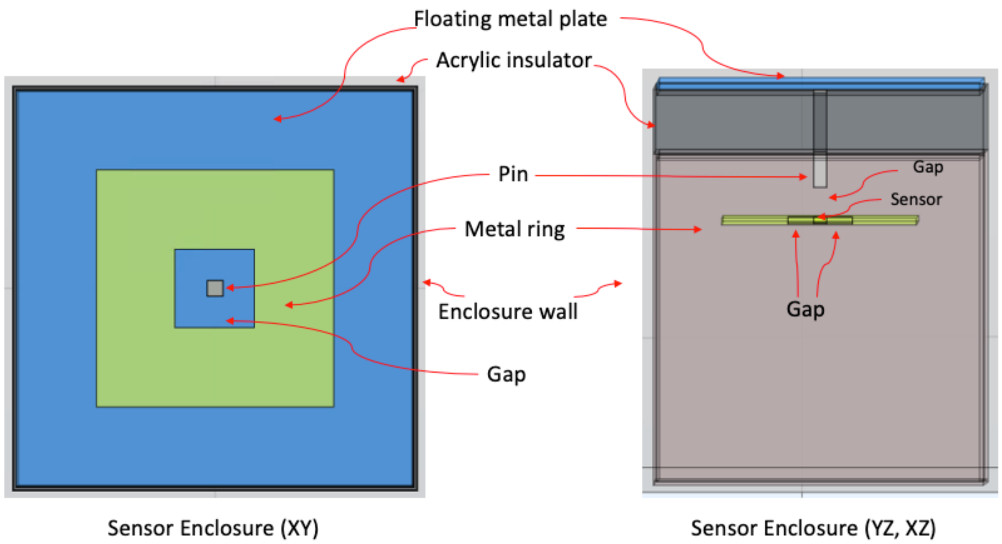

Figure 4.13: (a) Schematic of sensor enclosure faces. (Left) XY direction. (Right) YZ and XZ direction.

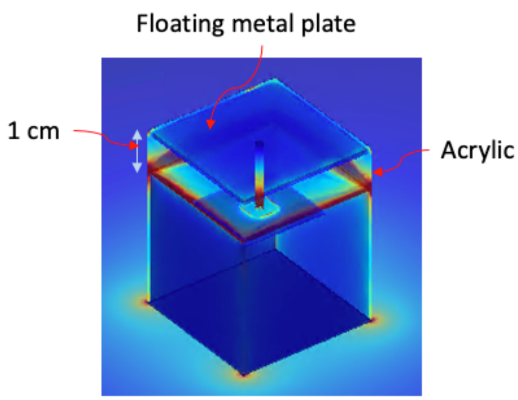

Figure 4.14: 3D electric field distribution for Case 7a.

Figure 4.15 shows the simulated results for this case. Simulated results show that having the elevated acrylic enclosure remarkably increases the electric field to about 5x for 5 mm acrylic height, 7x for 10 mm height and 8x for 15 mm height.

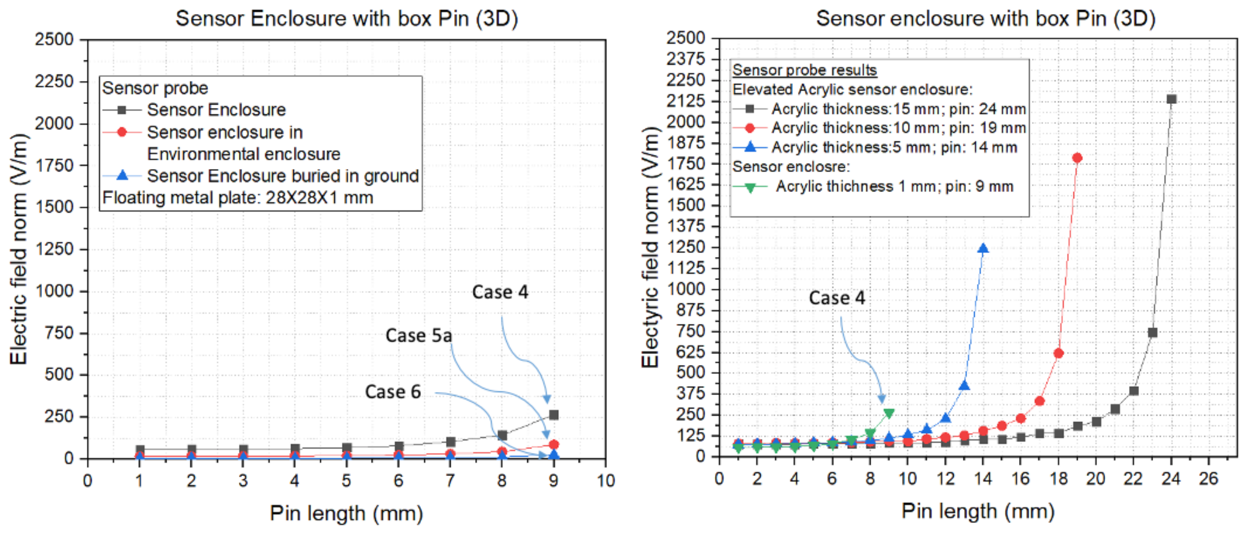

(a) (b)

Figure 4.15: Electric field on the sensor surface vs pin length change for elevated acrylic sensor enclosure (5 mm, 10 mm, 15 mm acrylic height).

4.7 Summary

The time it takes to run a 3D simulation using COMSOL Multiphysics software varies depending on factors such as model complexity, mesh element count, type of analysis, and hardware configuration. Larger models, finer meshes, and longer simulation times take longer to run. The time can range from minutes to days, depending on the specifics of the simulation. It is important to benchmark and optimize hardware and simulation settings to ensure a reasonable completion time.

In this chapter, the sensor was simulated in 3D and compared to the 2D results of the prior Chapter 3. It was observed that the 3D result showed a much higher electric field on the sensor due to better prediction of the electric field distribution around the floating metal plate in the third dimension. This was consistent with both the situations of Case 4 and Case 7a. It was also observed that the outer enclosure, which reduced the electric field to about 1/2 of the sensor enclosure alone for Case 4 in 2D, became nearly 6x smaller in the 3D simulation.

It is worth comparing the 2D and 3D simulation results. Figure 4.16 shows the normalized electric field comparison for 2D and 3D for four cases: sensor enclosure without top cover (Acrylic insulator and FMP), with cover but without pin, with pin 1 mm long and 10 mm above sensor, with pin 9 mm long 2 mm above sensor.

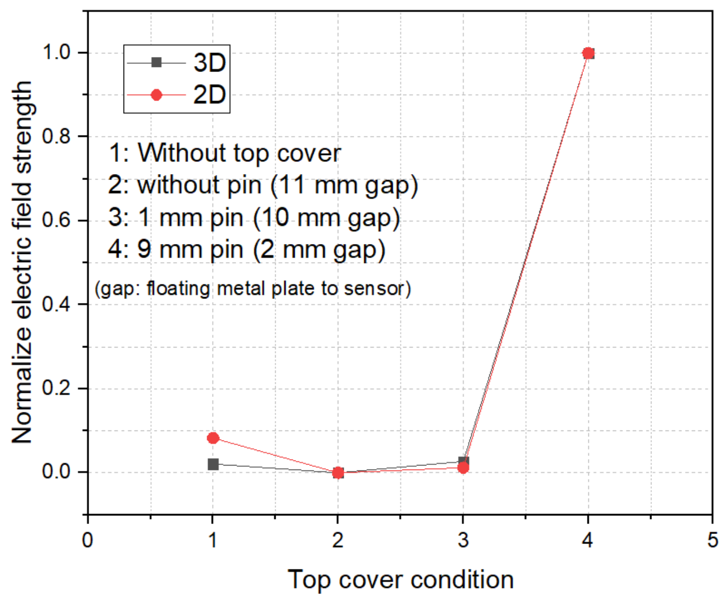

Figure 4.16: Normalized electric field on the sensor surface vs status of sensor enclosure top cover.

Chapter 5

DC electric field sensor enclosure experiment and results

Extensive study of the enclosure for the DC electric field sensor using 3D model simulation was presented in Chapter 4. These simulation results motivated the design and fabrication of a handheld, industry usable, DC electric field sensor enclosure. Chapter 5 describes the experiments which were done to study the physical sensor enclosure.

5.1 Introduction

Manitoba Hydro and other utilities desire small size, low cost, portable, and low power DC electric field sensors which can operate in any environmental condition. General laboratory instruments are difficult to handle in test site conditions and can often be not practical for industrial use. Therefore, the enclosure designed for the DC electric field sensor was developed to eliminate issues caused by surroundings that may negatively affect the sensor performance and measurements.

5.2 Design handheld DC electric field sensor enclosure and electronics

The choice of using a rectangular box as the outer casing for a direct current (DC) electric field sensor simulation is based on:

- *Electric field distribution*: The rectangular shape provides a uniform electric field distribution inside the box, which is important for the accurate measurement of the electric field.

- *Compatibility with other components*: The rectangular box must be compatible with other components, such as the electric field sensor and its associated electronics and must provide adequate protection and support for these components.
- *Cost and complexity*: The rectangular box must be simple and cost-effective to manufacture and assemble. The rectangular shape is a simple and straightforward design that is well suited for mass production.
- *Shape and dimensions*: The shape and dimensions of the rectangular box must be chosen carefully to ensure that it effectively blocks external electric fields and creates a uniform electric field environment for the electric field sensor. This can be determined through simulations, experiments, or other methods.
- *Faraday cage effect*: The rectangular box acts as a Faraday cage, effectively blocking external electric fields and creating a uniform electric field environment for the electric field sensor. This is important for ensuring accurate measurements of the electric field.
- *Size and shape of the sensor*: The size and shape of the sensor are important factors in determining the suitability of a rectangular box. The box needs to be large enough to accommodate the sensor, while also providing sufficient clearance and protection against any potential impacts or mechanical shocks. It is also important to consider whether the rectangular box is a good match for the shape of the sensor, and whether it allows for optimal orientation and alignment of the sensor.
- *Sensor packaging*: In addition to the rectangular box itself, it may also be necessary to include additional packaging materials or shock-absorbing elements to further protect the

sensor from any mechanical shocks or impacts.

Figure 5.1 is a picture of sensor enclosure that was used in the laboratory bench and high voltage lab experiments [42]. Figure 5.2 shows the cross section of the DC electric field sensor enclosure design. It consists of an aluminum frame giving mechanical support and serving to protect the delicate and fragile sensor and other electronics. Directly over the sensor, is an opening in the frame, that is covered by an insulator material (acrylic) supporting an electrically isolated metal plate. The metal plate is replaceable. In the center of this plate is a height adjustable pin in the middle, aligned over the sensor and extending inwards towards it. The sensor is in fixed position by a surrounding metal ring positioned on the horizontal stage. The sensor is located 14.6 mm below the floating plate. Figure 5.3 shows the enclosure without the side walls, to make the interior visible. Table 5.1 provides detailed parameters of the physical sensor enclosure.

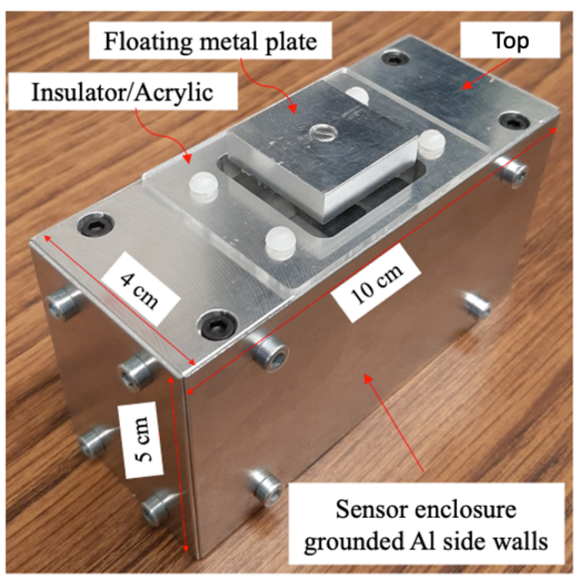

Figure 5.1: Handheld DC electric field sensor enclosure developed for outdoor testing.

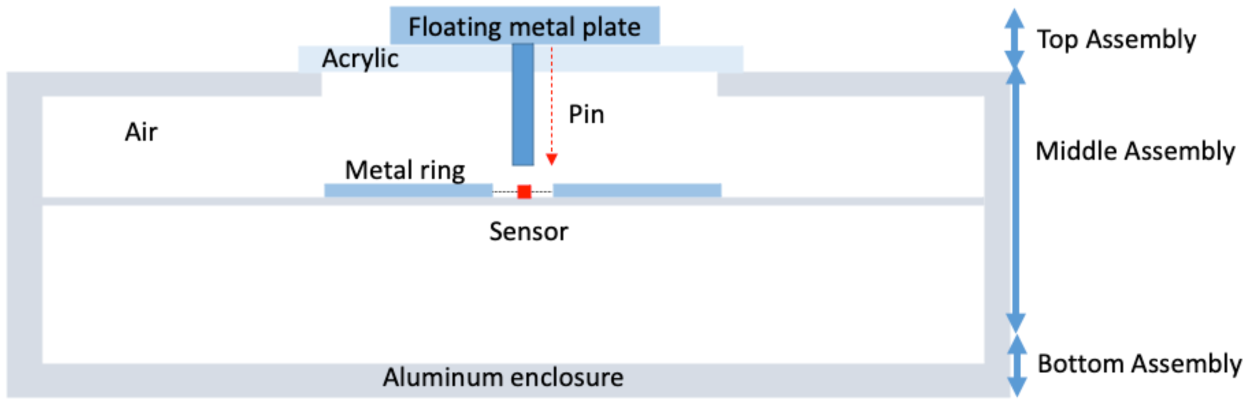

Figure 5.2: Illustration of schematic cross section view of the handheld sensor enclosure.

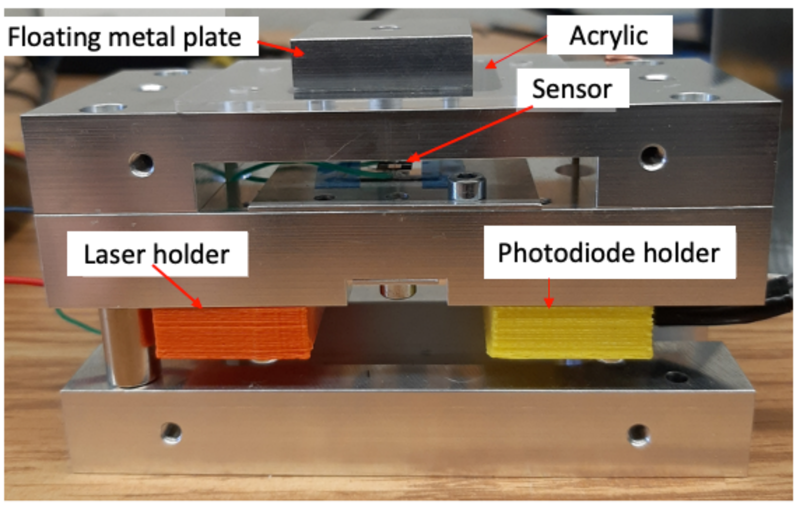

Figure 5.3: Sensor enclosure view without aluminium side walls.

Table 5.1: Attributed simulated optimized parameters to the physical sensor enclosure.

Element	Material	Shape	Size (mm)
Sensor enclosure (length, width, thickness)	Aluminum	Rectangular shaped hollow box	100 x 50 x 40
Enclosure walls (thickness)	Aluminum	Flat solid plates	1
Insulator (thickness)	Acrylic	Flat solid plate	1.5
Floating metal plate (rectangular solid)	Aluminum	Solid plate	25 x 25 x 7
Floating metal pin (diameter, length)	Aluminum	Solid cylinder	4.6 x 13.4
Sensor (square, rounded corners)	Silicon	Micromachined silicon wafer	2 x 2 x 0.3
Metal ring to sensor gap (width)	air		2
Gap sensor to pin (minimum height)	air		1
Distance from floating plate to sensor (maximum height)	air		14.6
Distance from voltage source to floating metal plate	air		25

Figure 5.4 shows partially fixed inner details of the sensor enclosure shown in the Figure 5.1. The floating metal plate is replaceable in case it is needed to use different sizes. The floating plate has a threaded hole with diameter of 4.6 mm, inside which is mounted the extension pin. The pin is also threaded, which allows height adjustment over the sensor. In this figure we can also see the mounted MEMS torsional electric field sensor device below the location of the floating metal plate. At the right bottom corner of the figure, it is also shown a MEMS tortional sensor made from silicon material, which is see 2 x 2 x 0.6 mm in size. The enclosure is designed for easy sensor replacement and changing sensor types (polyimide or silicon material torsional sensor, or other kind), if they share the same frame size.

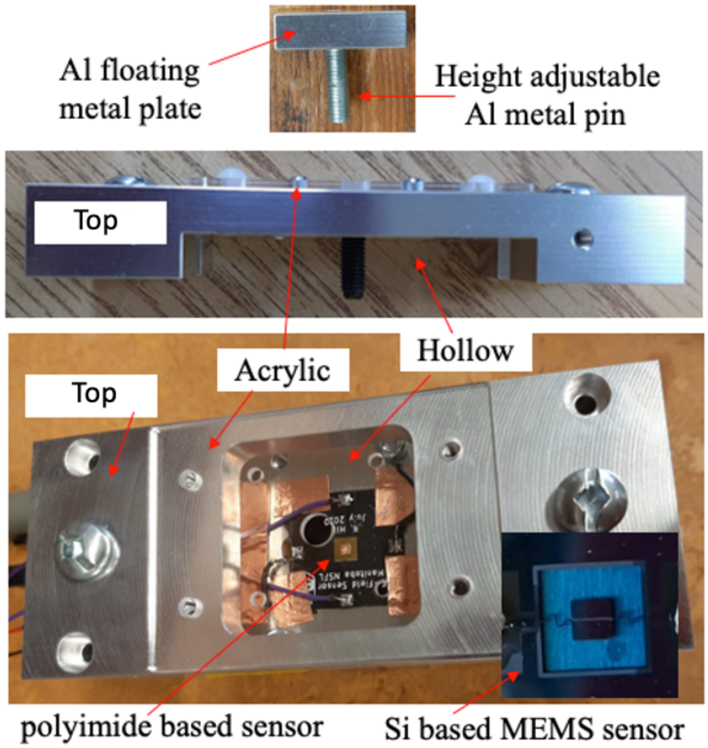

Figure 5.4: Inner illustration of partially assembled DC electric field sensor enclosure.

Figure 5.5 shows the middle assembly of the sensor enclosure. Left and right are two 3D printed polymer supports which are used to hold a laser diode and dual photodetector that interrogate sensor movement. All the wires are routed below the sensor layer, such as 5 V to laser, and ±12 V ac bias, and photodiode output, to minimize the interference.

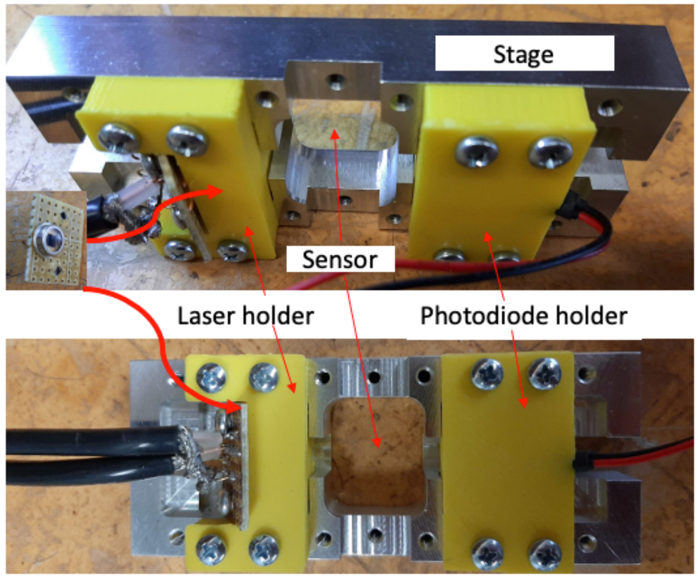

Figure 5.5: Side and bottom view of middle assembly.

Figure 5.6 shows two different types of sensors. Figure 5.6(a) is a MEMS torsional sensor fabricated from a silicon substrate, inside a 5 cm dish. Figure 5.6(b) is a close view of the same sensor. The silicon sensor was microfabricated in the Nano-Systems Fabrication Laboratory (NSFL) cleanroom in Electrical and Computer Engineering [42]. Figure 5.6(c) is the polyimide substrate version was fabricated using a commercial flexible PCB manufacturing process (PCBWay), which lowers the cost of fabrication [43]. It was released by laser micromachining in the NSFL. Figure 5.6(d) illustrates the sensor on its mounting assembly to enable connection to the electronics. Figure 5.6(e) shows the sensor mounted and seen though the transparent acrylic material. The experimental work in this chapter was done with sensor enclosure using the silicon substrate MEMS sensor shown in Figure 5.6(b).

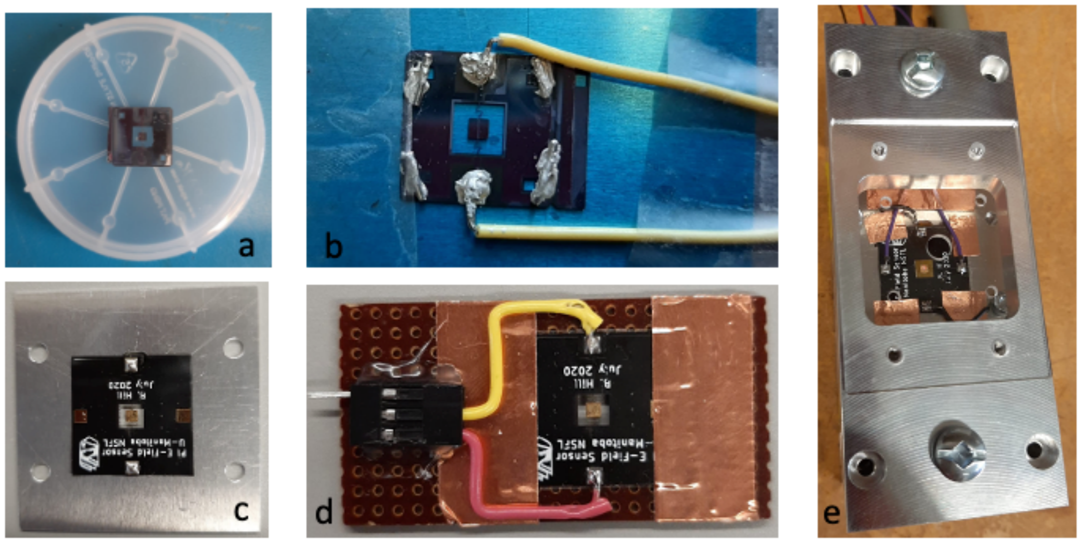

Figure 5.6: Micro sensors suitable for sensor enclosure. (a) and (b) are both 1 x 1 cm silicon substrate MEMS sensor. (c) Shows sensor device mounted on metal ring on. (d) Polyimide substrate sensor. (e) Mounted polyimide substrate sensor seen though the acrylic plate.

Figure 5.7 shows simplified handheld sensor enclosure with electronic system functional block diagram that replaced lab bench set up including functional generator, lock-in-amplifier, and digital multimeter. Final data samples retained by USB to process using PC.

a. In a DC electric field, if the sensor is grounded, the micro-mirror will be deflected by the electrostatic force on it,
b. Or if the two parts of the mirror are biased with opposite ac signals Vac and -Vac, the micro-mirror will be oscillating at the frequency same as the bias signal.
c. In either way, the deflection of the membrane is very small in the range from nm to µm. The most common method to measure this tiny displacement is beam-deflection method which is widely used in atomic force microscopy (AFM).
d. In this method, a laser beam from a laser diode is reflected off the back of the membrane and collected by a position sensitive photodetector.
e. The current signal from photodetector can be convert to voltage signal by using

transimpedance amplifier, then a lock-in amplifier (SR830) can be used to extract the signal at the frequency of bias signal.

f. After that the sensor response is measured with a digital multimeter (Agilent 34401A).

More details about the working principle and fabrication process are introduced in published conference proceedings [42-43]. As explained in publication [43], the amplitude of the membrane oscillation is proportional to the strength of the bias signal. Thus, a stronger bias signal results in higher sensor sensitivity. The thesis study [54] shows the sensor's fabrication process and its specifications, while conference paper [43] provides information about the custom electronics, measurement, and testing setup used in this experiment.

The oscillation of the silicon sensor mirror is detected by an optical interrogation system. The mirror reflects the laser beam to a dual photodetector. With the mirror oscillating, the spot on the photodetector will be oscillating at the same frequency, resulting in an ac output current from each part of the photodetector. These currents are be amplified by two transimpedance amplifiers followed by a differential amplifier. The total gain of this circuit is 10^5. Then, the signal is sent to a lock-in amplifier where the reference signal has same frequency as the bias signal V_{ac}. Figure 5.7 shows the simplified signal conditioning circuit. In this work the lock- in amplifier employed is a Stanford Research SR830. Finally, the output is displayed on an oscilloscope (Tektronix TBS 1052B-EDU) [42]. To enable better accuracy in the experiments in this Chapter, the output was acquired using a digital multimeter (Agilent 34401A model).

The Si-based MEMS sensor (chip B [54]) employed in this study has a resonance frequency of 1409 Hz. In terms of sensitivity, under the same lock-in amplifier settings (time constant of 1 second, sensitivity of 5 mV, and preamplifier gain of 10^6), the silicon sensor chip B exhibits a sensitivity of 25.2 mV/(V/m) (an 8.4 V response in a field of 333 V/m) and a noise of 0.3 (V/m)/√Hz.

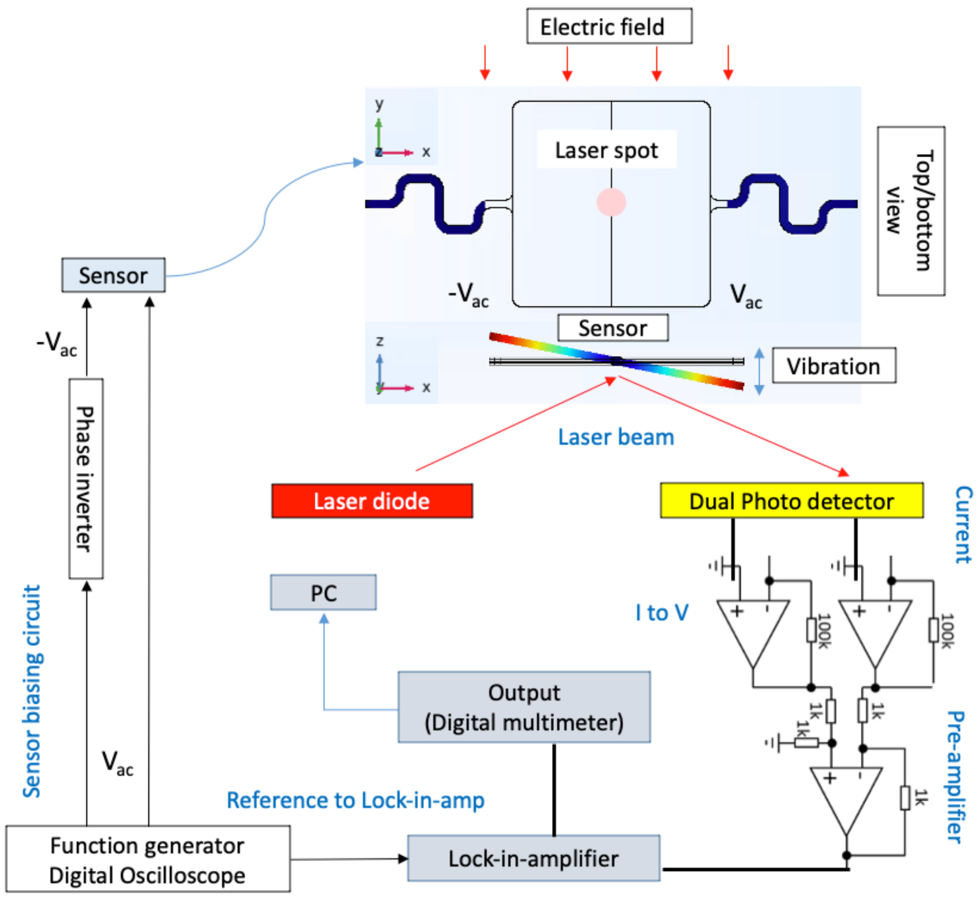

Figure 5.7: Simplified Sensor signal processing block diagram.

5.3 Simulation and experimental testing of fabricated sensor enclosure

Figure 5.8 shows the experiment setup established in the lab to measure DC electric field using sensor enclosure developed in this study. This test setup is representative of Case 6 in chapter 2, which is the sensor enclosure buried below a grounded surface. In this experiment, the grounded aluminum metal plate is placed over the sensor, with the sensor exposed to the electric field through a 4 cm x 5 cm rectangular hole in the grounded aluminum plate. The electric field is created using a metal plate over the sensor, separated 25 mm above the grounded plate using Teflon spacers.

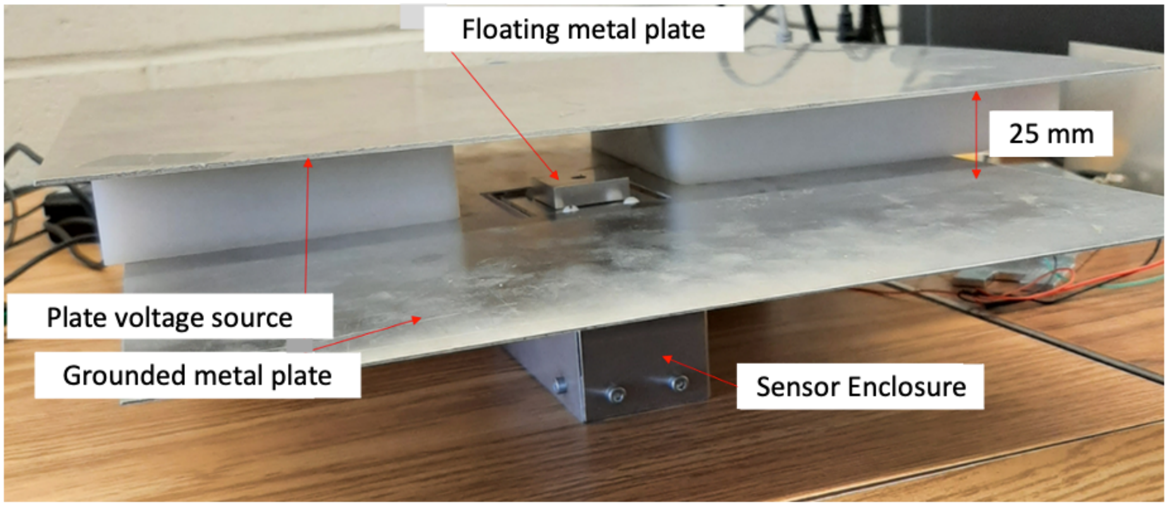

Figure 5.8: Experimental setup.

A simulation was performed to compare with sensor enclosure measurements. 3D simulations were used to model the enclosure using COMSOL Multiphysics software (Figure 5.9). The effect of the extension pin and its length was studied in the simulations, by varying the distance from the pin to the sensor from 0.2 mm to 1 mm with increments of 0.2 mm, and 1 mm to 13 mm with 1 mm increments. Simulation without the extending pin was also done, with the gap space being 14.6 mm. Figure 5.11 shows a perspective view of the simulated enclosure, which resembles the fabricated enclosure. It should be mentioned that these new simulations were done, since those in Chapter 3 and 4 did not have the same dimensions of the fabricated enclosure.

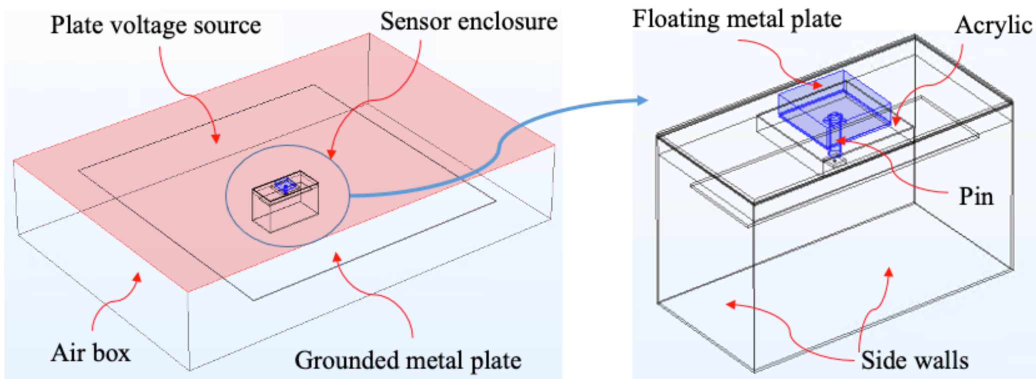

Figure 5.9: 3D schematic view of air box (left) and sensor enclosure (right).

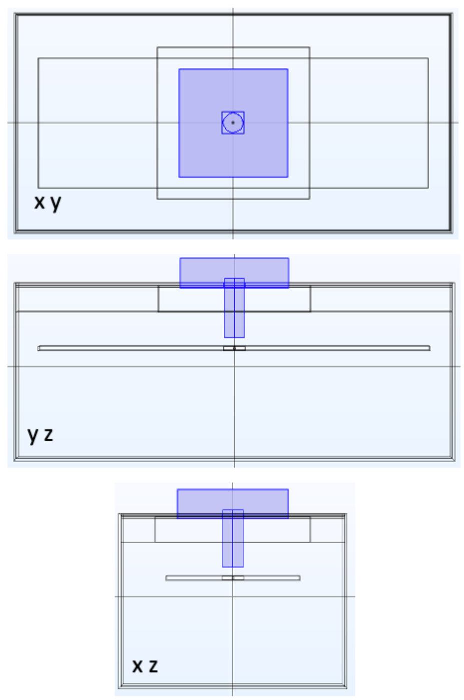

Figure 5.10: Rectangular shaped sensor enclosure perspective views

The experimental test had the top metal plate biased to 61 V, which generates a 2.44k V/m electric field between the plates. In the experiment, the pin height was adjusted to have 1 mm, 2 mm, 3 mm and 4 mm distance to the sensor. The distance was manually measured by using a caliper with a ±0.1 mm error. For the experiment, the pre-amplifier has a gain of 10^5, a SR830 lock-in amplifier (instrument) was used set to 300ms integration time and 20mV sensitivity. As tested, the sensor resonant frequency is 1410 Hz, with the ac bias on the sensor set to 12 V sine wave at this frequency. The output was measured using an Agilent 34461A digital multimeter.

Figure 5.11 measured results for the sensor response at different pin heights. We can see that the sensor has response of 6 V for 1 mm spacing (93.2% of 14.6 mm gap size), 2.8 V for 2 mm spacing (86.3% of gap), 1.7 V for 3 mm space (79.5% of gap), and 0.99 V for 4 mm space (72.6% of gap). When no pin is connected, the sensor response is 0.33 V (14.6 mm gap or 0%). Table 5.2 shows the simulated electric field for each pin to sensor gap spacing and compares with the experiment results. The gap of 2 mm has its results normalized to 1. Figure 5.12 shows simulation results taken from the model identical to the physical sensor enclosure (shown in Figure 5.1). Figure 5.13 shows results normalized to the gap of 2 mm, and we see close agreement between simulation and measurement. As we can see, the measured signal rises considerably when the pin length to sensor distance ratio is over 90%.

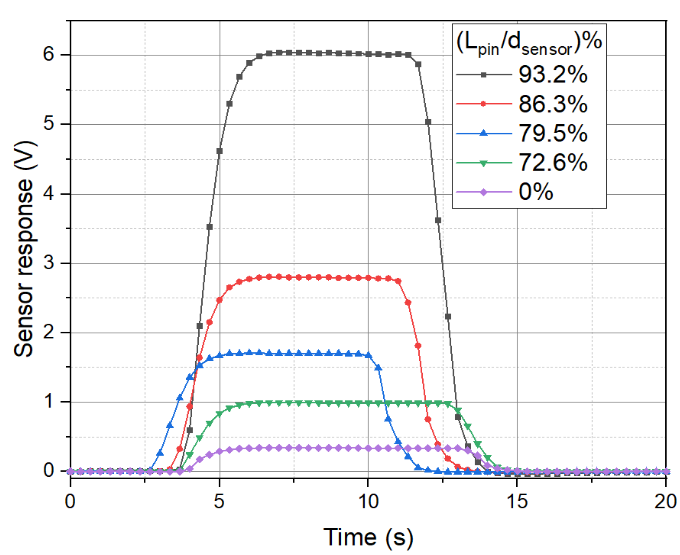

Figure 5.11: Sensor enclosure measurements.

Table 5.2: Simulation and Experiment results using Figure 5.1 (physical enclosure) and 5.9 (Simulation enclosure).

Simulation			Measurement	
Gap (mm)	Average field (V/m)	Normalization	Response (V)	Normalization
1	9159	1.97	6.0	2.2
2	4655	1.00	2.8	1.0
3	3076	0.66	1.7	0.61
4	2120	0.46	0.99	0.35
5	1606	0.35	-	-
6	1318	0.28	-	-
7	1079	0.23	-	-
8	925	0.20	-	-
9	835	0.18	-	-
10	767	0.16	-	-
11	712	0.15	-	-
12	682	0.15	-	-
13	556	0.12	-	-
14.6	524	0.11	0.33	0.12

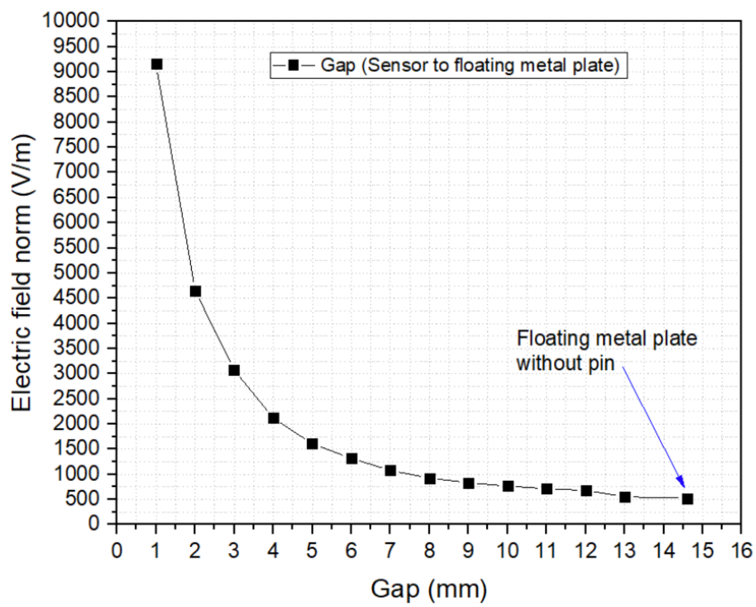

Figure 5.12: Sensor enclosure measurements.

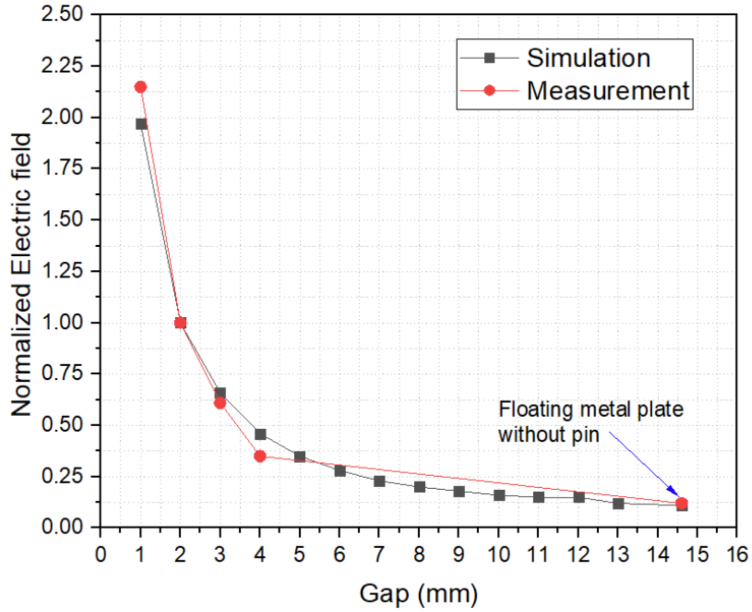

Figure 5.13: Results normalized for gap of 2 mm, showing test results vs. simulation results.

5.4 Capacitive model of the electric field sensor system

The enclosed MEMS electric field sensor consists of a grounded enclosure with a floating conductive metal plate on top assembly and a height-adjustable conducting pin extending into the enclosure. The sensor is designed to enhance the electric field by bringing the sensed field into the interior of the enclosure and close to the sensor. The mechanism for enhancing the electric field involves the use of a grounded platform inside the enclosure, which provides a reference potential for the sensor. The floating metal plate on top assembly creates a capacitor with the enclosure, and the height-adjustable conducting pin extends into the enclosure, creating another capacitor with the enclosure.

The enclosed MEMS electric field sensor consists of a grounded enclosure that contains a floating conductive metal plate on top assembly and a conducting pin that can be adjusted in height and extends into the enclosure. The goal of this design is to amplify the electric field by bringing the sensed field into the interior of the enclosure and close to the sensor. This mechanism works by creating two capacitors with the enclosure. The floating metal plate creates a capacitor with the enclosure, and the height-adjustable conducting pin also creates a capacitor with the enclosure. The grounded platform inside the enclosure serves as a reference potential for the sensor. Together, these components create a mechanism for enhancing the electric field, making the sensor more sensitive to changes in the electric field within the enclosure.

The electric field incident on the sensor is influenced by the capacitance of the interior enclosure and the capacitance of the pin seen by the sensor. As the height of the conducting pin is adjusted, the capacitance of the pin changes, altering the electric field experienced by the sensor. A higher capacitance of the pin results in a higher sensitivity of the sensor, as the electric field is amplified by the change in capacitance.

To further enhance the electric field, simulations and experimentation are conducted to investigate the effect of pin height on sensor sensitivity. By varying the height of the conducting pin, the capacitance of the pin can be controlled, and the electric field experienced by the sensor can be optimized. The simulation involves modeling the electric field incident on the sensor using finite element analysis, while experimentation involves measuring the output signal of the sensor as a function of pin height.

In conclusion, the enclosed MEMS electric field sensor enhances the electric field by using a grounded enclosure with a floating conductive metal plate on top assembly and a height-adjustable conducting pin extending into the enclosure. The sensor utilizes the capacitance of the interior enclosure and the capacitance of the pin seen by the sensor to enhance the electric field. The sensitivity of the sensor can be optimized by adjusting the height of the conducting pin and by controlling the capacitance of the pin.

The shielding effect reduces the field to the sensor, the deeper the sensor, the weaker the strength of the field. As the metal floating plate is an equipotential body, if a pin is extended into the box, it can bring the external field inside. Figure. 5.14 shows the simulated electric field distribution for a box opening in a few different scenarios. The blue arrows represent the electric field vector, where the length of it indicates the strength of the field at that point. As we can see in Figure. 5.14 (a) and (b), when the depth of the sensor increases, the strength of the field on the sensor is significantly decreased. A metal pin extending from the floating plate to the inside of the box helps bringing the field inside. As we can see in Figure. 5.14 (c) and (d), when the pin length increases to the area close to the sensor, the electric field strength on the sensor increases significantly. Both Figure 5.14 (c) and (d) show stronger field compared to Figure 5.14 (b).

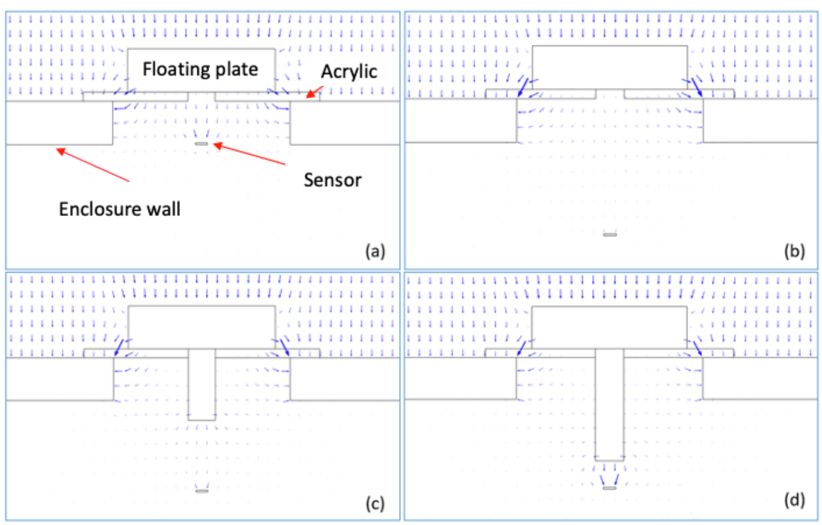

Figure 5.14: Electric field distribution at various pin length.

The sensor operation can be explored in terms of charge distribution. Figure 5.15 shows the model of a floating plate with a pin and sensor in an electric field. The figure also shows the enclosure box opening region, ignoring the fringing effect and other components in the enclosure box such as laser diode, photodiode, cables, etc. This can be viewed as a circuit consisting of three capacitors, C_1 between the floating plate to the plate of the voltage source, C_2 between the floating plate and the sensor, and C_3 between the floating plate and the grounded sensor stage and enclosure box wall. The equivalent circuit has C_2 and C_3 in parallel and in series with C_1. The sensor measures the electric field of C_2, which is related to the potential of V_2 in this circuit. If the floating plate initially possesses a zero charge, in an electric field E_1 generated by a DC voltage source V_1, the voltage on C_2 is V_2, and it can be calculated from the capacitive voltage divider circuit, as shown in equation (5.1):

$$V_2 = V_1 \frac{\frac{1}{C_2+C_3}}{\frac{1}{C_2}+\frac{1}{C_2+C_3}} = V_1 \frac{V_1}{1+(\frac{C_2+C_3}{C_1})} \quad (5.1)$$

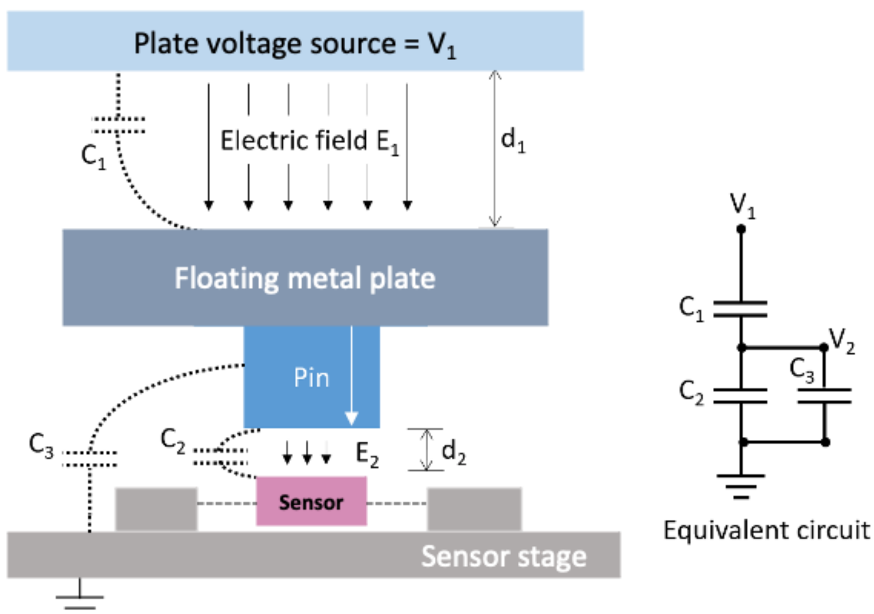

Figure 5.15: Floating plate with the pin in an electric field and equivalent circuit.

Considering the electric field strength on the sensor is related to the distance separating the pin to the sensor, the electric field in C_2 can be written as:

$$E_2 = \frac{V_2}{d_2} \quad (5.2)$$

Substituting (5.1) into (5.2), we obtain:

$$E_2 = \frac{V_1}{d_2(\frac{C_2+C_3}{C_1})} \quad (5.3)$$

Equation (5.3) indicates that the strength of the field is determined by both the distance from the pin to the sensor d_2, and the ratio of C_2+C_3 over C_1, where C_1 is constant, C_2 and C_3 are related to the pin height d_2. When d_2 increases, both C_2 and C_3 will be reduced, and vice versa. It is of interest to find out the trend of E_2 when d_2 changes. Table 5.4 shows the results. As we can see, with d_2 increasing the denominator of (5.3) will increase. In other words, E_2 will be enhanced when the pin is closer to the sensor, and the rate of increase is rapid for small d_2 values. Different enclosure box designs will vary C_1 and C_3, affecting the specific field seen by the sensor, however, the overall trend will be the same with decreasing d_2.

Table 5.3 shows the results of the calculated capacitances (C_1, C_2, C_3) for various pin lengths, and the associated values for the denominator of equation 5.3 (designated as "X" in the inset of Figure 5.16).

Table 5.3: Simulated capacitances at variant pin height

Gap (mm)	X= $d_2(1+\frac{C_1}{C_2+C_3})$	C_1 (pF)	C_2 (pF)	C_3 (pF)
1	5.6	0.45	0.79	1.95
2	10.6	0.45	0.41	1.88
3	15.6	0.45	0.26	1.83
4	20.2	0.45	0.19	1.79
5	24.9	0.45	0.14	1.76
6	29.5	0.45	0.12	1.73
7	34	0.45	0.01	1.71
8	38.6	0.45	0.009	1.69
9	43.1	0.45	0.008	1.68
10	47.6	0.44	0.007	1.67
11	52.1	0.44	0.007	1.66
12	56.7	0.44	0.007	1.65
13	61.3	0.44	0.007	1.65
14.6	68.8	0.44	0.007	1.5

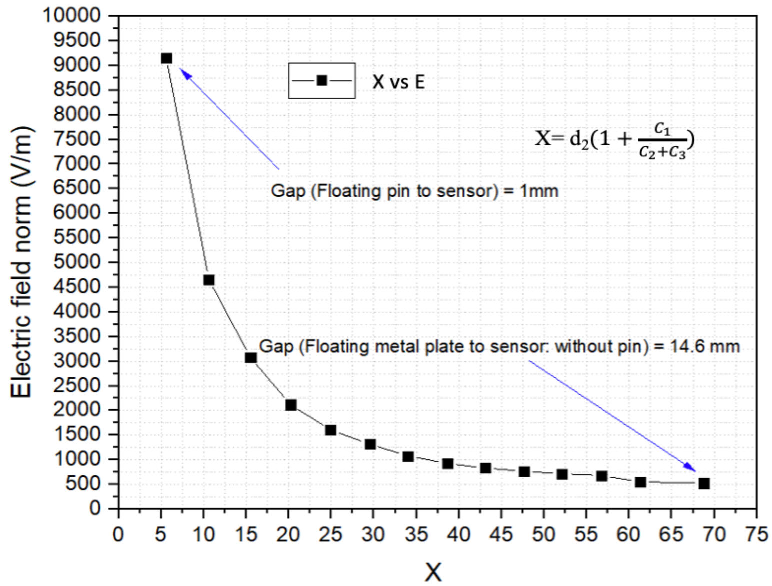

Figure 5.16: Electric field vs X.

5.5 Summary

The performance of a DC electric field sensor inside an enclosure was simulated and experimentally validated. A capacitance model was presented showing how the sensor signal is affected with the enclosure interior, and the spacing of the pin extending to the sensor. Simulation results showed a good agreement with the measured sensor signal with the pin spacing. When the pin was placed at 1 mm above the sensor, a field was measured that was 18.3 times stronger than when the pin was not present. This shows that a proper enclosure design can itself be used to augment the sensitivity of enclosed DC electric field sensors.

Chapter 6

Conclusions and future work

This thesis successfully demonstrated simulations and experimental results of a MEMS DC enclosed electric field sensor in a laboratory environment. The usage of a DC electric field sensor inside an enclosure was modeled and simulated. Performing 2D simulations before 3D simulations allowed for quicker design iteration and optimization. Optimized 2D simulations were then validated by 3D simulations to provide a more accurate representation of the system behavior. The 3D model was used to predict the actual DC electric field inside the enclosure. Simulation parameters were attributed to a hand-made physical sensor enclosure, which was then simulated to validate experimental results. A capacitance model was built to represent the enclosure, and it was used to model how an extension pin into the structure above the sensor can mitigate field attenuation and even enhance the field seen by the sensor.

The movement of the silicon sensor mirror is detected by an optical interrogation system. The resulting signal is then amplified using two transimpedance amplifiers and a differential amplifier with a total gain of 10^5 during the experiment. The output signal is further processed using a lock-in amplifier and displayed on an oscilloscope. To ensure accuracy, a digital multimeter was utilized to acquire the output signal.

The simulation and experimental results showed good agreement and correlated well with the measured sensor signal and the pin spacing. When the pin was placed 1 mm above the sensor, a stronger field was measured, which was 18.3 times stronger than the measurement without the pin. This demonstrates that a well-designed enclosure can be used to enhance the sensitivity of enclosed DC electric field sensors.

Future works

Future studies of these enclosures aim to integrate with other sensor types, such as field mills, to eliminate the potential disadvantages of locating sensors inside protective enclosures. Different parameters and materials (insulators) can be used to model various applications that can be employed in different environmental conditions.

Prior research conducted by S. Liyanage [29] showed that sensors utilizing laser interrogation of sensor platform movement will provide the foundation for future development. These sensors require sensor platforms with sufficient size (around 1 x 1 mm) for laser reflection, and the objective is to increase their operational resonance frequency to over 1 kHz by utilizing stiffer and lighter structures and investigating perforations on the membrane surface to reduce damping caused by air effects. Furthermore, it is necessary to develop perforated surfaces that do not affect laser reflectivity. Sensors that utilize capacitive interrogation of sensor platform movement have the potential for smaller mass structures, allowing for significantly higher resonance frequencies. These sensors typically have two capacitive position sensing electrodes positioned either below or beside the sensor membrane, in the form of interdigitated electrodes. Further experimentation is needed to fully explore their capabilities.

Capacitive detection electrodes offer isolation from the electric field, but their positioning requires a new fabrication process using a bonded two-wafer process like MicraGEM fabrication process. Further exploration is needed.

The presently tested enclosure requires further optimization and modification to be suitable for underground and underwater DC electric field measurements. The focus of this endeavor will be on developing new sensor generations that incorporate laser interrogation for monitoring sense membrane movement. Although we have a working prototype based on this principle, additional effort is required to enhance the laser optical system's durability and compactness. Furthermore, the sensor designs will emphasize higher resonance frequency for quicker event detection and higher AC bias voltages for increased sensitivity. Multiple initiatives will be required to pursued to improve the sensor.

Manitoba Hydro needs to scale this DC electric field sensor is to measure and monitor the electric fields that are present in their power transmission and distribution systems. These electric fields can be generated by the high voltage lines and equipment used to transmit electricity over long distances. Monitoring the electric fields is important because they can affect the performance and safety of the power grid. Electric field strength of a power transmission line can depend on various factors such as the voltage of the transmission line, the distance between the conductors, the spacing of the towers or poles, and the weather conditions and required those measurement to validate this sensor. It's worth noting that power transmission companies like Manitoba Hydro typically have safety and regulatory standards they must adhere to, including limits on the maximum electric field strengths allowed around their power lines. These limits are set by government agencies and are designed to protect public safety and minimize any potential health risks associated with exposure to electric fields. Therefore, wide range of electric field measurement should be conducted in outdoor environment.

References

[1] S. Isik, C. Shafai, "Simulation based modelling of sensor enclosure to enhance dc electric field strength on MEMS-based sensors" 48th international conference on Micro and Nano Engineering - Eurosensors (MNE-ES), 19 - 23 September, Leuven, Belgium, 2022.

[2] L. Sher, "Effects of natural and man-made electric/electromagnetic fields on human health: a possible mechanism,", vol. 49, , Issue 1, pp. 31–34, ISSN 0306-9877, 1997.

[3] M. Singh, V. Khadkikar, A. Chandra, and R.K. Varma, "Grid Interconnection of Renewable Energy Sources at the Distribution Level With Power-Quality Improvement Features," IEEE Transactions on Power Delivery, vol. 26, pp. 307-315, 2011.

[4] N. Kirby, Lie Xu, M. Luckett, and W. Siepmann, "HVDC transmission for large offshore wind farms," Power Engineering Journal, vol. 16, pp. 135-141, 2002.

[5] K. Zhu, W.K. Lee, and P.W.T. Pong, "Non-Contact Voltage Monitoring of HVDC Transmission Lines Based on Electromagnetic Fields," IEEE Sensors Journal, vol. 19, pp. 3121-3129, 2019.

[6] P.S. Maruvada, R.D. Dallaire, R. Pedneault, "Development of field-mill instruments for ground-level and above-ground electric field measurement under HVDC transmission lines," IEEE Transactions on Power Apparatus and Systems, vol. PAS-102, pp. 738-744, 1983.

[7] X. Qiao, Z. Zhang, X. Jiang, and T. Liang, "Influence of DC Electric Fields on Pollution of HVDC Composite Insulator Short Samples with Different Environmental Parameters," Energies, vol. 12, 2304, 2019.

[8] G.H. Vaillancourt, S. Carignan, and C. Jean, "Experience with the detection of faulty composite insulators on high-voltage power lines by the electric field measurement method," IEEE Transactions on Power Delivery, vol. 13, pp. 661-666, 1998.

[9] C.J. Miller, "The measurement of electric fields in live line working," IEEE Transactions, vol. PAS-86, pp. 493-498, 1967.

[10] E.L. Harris, B.D. Rindall, N.J. Tarko, and O.C. Noris-Elye, "The effect of a helicopter on DC fields and ions," IEEE Transactions on Power Delivery, vol. 8, pp. 1837-1841, 1993.

[11] D. R. Macgorman et al., "Coordinated lightning, balloon-borne electric field, and radar observations of triggered lightning flashes in North Florida", J. Geophys. Res. Lett. 42 (13), 5635, 2015.

[12] Jennifer G. Wilson and Kenneth L. Cummins, "Thunderstorm and fair-weather quasi-static electric fields over land and ocean," Atmospheric Research, vol. 257, pp. 105618, 2021.

[13] Pena, Jesus and Salgado-Meza, P. and Florez-Villegas, L. and Nunez, Luis. "A lightning monitoring system for studying transient phenomena in cosmic ray observatories", 2022.

[14] Fan, Y., Du, X., An, Z. et al. Earthquake-related Electric Field Changes Observed in the Ionosphere and Ground", Acta Geophys. 63, 679–697 ,2015.

[15] P. Yu et al. "Analysis of the natural electric field at different sea depths", JINST 16 P01006 2021.

[16] Messerli, Mark A., and David M. Graham. "Extracellular Electrical Fields Direct Wound Healing and Regeneration." The Biological Bulletin (Lancaster), vol. 221, no. 1, Marine Biological Laboratory, 2011, pp. 79–92.

[17] Nuccitelli, Richard, et al. "The Electric Field Near Human Skin Wounds Declines with Age and Provides a Non-Invasive Indicator of Wound Healing." Wound Repair and Regeneration, vol. 19, no. 5, pp. 645–55, 2011.

[18] Paradiso, J. A., & Gershenfeld, N. "Musical Applications of Electric Field Sensing". Computer Music Journal, 21(2), 69–89, 1997.

[19] I. Hieda and K. C. Nam, "Electric Field Measurement of the Living Human Body for Biomedical Applications: Phase Measurement of the Electric Field Intensity," International Journal of Antennas and Propagation, vol. 2013, pp. 1-6, 2013.

[20] F. X. Hart and J. R. Palisano, "The Application of Electric Fields in Biology and Medicine," in Electric Field, M. Sheikholeslami Kandelousi, Ed. Rijeka, Croatia: IntechOpen, Dec. 2017. [Online]. Available: https://www.intechopen.com/chapters/57684.

[21] M.N. Horenstein, and P.R. Stone. "A Micro-Aperture Electrostatic Field Mill Based on MEMS Technology," Journal of Electrostatics, vol. 51-52, pp. 515–21, 2001.

[22] Z. Chu, C. Peng, R. Ren, B. Ling, Z. Zhang, H. Lei, and S. Xia, "A High Sensitivity Electric Field Microsensor Based on Torsional Resonance," Sensors, vol. 18, 286, 2018.

[23] P. Yang, C. Peng, H. Zhang, S. Liu, D. Fang, and S. Xia, "A High Sensitivity SOI Electric-Field Sensor with Novel Comb-Shaped Microelectrodes." IEEE International Solid-State Sensors, Actuators and Microsystems Conference, pp. 1034-37, June 2011.

[24] S. Ghionea, G. Smith, J. Pulskamp, S. Bedair, C. Meyer, and D. Hull, "MEMS Electric-Field Sensor with Lead Zirconate Titanate (PZT)-Actuated Electrodes," IEEE Sensors Conference, Baltimore, USA, November 2013.

[25] G. Wijeweera, B. Bahreyni, C. Shafai, A. Rajapakse, and D.R. Swatek, "Micromachined Electric Field Sensor to Measure ac and dc Fields in Power Systems," IEEE Transactions on Power Delivery, vol. 24, pp. 988-995, 2009.

[26] A. Kainz, H. Steiner, J. Schalko, A. Jachimowicz, F. Kohl, M. Sifter, R. Beigelbeck, F. Keplinger, and W. Hortshitz, "Distortion-free measurement of electric field strength with a MEMS sensor," Nature Electronics, vol. 1, pp. 68-73, 2018.

[27] T. Kobayashi, S. Oyama, M. Takahashi, R. Maeda, and T. Itoh, "Microelectromechanical

Systems-Based Electrostatic Field Sensor Using Pb(Zr,Ti)O3Thin Films," Japanese Journal of Applied Physics, vol. 47, pp. 7533-7536, 2008.

[28] T. Chen, C. Shafai, A. Rajapakse, J.S.H. Liyanage, and T. Neusitzer, "Micromachined ac/dc electric field sensor with modulated sensitivity," Sensors and Actuators A, vol. 245, pp. 76-84, 2016.

[29] S. Liyanage, C. Shafai, T. Chen, and A. Rajapakse, "Torsional Moving Electric Field Sensor with Modulated Sensitivity and without Reference Ground," Eurosensors Conference, vol. 1, pp. 350-353, Paris, France, September 2017.

[30] W. Xiaolong, P. Yang, C. Zhaozhi, C. Peng, L. Yutao, and W. Shuang, "MEMS-Based Electric Field Sensor with Environmental Adaptability Consideration and Its Application in the Near-Ground Atmosphere," Journal of Physics: Conference Series, vol. 1775, 12003, 2021.

[31] X. Wen, P. Yang, Z. Zhang, Z. Chu, C. Peng, Y. Liu, S. Wu, B. Zhang, and F. Zheng, "Resolution-Enhancing Structure for the Electric Field Microsensor Chip," Micromachines, vol. 12, 936, 2021.

[31] Y. Yan, Y. Hu, L. Wang, X. Qian, W. Zhang, K. Reda, J. Wu, and G. Zheng, "Electrostatic sensors – Their principles and applications," Measurement, vol. 169, pp. 108742, 2021.

[32] R. K. Adair, R. D. Astumian, and J. C. Weaver, "Detection of weak electric fields by sharks, rays, and skates," Chaos, vol. 8, no. 3, pp. 576-587, Sep. 1998.

[33] B. Brown, J. Hutchison, M. Hughes, D. Kellogg, and R. Murray, "Electrical characterization of gel collected from shark electrosensors," Phys. Rev. E, vol. 65, pp. 061903-1-5, June 2002.

[34] E. E. Josberger, P. Hassanzadeh, Y. Deng, J. Sohn, M. J. Rego, C. T. Amemiya, and M.

Rolandi, "Proton conductivity in ampullae of Lorenzini jelly," Science Advances, vol. 2, no. 5, e1600112, 2016. [Online]. Available: https://advances.sciencemag.org/content/2/5/e1600112.

[35] Fields, R. (2007). The Shark's Electric Sense. Scientific American. 297. 74-80.

[36] Bateman, M. G., Stewart, M. F., Podgorny, S. J., Christian, H. J., Mach, D. M., Blakeslee, R. J., Bailey, J. C., & Daskar, D. (2007). A Low-Noise, Microprocessor-Controlled, Internally Digitizing Rotating-Vane Electric Field Mill for Airborne Platforms, Journal of Atmospheric and Oceanic Technology, 24(7), 1245-1255.

[37] Wijeweera, G.; Shafai, C.; Rajapakse, A. Measuring power system voltage remotely using micromachined electric field sensor. In Proceedings of the 1st Microsystems and Nanoelectronics Research Conference, Ottawa, ON, Canada, 15 October 2008; pp. 209–212.

[38] Wen, Xiaolong & Yang, Pengfei & Zhaozhi, CHU & Peng, Chunrong & Yutao, LIU & Shuang, WU. (2021). MEMS-based electric field sensor with environmental adaptability consideration and its application in the near-ground atmosphere. Journal of Physics: Conference Series. 1775. 012003.

[39] A micromachined DC electric field sensor using a torsional micro mirror, Hiniduma Liyanage, Janaranjana Sampath 2017. https://mspace.lib.umanitoba.ca/handle/1993/32687

[40] Wang, Xiaolong & Yue, Hui & Liu, Guangliang & Zhao, Zhao. “The Application of COMSOL Multiphysics in Direct Current Method Forward Modeling”, Procedia Earth and Planetary Science. 3. 266-272.

[41] A 3-degree-of-freedom low power and large displacement MEMS Lorentz force micro-mirror, Afsharipour, Elnaz, 2019. https://mspace.lib.umanitoba.ca/handle/1993/33966

[42] T. Chen, S. Isik, C. Shafai and L. Shafai, "MEMS Electric Field Sensor with Biased Electrically Floating Cover to Measure Electric Field in Ionic Environments," 2022 12th International Conference on Power, Energy and Electrical Engineering (CPEEE), pp. 175-(Sadna Isik, Simulation based modelling of sensor enclosure to enhance dc electric field strength on MEMS-based sensors, 2022)179, 2021.

[43] T. Chen, B. Hill, S. Isik, C. Shafai and L. Shafai, "DC electric field sensor based on polyimide substrate, "IEEE Sensors, pp.1-4, 2021.

[44] J.N. Chubb, "Two New Designs of "Field Mill" Type Fieldmeters not Requiring Earthing of Rotating Chopper," IEEE Transactions on Industry Applications, vol. 26, pp. 1178-1181, 1990.

[45] C. Peng, X. Chen, Q, Bai, L. Luo, and S. Xai, "A Novel High Performance Micromechanical Resonant Electrostatic Field Sensor Used in Atmospheric Electric Field Detection," MEMS 2006, Istanbul, Turkey, p. 698-701, January 2006.

[46] C.H. Hsu, R.S. Muller, "Microelectromechanical Electrostatic Voltmeter," Transducers'91, International Conference on Solid-State Sensors and Actuators, San Francisco, 1991.

[47] P.S. Riehl, K.L. Scott, R.S. Muller, "Electrostatic Charge and Field Sensors Based on Micromechanical Resonators," Journal of Microelectromechanical Systems, v. 12, pp. 577-589, 2003.

[48] J.S. Shafran, "A MEMS-based high-resolution electric- field meter," M.Eng. thesis, Massachusetts Institute of Technology, Cambridge, Massachusetts, 2005.

[49] X. Chen, C. Peng, H. Tao, C. Ye, Q. Bai, S. Chen, S. Xia, "Thermally driven micro-electrostatic fieldmeter," Sensors and Actuators A, vol. 132, pp. 677-682, 2006.

[50] B. Bahreyni, G. Wijeweera, C. Shafai, A. Rajapakse, "Design And Testing Of A Field-

Chopping Electric Field Sensor Using Thermal Actuators With Mechanically Amplified Response," Transducers'07 Conference on Solid-State Sensors, Actuators & Microsystems., Lyon, France, pp. 1397-1400, 2007.

[51] G. Wijeweera, B. Bahreyni, C. Shafai, and A. Rajapakse, "Low Power Consuming MEM Sensors for Power Engineering Applications," Cigré Canada Conference on Power Systems, Winnipeg, Canada, October 2008.

[52] A. Roncin, C. Shafai, and D.R. Swatek, "Electric Field Sensor Using Electrostatic Force Deflection of a Micro-Spring Supported Membrane," Sensors & Actuators A, vol. 123-124, pp. 179-184, Sept. 2005.

[53] T. Chen and C. Shafai, "Electric Field Sensor Using Electrostatic Force Deflection of a Micro-Spring Supported Membrane," presented at the 2013 IEEE Power & Engineering Society (PES) General Meeting, Vancouver, Canada, Jul. 21-25, 2013, pp. 1-4.

[54] Investigation of a Flexible Printed Circuit Board MEMS Electrostatic Field Sensor, Brandon Hill, 2023. https://mspace.lib.umanitoba.ca/bitstream/handle/1993/37089